Magnetic Properties of Some of the Steels Used in the Construction of the ZEUS Detector

by

Fawzi A. Ikraiam

A Thesis

Submitted to the Faculty of Graduate Studies

in Partial Fulfillment of the Requirements

for the Degree of

Master of Science

Department of Physics

University of Manitoba

Winnipeg, Manitoba

ISBN 0-315-77947-0

MAGNETIC PROPERTIES OF SOME OF THE STEELS USED IN THE CONSTRUCTION OF THE ZEUS DETECTOR

BY

FAWZI A. IKRAIAM

A thesis submitted to the Faculty of Graduate Studies of the University of Manitoba in partial fulfillment of the requirements of the degree of

MASTER OF SCIENCE

To my dear parents, Aisha and Abdulkreim

Acknowledgments

I am very grateful to my supervisor, Dr. G.R.Smith for his support, guidance, and assistance during the course of this project.

I would like to thank J.J.G.Durocher for his assistance during the experiment and for many valuable suggestions.

I would also like to thank my friends; Ali, Hussein, Hamish, John, Ibraheim and Phil whose assistance I gratefully acknowledge.

I wish to express my deepest appreciation to my dear wife, my dear daughter, and my dear son for providing encouragement and loving distraction.

I wish to extend my appreciation to my parents and family for their continued support and encouragement from the other side of the world.

Finally, I give my thanks to Allah for His grace and blessings through this long effort.

Abstract

The high energy resolution and the large dynamic range of the ZEUS calorimeter put extreme requirements on linearity and gain stability of the photomultiplier tubes used in the detector. For tracking analysis of the physics events from ZEUS, an understanding of the changes in the solenoidal magnetic field due to the presence of the different types of construction iron in the detector is necessary.

Several samples of the steel used in the construction of the ZEUS detector were obtained. Ring samples were machined out of these steels. The rings then were wrapped with about 450 turns of fine copper wire as a pick-up coil and about 250 turns of a coarse magnet wire to energize the samples. These ring samples were investigated for magnetization, coercive force, remanence, and permeability. The phenomena of magnetization and especially of the hysteresis properties of the steels give evidence that the magnetic properties of the samples are sensitive functions of the structure and constitution. Hysteresis is affected by a number of factors, among which are composition of the material, heat treatment, fabrication and temperature.

Magnetic properties of the samples are discussed. It is found that the coercive force of the samples, which is a measure of quality of the material, ranges from 180 to about 350 A/m and that the remanent field ranges from about 0.3 to 0.9 tesla.

Table of Contents

List of Figures

List of Tables

CHAPTER 1

Introduction

1.1 ZEUS: A Detector for HERA

Electron-proton interactions have been one of the most important experimental methods used to study the structure of matter [DH86]. The interactions provide better understanding of the structure of the nucleon and the weak current coupling to quarks and leptons. The Deutsches Elektronen-Synchrotron Laboratory, DESY, located in Hamburg, has constructed the Hadron Electron Ring Accelerator, HERA, which will provide colliding beams of 820 GeV protons and 30 GeV electrons. HERA offers exciting and unique physics opportunities. The HERA machine design parameters are summarized in table 1 [ZD86]. Using HERA, physicists will be able to examine electron and quark substructure to distances of a few 10^{-20} m and search for new mediators of the neutral (NC) and charged current (CC) interactions with masses up to 800 GeV. Next to electron-quark scattering, photon-gluon and W-gluon fusion will play an important role. The measurements of NC and CC scattering put a premium on the detection of the electrons and the quark jets. Particles and jets with energies up to 820 GeV have to be measured with high precision. This calls for a detector which employs a calorimeter of the best possible hadron energy resolution to make the most accurate measurements of the NC and CC cross sections. These measurements of the proton structure functions provide access to three different areas of physics. These areas are electron-quark substructure, properties of the electroweak current and Quantum Chromodynamics (QCD) interactions. ZEUS is

Table 1.1 Design Parameters of HERA.

	p–ring		e–ring	units
Nominal energy	820		30	GeV
c.m. energy		314		GeV
Q^2_{max}		98.400		GeV^2
Luminosity		$1.5 \cdot 10^{31}$		cm^2s^{-1}
Polarization time			28	min
Number of interaction points		4		
Crossing angle		0		mrad
Free space for experiments		± 5.5		m
Circumference		6336		m
Length of straight sections		360		m
Bending radius	588		608	m
Magnetic field	4.65		0.165	T
Energy range	300–820		10–33	GeV
Injection energy	40		14	GeV
Circulating current	160		58	mA
Total number of particles	$2.1 \cdot 10^{13}$		$0.8 \cdot 10^{13}$	
Number of bunches		200		
Number of bunch buckets		220		
Time between crossings		96		ns
Emittance (ϵ_x/ϵ_y)	0.71/0.71		3.4/0.7	10^{-8} m
Beta function (β^*_x/β^*_y)	10/1.0		2/0.7	m
Beam tune shift (Q_x, Q_y)	0.0026/0.0014		0.023/0.026	
Beam size at crossing σ^*_x	0.27		0.26	mm
Beam size at crossing σ^*_y	0.08		0.07	mm
Beam size at crossing σ^*_z	11		0.8	cm
Energy loss /turn	$1.4 \cdot 10^{-10}$		127	MeV
Critical energy	10^{-6}		111	keV
Max. circumf. voltage	0.2/2.4		260	MV
Total RF power	1		13.2	MW
RF frequency	52.033/208.13		499.667	MHz
Filling time	20		15	min

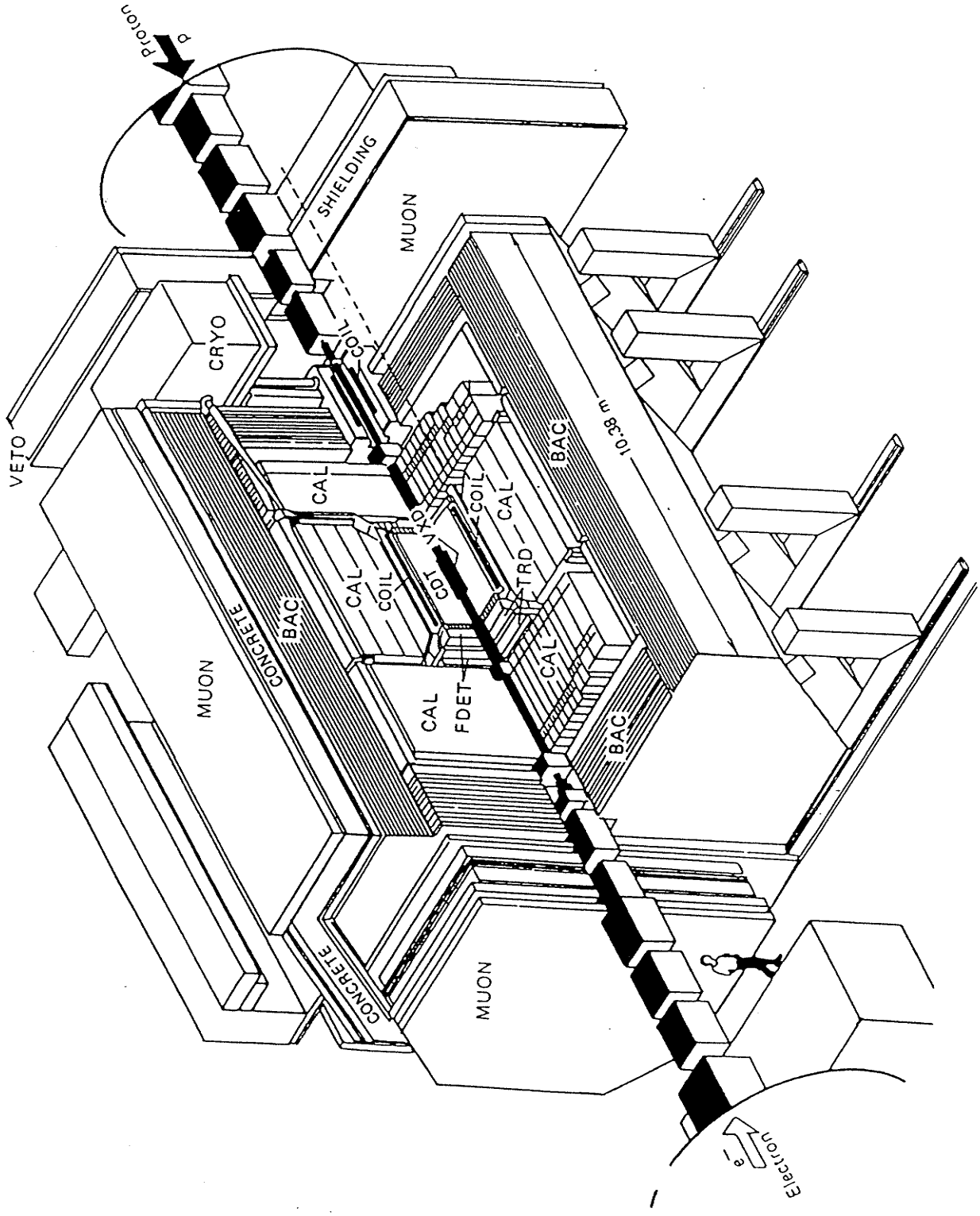

Figure 1.1 Isometric view of the ZEUS detector.

a detector capable of exploiting the physics possibilities provided by HERA. ZEUS has been designed with the following components and properties:

(1) hermetic electromagnetic and hadronic calorimeter with uniform response to electrons and hadrons and the best possible hadron energy resolutions.

(2) high precision charged particle tracking detectors covering the whole solid angle with special emphasis on resolving tracks travelling in the proton direction where the track densities are high.

(3) electron and muon identification, in particular for the isolated tracks expected from exotic processes.

(4) a leading proton detector to obtain fully contained events.

(5) electron and muon tagging for a luminosity measurement and for the identification of the photoproduction processes.

Figure 1.1 shows an isometric view of the detector. The essential components within a thin magnetic solenoid (SOLENOID) are the vertex detector (VXD), central track detector (CTD) transition radiation detector (TRD) and planar chambers (FTD, RTD). Surrounding the SOLENOID are an electromagnetic (EMC) and a hadron calorimeter (HAC) completely covering the solid angles. A backing calorimeter (BAC), barrel and rear muon detector (MU), and a forward muon spectrometer (FMU) are also identified [ZE86].

The high resolution calorimeter consists of depleted uranium plates interleaved with plastic scintillator. Balancing the thickness of absorber and scintillator achieves approximately equal response to electrons and hadrons along with optimal energy

resolution. The scintillator plates are read out via wave length shifter bars, light guides and photomultipliers. The backing calorimeter uses as absorber iron plates which form the magnet yoke [ZE86].

The calorimeter is divided into three main components; the forward calorimeter (FCAL), the barrel calorimeter (BCAL) and the rear calorimeter (RCAL), as shown in figure 1.2. The structure of the three CAL components is similar. Each calorimeter unit (FCAL, RCAL, or BCAL) consists of a back beam and two C-arms, or C-legs, as shown in figure 1.3 [ZE89].

The central track detector consists of a cylindrical jet-type drift chamber with an outer radius of 85 cm and an overall length of 240 cm. The vertex detector, which is used to detect decays of short lived particles, has a time-expansion type drift cell. The muon spectrometer employs drift and limited streamer tube chambers plus scintillator counters. Both the barrel and the forward muon detector systems provide event triggers which may be used for exotic and heavy flavour physics, as well as for cosmic ray tests. The muon detector is constructed using double-layers of limited streamer tubes of non-flammable construction [ZE86].

The magnetic solenoid is superconducting and provides a field of 1.8 T which ensures accurate measurement of charged tracks through the central, forward and rear tracking detectors. It has an inner radius of 86 cm, a length of 280 cm and is 0.8 radiation lengths thick [ZE86].

More information about the different elements of the ZEUS Detector and how they operate may be obtained from the technical proposal for the detector [ZD86].

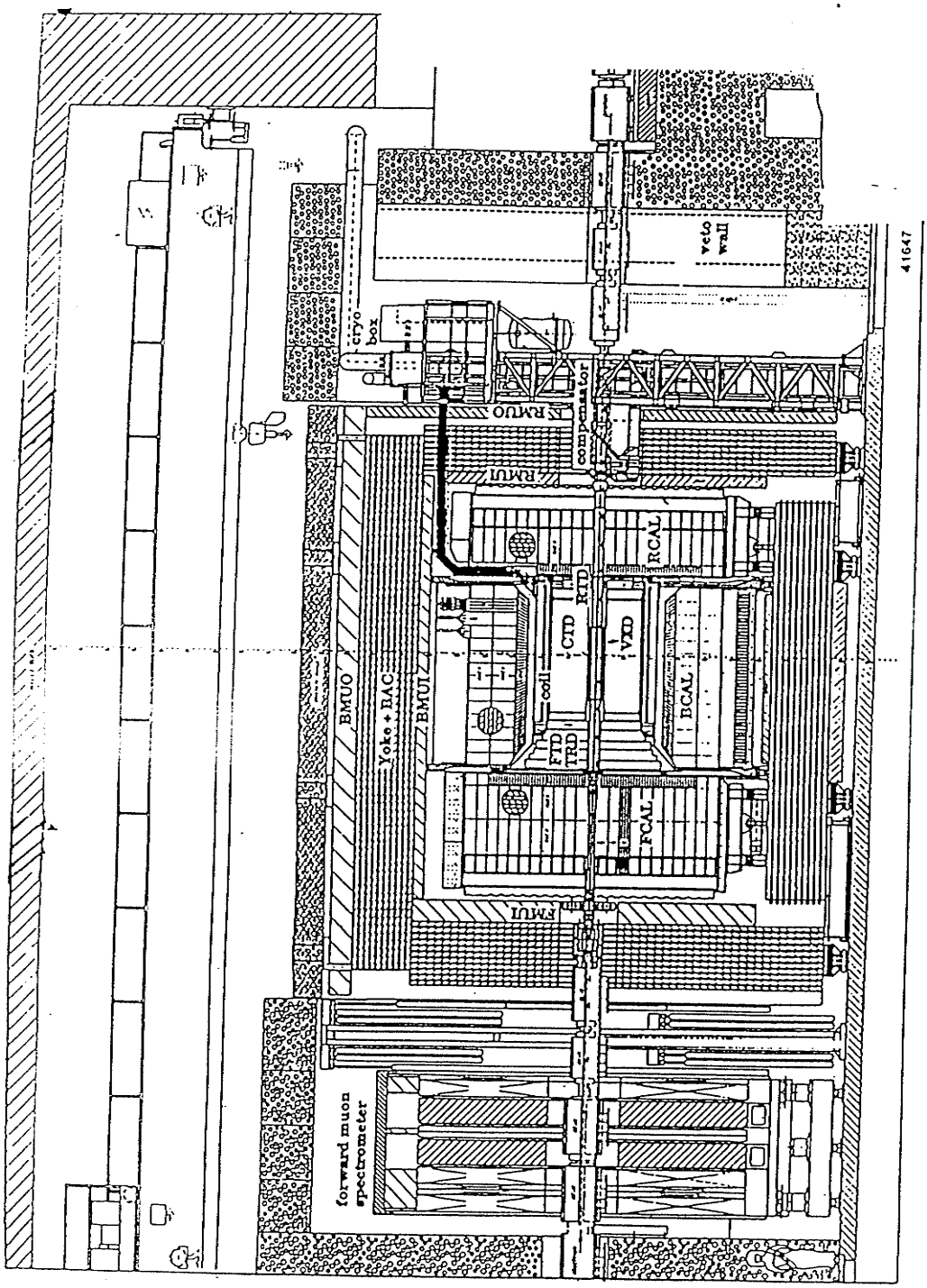

Figure 1.2 Section of the ZEUS detector along the beam.

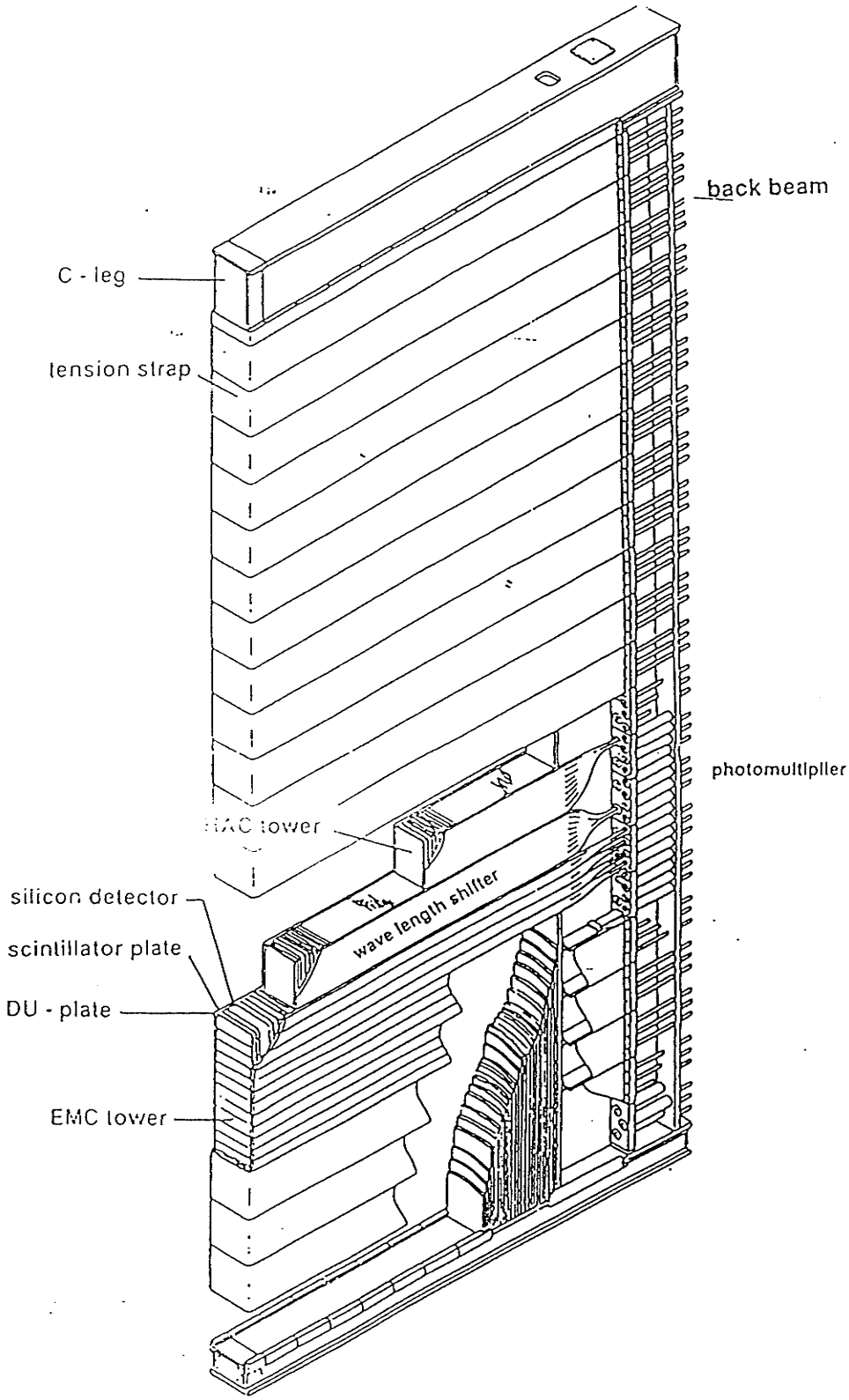

Figure 1.3 Isometric view of the largest FCAL module.

1.2 Purpose of This Study

Canada participates as a major partner in the international collaboration building ZEUS. ZEUS represents a significant opportunity for Canadian physicists to work at one of the important frontiers in elementary particle physics.

Canada has responsibility for half the forward and rear calorimeters (FCAL and RCAL) along with the third level trigger system. Reading out the calorimeters using photomultiplier tubes (PMTs) involves a special difficulty because proper operation of the PMTs requires that ambient magnetic fields must not exceed 10^{-6} T. The magnetic field of the solenoid, in the regions of the PMTs can be as high as 0.2 T so that a reduction of several orders of magnitude in field intensity is required. In ZEUS, this reduction is provided by bulk magnetic shielding tubes for the PMTs and the construction iron contained within the calorimeter units [ZD86].

The ZEUS calorimeter puts quite extreme requirements on linearity and gain stability of the PMTs. The PMTs must be shielded against a magnetic field which is < 0.06 T except for the RCAL where the field might go up to about 0.2 T. The shield has to reduce the magnetic field between photocathode and anode to values of about 5 A/m (10^{-6} T in air) for fields transverse to the PMT axis and to 100 A/m (20×10^{-6} T in air) for longitudinal fields [ZD86].

One solution is to encase the PMT in one or more concentric cylindrical shells made from high permeability materials. However in regions of large field intensities a combination of additional bulk shielding, and magnetic flux redirection is required for the successful operation of the PMT's [ZD86].

Because modelling of the magnetic field is important to effective analysis of the data from ZEUS, an understanding of the changes in the solenoidal magnetic field due to the presence of all the different types of construction steel in the detectors is necessary. Also the forces on the solenoid and calorimeters are very much dependent on the magnetization curves. For this reason, the ZEUS project initiated a series of calculations [CO91] and measurements [MA91] of the solenoidal field in the presence of different types of steel. The final predictions of these modifications of the magnetic field depend on the magnetic properties of the various types of steel used in the construction of the detector. Hence this detailed study of the **B** versus **H** characteristics of these steels was undertaken.

1.3 Locations of the different steels under study in ZEUS

Figure 1.3 shows a three dimensional view of an FCAL module in the orientation in which it is installed in the ZEUS detector.

The various types of steel, which are to be tested for their magnetic properties, are machined into ring samples for reasons to be explained later. The steels used in the construction of the modules are as follows:

(1) Canadian steels I and II in the back beam.

(2) C-Arm steel in the Canadian C-arm.

(3) The German steel in the Dutch back beam.

(4) The Dutch steel in the Dutch C-arm.

(5) The US steel in the BCAL units.

Table 2 section 4.6 (p.71) lists the geometric dimensions and coil number for all the ring samples which were obtained from the above mentioned steels.

There are also four steels from ZEUS which were not studied for their magnetic properties. These steels are the main yoke, compensator yoke, FCAL-HAC1 cladding and FMU toroids. No samples of these steels were available for analysis when this study was undertaken. However, a thin sample from the FCAL-HAC1 cladding unit has recently been made available. An attempt will be made to fabricate a sample from this material for future analysis. The use of magnetic cladding steel for the FCAL-HAC1 uranium was selected to assist in the balance of forces on the ZEUS superconducting solenoid.

Chapter 2

Magnetism in matter

2.1 Introduction

Materials may be classified into five types according to their magnetic properties. These five different categories are named diamagnetic, paramagnetic, ferromagnetic, antiferromagnetic, and ferrimagnetic. These different magnetic behaviours are attributed to three main causes; electron orbital motion, electron spin, and nuclear spin. Nuclear spin is usually very weak. All of these effects may be represented by equivalent atomic currents flowing in circular loops. Each of these atomic current loops may be represented by its magnetic, or dipole, moment, **m**.

When dealing with magnetic materials, it is convenient to speak of the relative permeability κ defined as $\kappa = \mu/\mu_o$

where: μ is the permeability in units of henrys/meter.

μ_o is the permeability of vacuum, or free space, in units of henrys/meter. Thus the relative permeability is a dimensionless quantity and has a magnitude of unity for vacuum. The relative permeability is slightly larger than unity for paramagnetic materials and is slightly less than unity for diamagnetic substances. For ferromagnetic materials, the value of relative permeability is generally much greater than unity [KR53].

For diamagnetic materials, the net magnetic moment of each molecule, in the absence of an external magnetic field, is zero. The application of an external

magnetic field induces a slight net molecular moment directed opposite to the external field which produces a relative permeability slightly less than unity.

In paramagnetic materials, there are net permanent magnetic moments which are randomly oriented. Applying an external magnetic field causes some of these magnetic moments to align in the same direction as the magnetic field inducing a relative permeability slightly greater than unity.

In ferromagnetic materials, molecules possess atomic magnetic dipole moments which are aligned parallel to each other in certain regions, called *domains*. These alignments are caused by the strong interactions between neighbouring moments. The alignments persist in the material even after the applied external magnetic field is removed.

In antiferromagnetic materials, the adjacent molecules also have magnetic moments of equal strength, however their alignment is antiparallel to each other.

Finally, in the case of ferrimagnetic materials, the adjacent molecules have magnetic moments which are not only antiparallel but moreover are of different strengths. Figure 2.1 illustrates a one-dimensional model of these different types of magnetic materials [KR53].

2.2 Ferromagnetism

While all materials show some magnetic effects, these effects are weak except in the case of ferromagnetic materials, as described briefly in the previous section. Ferromagnetism occurs in materials such as iron, cobalt, nickel, and their alloys.

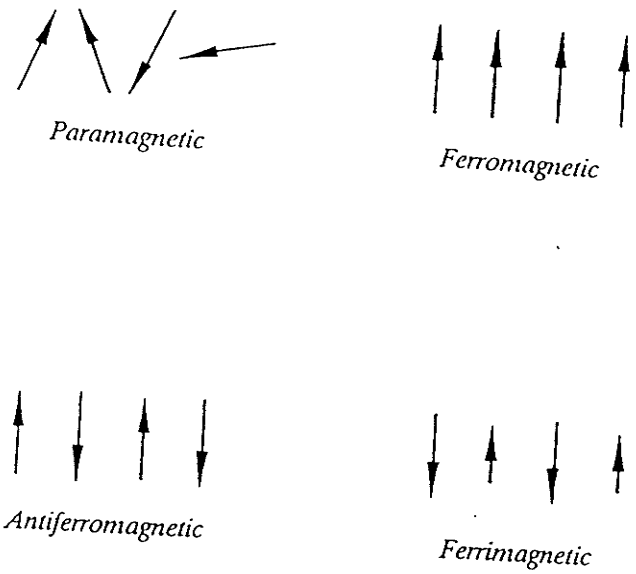

Figure 2.1 A one-dimensional model for the alignment of magnetic moments for the different types of magnetic materials.

When a small external magnetic field is applied to these substances, a large degree of alignment of internal dipole moments is attained. In some cases these aligned dipoles can persist after the external magnetic field is removed. This is due to the strong forces among these dipole moments. These forces are predicted by quantum mechanics and cannot be " explained " in terms of classical physics [RE66]. The magnetic moment of a dipole is defined as

$$\mu = m\mathbf{d} \qquad (2.2.1)$$

where: $\mathbf{d}$ is a vector pointing from negative to positive pole, and the quantity m is the pole strength.

The positive pole of a magnet is also called a " north-seeking pole ", or simply its north pole, and the negative pole is called a " south-seeking pole ", or a south pole. All magnetized materials have both a north and a south pole. These poles always appear in pairs and can not be separated, making a very important distinction between electric charges, which can be isolated, and magnetic poles [BO51].

Atomic theory has shown that the magnetic dipole moments observed in bulk matter arise from two origins. The first one is the motion of electrons about their atomic nucleus (orbital angular momentum) and the other is the rotation of the electron about its own axis (spin angular momentum). However the spin contribution is often more important than that of the orbital motion.

To explain the phenomenon of ferromagnetism, Weiss [WE07] postulated the existence of small regions that are spontaneously magnetized within the material. These regions are called *domains*. The direction of alignment varies from one

domain to another inducing a net magnetic moment of zero magnitude, due to moments cancelling each other, for that particular substance in the absence of an external magnetic field.

Domains can have different shapes and sizes, ranging in size from a few micrometers to a few millimetres, depending on the material and its past history. Each domain has many magnetic dipoles which are produced as a result of the electron spin. These dipoles are aligned in parallel by the strong forces among neighbouring dipoles. Figure 2.2a illustrates a typical magnetization curve and figure 2.2b illustrates the corresponding relation of the permeability μ as a function of the applied field **H**. The curve rises from a point on the μ-axis above the origin (the initial permeability is non-zero) to a maximum, μ_{max}, then falls off [BO51] & [WA86]. The maximum permeability, μ_{max}, occurs at that point on the magnetization curve with the largest ratio of B to H.

As stated earlier, in the absence of an external magnetic field, there is usually no spontaneous magnetic field in the material as a whole. This absence of magnetic field corresponds to point O in the magnetization curve shown in figure 2.2a. Figure 2.3a illustrates the corresponding situation for the domains. If an external magnetic field **H** is applied, for example, in the x-direction, those domains which possess moments in the direction of the applied field increase their size at the expense of neighbouring domains, and the internal magnetic field increases greatly over the external field alone. This result corresponds to that portion of the magnetization curve from point O to point P_1 shown in figure 2.2a. Figure 2.3b illustrates the

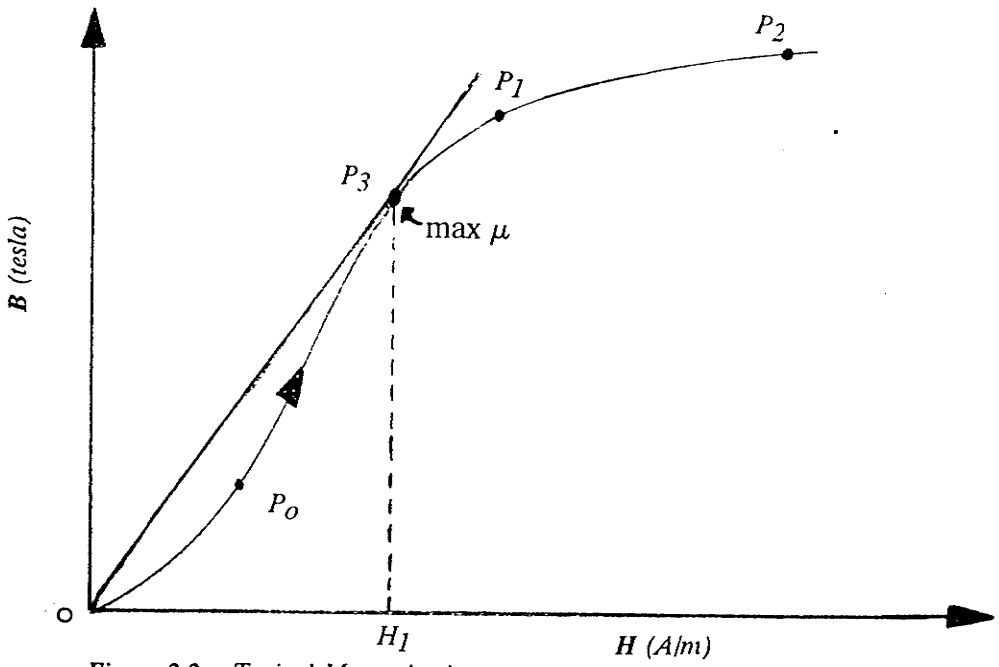

Figure 2.2a Typical Magnetization curve.

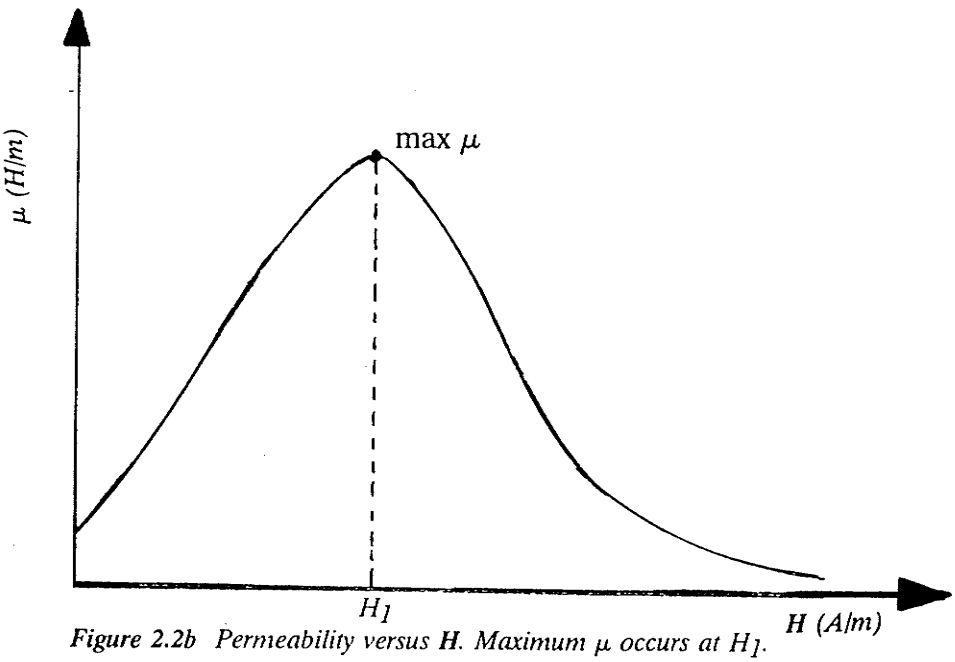

Figure 2.2b Permeability versus H. Maximum μ occurs at H_1.

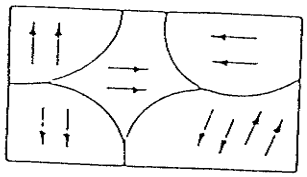

(a) In the absence of an applied field.

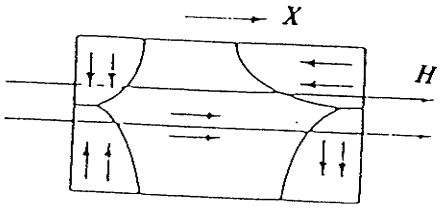

(b) In the presence of an applied field.

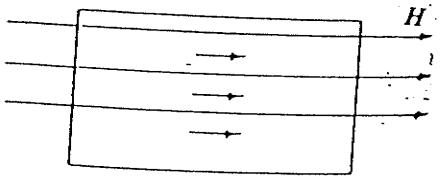

(c) All domains align with the external field at saturation point.

Figure 2.3 Domains in a ferromagnetic material.

corresponding situation for the domain. If the magnetizing field **H** is strong enough, one domain takes over entirely, and the material is said to be "saturated". This saturation point is represented by point P_2 in figure 2.2a. Figure 2.3c shows the corresponding state of the domains. Beyond point P_2 in figure 2.2a, the magnetic flux density, **B**, increases with **H** at a rate equal to μ_o.

Even though this picture of the magnetization process is an oversimplified one, it accounts qualitatively for many of the important phenomena. Another process, also occurs which was not previously mentioned. Not only do domains change in size when an external field is applied, but the length of specimen also changes during magnetization. This phenomenon is known as *magnetostriction* [HO52]. However, this effect can occur only if the specimen is not rigid. Non-rigid materials can deform under the influence of the external field. Magnetostriction is generally on a very small scale and can be neglected for most materials [WA86].

In 1932 Bloch [BL32] predicted theoretically that the boundaries between the different domains are not sharp on an atomic scale but they spread over a certain thickness. Through this thickness the direction of spins changes gradually from one domain to the next. This region is called a *domain wall* or sometimes it is called a *Bloch wall.*

The process of shifting domain boundaries in response to an external magnetic field is not entirely reversible. As the applied magnetic field **H** is increased, the conditions for minimum energy are changed. The new domain structure represents minimum energy under these new conditions. Over the first portion OP_o of the

magnetization curve in figure 2.2a, the domain wall motion is approximately reversible. If the magnetic field **H** is reduced to zero, the domain walls move back to their original position and the magnetization returns to zero along P_oO. Beyond P_o, the domain wall motion is irreversible. If the applied field **H** is reduced, there will be a return to randomly oriented domains, but that return will be far from complete. Now when the external field **H** is removed, a residual, or remnant, dipole field remains in the substance. By point P_1, the domain walls have moved about as much as they can and the walls movement ceases approximately at this point. However, there are still some domains left whose magnetic moments are not completely aligned with the applied field. As the applied field is increased further along the portion P_1P_2, these nonaligned domain slowly rotate to line up with the applied field. This process is called domain rotation. At point P_2, we have reached saturation. Further increase in **H** does not change **B** appreciably [SK68].

Ferromagnetic materials are commonly used for transformers and permanent magnets. For permanent magnets, a flat topped wide hysteresis curve is required so that the magnetization remains at high levels even after the removal of the external field. This implies a large area enclosed by the hysteresis curve and, consequently, high losses. This type of material is called a hard magnetic material. For transformers and motors, this type of material is inappropriate since it involves significant energy losses. Instead, a material is needed in which the domain wall movement is nearly reversible and that has a narrow hysteresis curve, and a high permeability. This type of material is called a soft magnetic material [FE66].

2.3 Magnetization Curves

The permeability μ of a material is given by

$$\mu = B/H = \kappa \mu_o \qquad (2.3.1)$$

where: B is the magnitude of flux density **B** in units of webers/meters^2.

H is the magnitude of field **H*** in units of amp/meter.

μ_o is the permeability of vacuum and has a magnitude of $4\pi x10^{-7}$ H/meter.

κ is the relative permeability of material (dimensionless).

The permeability, μ, represents the relative increase in the flux caused by the presence of the magnetic material [BO51]. It is very important to note that the permeability μ, or the ratio **B/H**, is not a constant for ferromagnetic substances but is dependent upon the initial conditions, the past history of the material and the value of **H**.

A "permeability" μ, for ferromagnetics, must never be defined simply as *the* value of B/H. It must be defined as a value of B/H, of dB/dH, or of $\Delta B/\Delta H$. Such special definitions lead to such concepts as initial permeability, differential permeability, and incremental permeability, respectively. A plot of μ as a function of **H** is shown in figure 2.2b, where the maximum μ is found at the point where the line joining the origin to a point on the magnetization curve is tangent to the curve. This corresponds to the line from point O to point P_3 in figure 2.2a.

If the sample is initially unmagnetized (virgin), i.e **B**=0, and the field **H** is slowly

---

**H is sometimes called "magnetic field intensity" but this name is not particularly appropriate since it implies that H is analogous to the electric field intensity E which is not the case. In force expressions B, as opposed to H, enters those expressions; H is also called "the magnetizing force" [KR53]p.215.*

increased in magnitude from zero, the flux density will change nonlinearly with **H** as shown in figure 2.2a. The relative permeability of a particular point on the magnetization curve is given by $\kappa = B/(\mu_o H)$ where B is the ordinate of that point and H is the abscissa of the point.

The point P_2 in figure 2.2a, as stated earlier, is called the saturation point, beyond which $d\mathbf{B}/d\mathbf{H} = \mu_o$, i.e the substance has stopped contributing to the flux density; any further increase of **H** will result in that much increase of **B** as in a vacuum. However, for many materials, the values of **H** required to reach this point are impractically large [WA86]. The maximum permeability occurs at that point on the magnetization curve where the ratio **B/H** is the largest.

The magnetization curve may be divided into two main portions. The first portion is the steep section where this corresponds to the condition of easy magnetization. The second portion is the flattened section which corresponds to a condition of difficult, or hard, magnetization. Figure 2.4 shows the two regions [KR53].

Since a domain contains millions of atoms and it changes its orientation from one direction of easy magnetization to another in a period measured in thousandths of a second, the magnetization proceeds by steps rather than in a smooth fashion. These steps may be observed by using sensitive measuring devices. Figure 2.4 shows an enlarged portion of the magnetization curve which illustrates these steps [KR53]. The steps are called Barkhausen steps or jumps [KR53], named after their discoverer.

If the magnetic field strength **H** is now reduced, the same magnetization curve

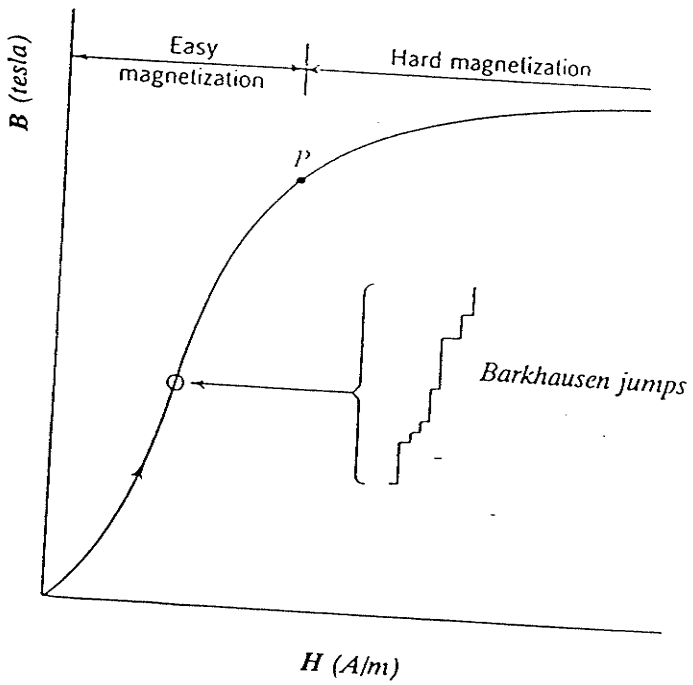

Figure 2.4 Regions of easy and hard magnetization of the magnetization curve.

will *not* be retraced. Instead, as indicated by the directions of the arrowheads in figure 2.5 [KR53], **B** decreases more slowly and will have a finite value at zero excitation field. That value of **B** will be near its saturation value. Thus there is a residual flux density at zero excitation field. The retention of magnetization in zero field is known as *remanence* and its value is shown as B_r in figure 2.5. On applying an **H** field in the opposite direction the value of **B** falls; reaching zero at $\mathbf{H} = -\mathbf{H}_c$. This value of the field strength is known as *the coercive force*. Ferromagnetic materials are often classified as hard or soft, depending on whether the value of coercive force is large or small, respectively. As the magnitude of the **H** field is further increased in the opposite direction, a reverse flux density is set up which quickly reaches the negative saturation value. If the reverse field is now removed by applying a positive field until $\mathbf{H}=0$, we find that again $\mathbf{B}\neq 0$ and there is a residual magnetization, or flux density, $-B_r$. To reduce **B** to zero, a coercive force $+\mathbf{H}_c$ must be applied. The **B** versus **H** curve eventually closes and the resulting curve is known as *a hysteresis*** *loop*, named by J.Ewing [EW89]. This is illustrated in figure 2.5 [KR53]. If the material is carried to saturation at both ends of the hysteresis loop, the resultant loop is called the saturation, or major, hysteresis loop [KR53]. For easily magnetized materials the hysteresis loop is thin with a small area enclosed. On the other hand, the hysteresis loop for hard magnetic materials is wider with a greater area enclosed.

** *The word hysteresis is derived from the Greek word hystereein which means to be behind [WA86]p.340.*

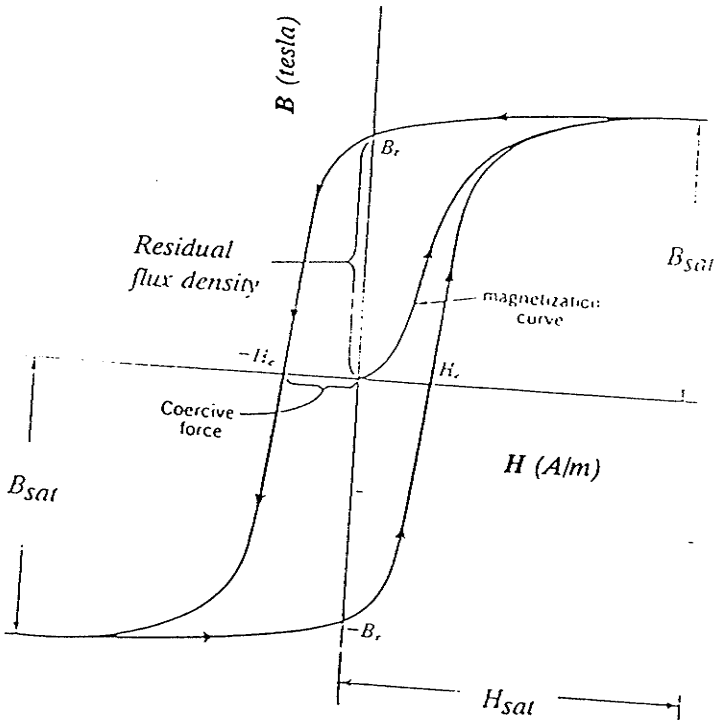

Figure 2.5 *Hysteresis loop.*

Thus it is seen that the relation between **B** and **H** is not only nonlinear, but it is not single valued either. Furthermore, the change in the **B** field always lags behind the change in the **H** field [WA86].

Typically, the magnetization and hysteresis curves are different for different materials. In addition to the nonlinear relation between **B** and **H**, the shape of the hysteresis curves depends strongly on the chemical composition of the substance, the details of its preparation, temperature and finally on the subsequent physical treatment of the material.

2.4 Demagnetization

Demagnetization, or deperming, is a process where the residual magnetization of a material is removed so that the residual flux density has a zero value when $\mathbf{H}=\mathbf{0}$.

The residual flux density can be reduced to zero by applying the coercive force $\mathbf{H}_c$. But when this is done, the residual flux density will rise to some value B_o as shown in figure 2.6. Where by increasing -H to slightly larger value than $-H_c$ and then decreasing it to zero, the condition of $\mathbf{B}=\mathbf{0}$ when $\mathbf{H}=\mathbf{0}$ may be achieved. This is shown by the dashed lines in figure 2.6 [KR53]. However, this procedure requires an accurate knowledge of **B** and **H**, the past history of the material, and the hysteresis loop of the material. Another way of achieving the same state is by heating the sample above the transition temperature and cooling in zero field. It is observed experimentally that heat and mechanical shock tend to return the material to the original unmagnetized state. In fact, if the temperature is raised sufficiently high, the

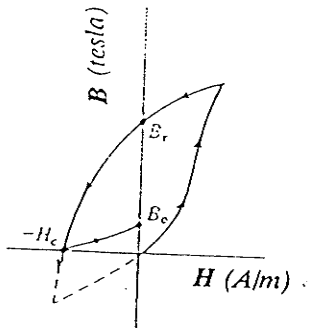

Figure 2.6 Part of the hysteresis loop showing the reduction of B to zero.

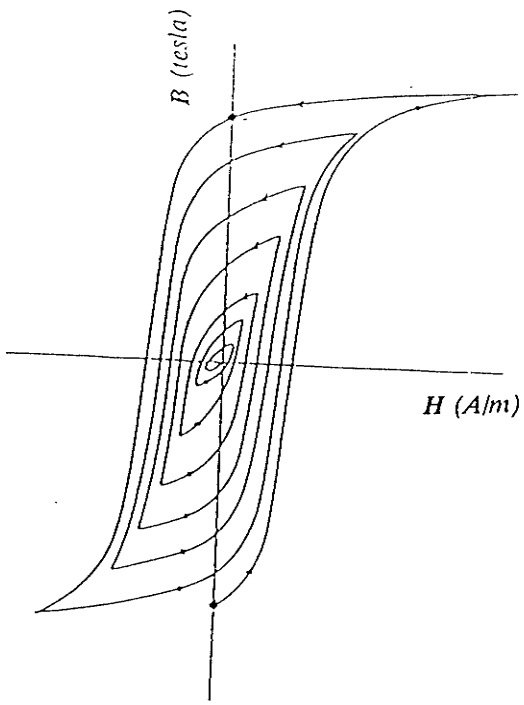

Figure 2.7 Demagnetizing a specimen by the method of deperming.

domains themselves are demagnetized and ferromagnetism disappears. The temperature at which this occurs is called the Curie point (about 770 °C for iron) [BO51].

A simpler method is called demagnetization, or deperming, by reversals which produces the same results. This is the method used in our experiment. In this method, an alternating current, larger than the current used to produce the hysteresis loop, is introduced into the primary windings and gradually reduced on each reversal so that the material, eventually, is found in a demagnetized state when the external applied field is removed, as illustrated in figure 2.7. This process could be completed in just a few seconds if the material which is to be demagnetized is of small size. On the other hand, a longer time may be required for each reversal for a large magnetic specimen because of the time lag between the field strength and the corresponding induction. This is may be attributed to the slow decay of the induced eddy currents and the longer time it takes for a particular domain to change its polarity [KR53]. Eddy, or circulating, currents are induced by the electromotive force generated in the plane at right angles to the direction in which the flux is changing [BO51]. These currents are affected by a number of factors, such as the resistivity of the substance, the geometry of material, the permeability and the frequency of the changing flux. The direction of the eddy currents is always opposite to that of the applied magnetizing current giving rise to them [BO51].

Eddy currents are unwanted because the heat produced not only represents a power loss but must also be dissipated [TI82]. However, in our experiment, this

problem is not present due to the small size of the different specimens and the short time required to demagnetize each sample.

Chapter 3

Experimental Techniques

3.1 Introduction

Magnetic effects in most materials are weak except for the group of substances known as ferromagnetic materials. The permeability of these materials is not a constant but is a function of the magnitude of the applied field, temperature and the past history of the substance. In this chapter an experimental method will be described to study the magnetic behaviour of the steel samples from the ZEUS detector.

3.2 Sample Preparation

A specimen of the material to be tested is machined into a ring (torus)***. The measurement of the magnetization curves by the ring method was used by Rowland in 1873, hence this type of ring is sometimes called a Rowland ring. The ring specimen is, in many respects, nearest to the ideal when considering basic testing principles. Then two separate coils of insulated wire are wound around the ring. The two coil windings are the magnetizing **H** coil and the pickup **B** coil. First, the pickup -, or flux-sensing, or secondary, winding is put on and wound uniformly around the ring. The primary, or magnetizing, winding is wound uniformly on top of the pickup coil. The wire that is used for the primary winding should be large enough

***This was done at the machine shop at the University of Manitoba.*

to avoid heating which may result in variations in current. Figure 3.1 illustrates such a ring sample. When the sample is ready for experimentation, it is mounted on a board with appropriate leads connected to the ends of both the primary and pickup coils.

In principle, the coil may be uniformly distributed around the ring or concentrated in a part of the ring. However, with a uniformly distributed winding the magnetic field is confined to the ring. With a concentrated winding there is some flux density leakage into the air outside the ring. This leakage flux has escaped from the magnetic circuit formed by the ring. However, the effect of leakage flux in the case of concentrated windings may, in many cases, be neglected when one is dealing with samples that have a large permeability compared with that of air [BO51]. In our experiment, we have adopted the method of uniformly distributed winding.

3.3 Advantages of the Ring Sample

Using a ring specimen has many advantages. The first one is that there are no air gaps or joints in the sample. These discontinuities produce surfaces perpendicular to the lines of **H** and surface pole densities are induced on these surfaces. The surface pole densities dominate the magnetic field and are avoided by the ring sample. Since the specimen is gapless (i.e. the magnetic field **H** is uniform around the ring), there will be no sources of **H** "poles", and therefore no demagnetizing field. Secondly, the magnetic field **H** is uniform, to first approximation, in the cross section throughout the length of the ring sample. Thirdly, since the radius r of the toroid

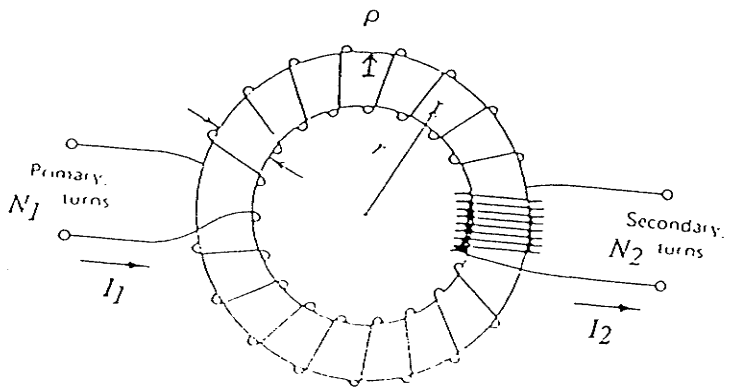

Figure 3.1 The ring sample, showing only parts of the primary and secondary windings, where in fact N_1 and N_2 cover the ring completely.

is large compared with the cross-section radius ρ, the magnetizing field **H** can be derived accurately from a knowledge of the magnetizing current, I, the dimensions of the specimen, and the number of turns in the primary windings, and no independent measurement of the magnetizing force is required. That is

$$\int \nabla \times \mathbf{H} \cdot d\mathbf{S} = \oint_S \mathbf{H} \cdot d\mathbf{l} \qquad (3.3.1)$$

$$\Rightarrow \qquad (2\pi r)H = N_1 I \qquad (3.3.2)$$

where: N_1 is the number of turns of the primary windings and

S is a surface bounded by an arbitrary path of integration.

Table 2 section 4.6 (p.71) lists the geometric dimensions and coil numbers for all of the samples.

3.4 Apparatus

The sample is then connected into the apparatus which consists of a waveform generator, a power supply, a 0.1 Ohm resistor, a Hewlett-Packard (HP) digital multimeter (DVM), a monostable multivibrator, and a personal computer (PC) with a general purpose interface bus (GPIB) board. Figure 3.2 shows a block diagram of the equipment setup.

A description of the apparatus used in the experiment is as follows:

(1) Microdot F230B Waveform Generator:

The Microdot F230B is a high frequency Waveform Generator, providing a continuously variable selection of frequencies from 0.005 Hz to 3 MHz. The F230B

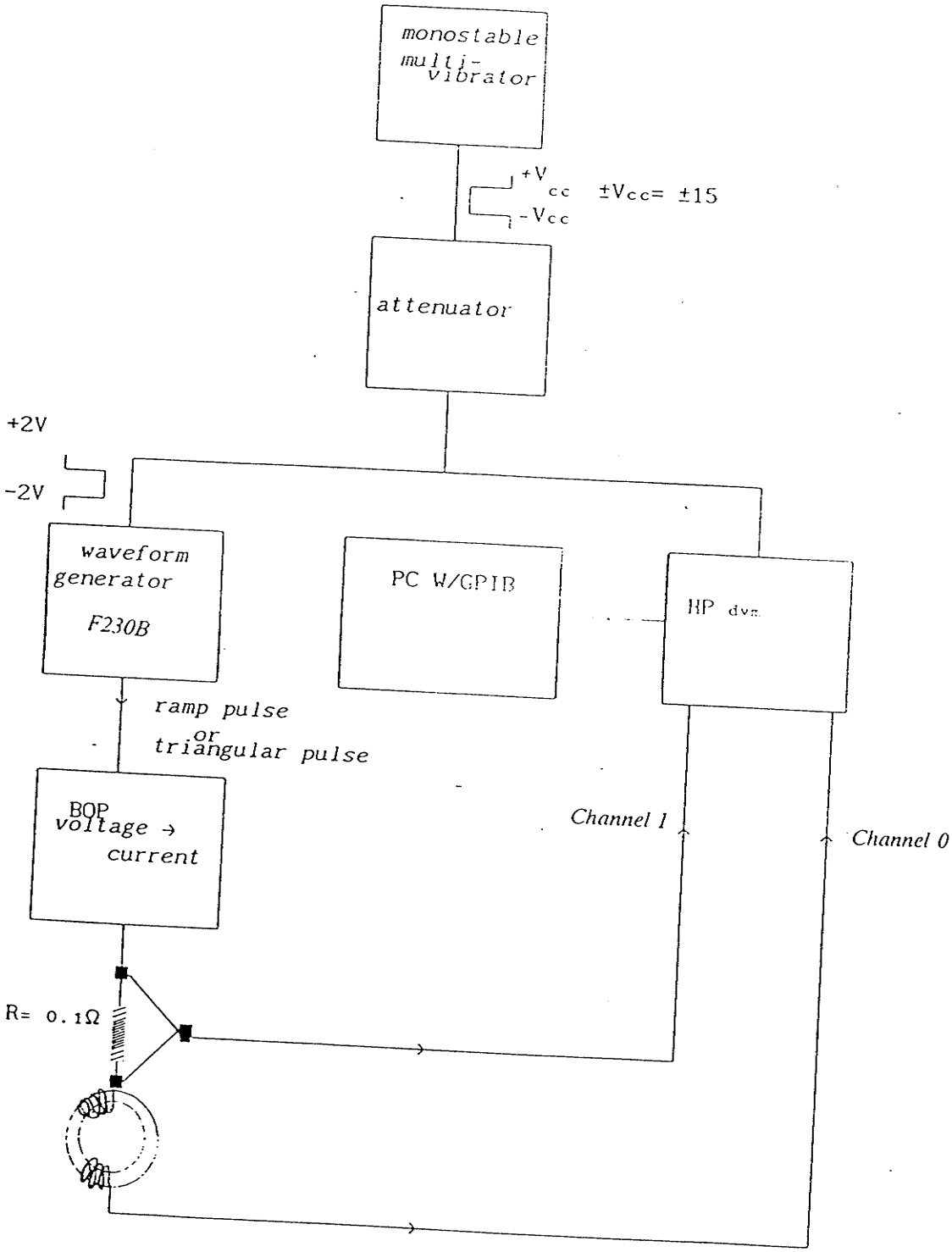

Figure 3.2 A block diagram of the equipment setup.

provides Square, Sine, Triangle, and Ramp wave forms. It also contains an internal Sawtooth Generator which enables it to be operated as a Sweep Generator, Pulse Generator or Tone burst Generator. The two wave forms which are used in our experiment are the triangular and the ramp, or sawtooth, wave forms. The triangular wave is used to generate the hysteresis loops and the sawtooth wave is used for the magnetization curves. Figure 3.3 shows a simplified block diagram of the F230B instrument [MI70].

(2) Kepco Bipolar Operational Power Supply (BOPS):

The Kepco BOPS is an all solid-state design, featuring IC operational amplifiers (op amp) and silicon power transistors mounted on special fan-cooled heat sinks. It is a fast programmable power supply with considerable bandwidth. The BOPS has two bipolar control channels, one for the voltage mode and the other for the current mode. Each mode is individually selectable and controllable either from their front panel controls, or by remote signals. The current channel is the one which is used in our experiment. Figure 3.4 shows a circuit diagram of the BOPS current control channel. More information about the Kepco BOPS may be obtained from the instruction manual of the instrument [KE79].

(3) A 0.1 Ohm can resistor:

The resistor is a wire wound resistor manufactured by Leeds & Northrup Co. It has four leads, two of which are for input (current) and the other two for output

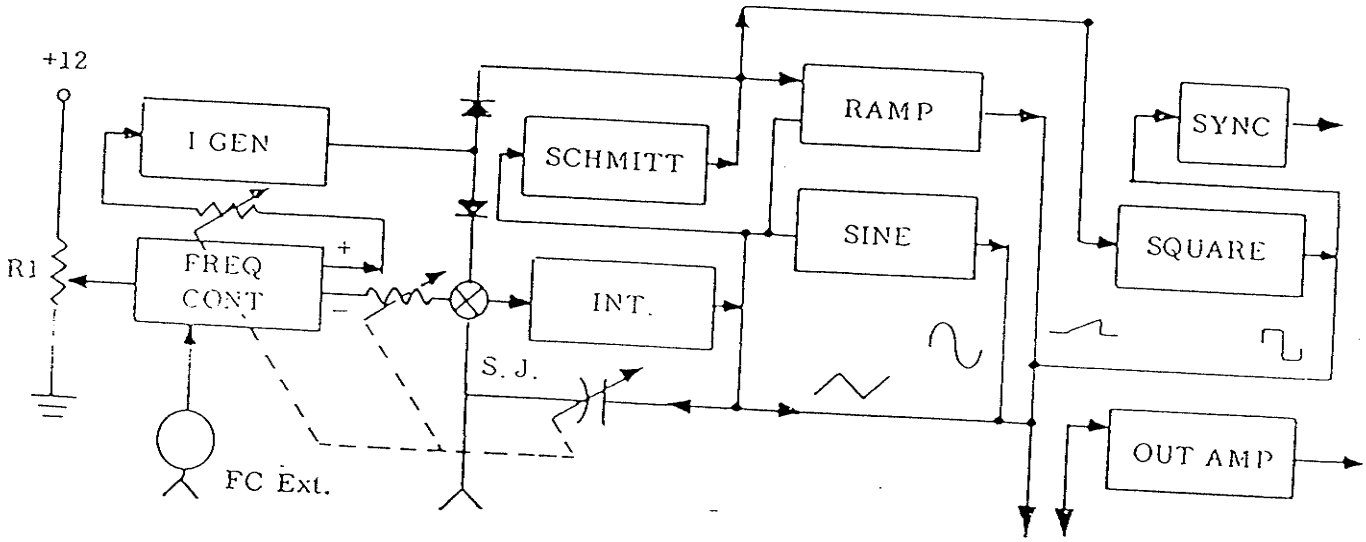

Figure 3.3 Simplified block diagram of the F230 Wave Generator.

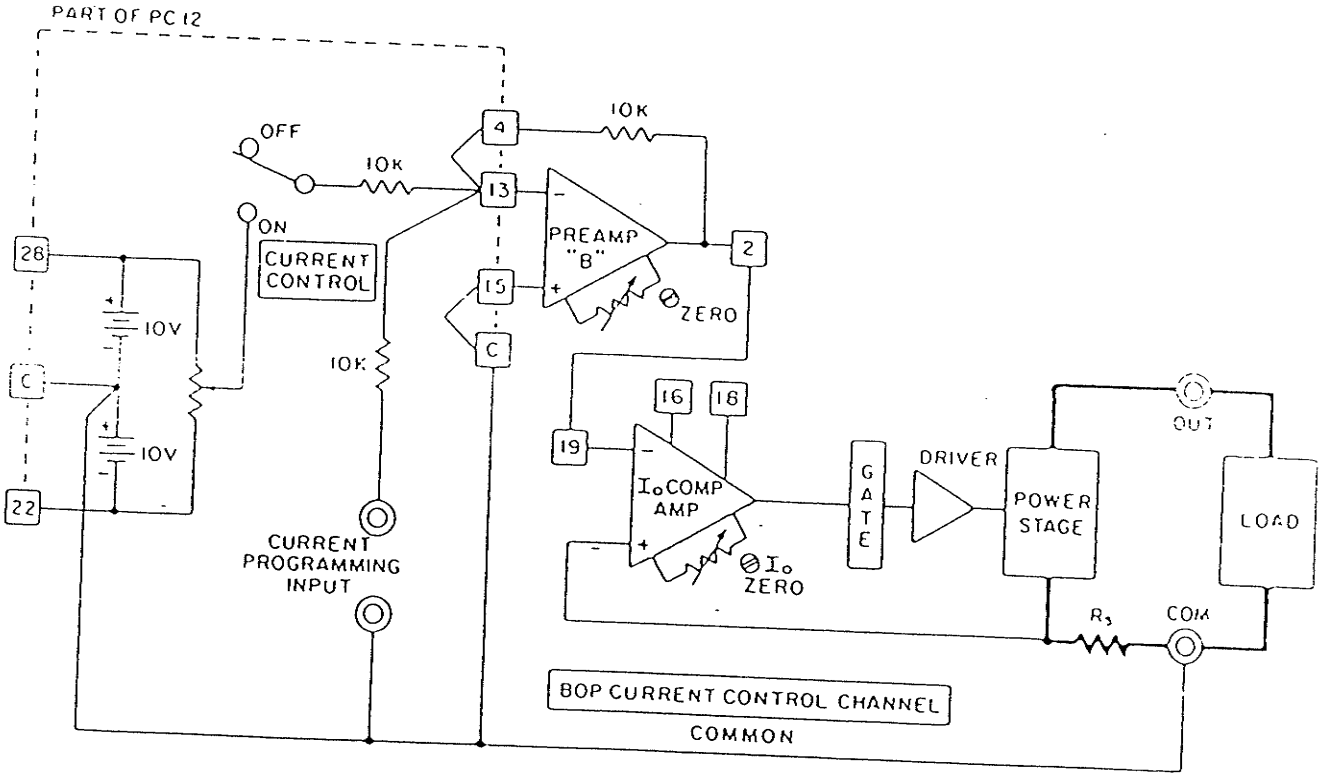

Figure 3.4 A circuit diagram of the BOP current control channel.

(voltage). The resistor is used to measure current values through the primary windings from which the magnitude of the **H** field can be calculated.

(4) Shopmade 400 ms monostable multivibrator (MOV):

The monostable multivibrator, or the one shot, has only one stable state and one unstable, or transient, state. The normal state of the circuit is the stable mode. A trigger pulse flips the circuit into its unstable state. The circuit stays in the unstable state for a fixed time, depending on the circuit time constant, 400 ms in our experiment, and then it flips back into its stable mode again. The time constant of the circuit is determined by the product of R and C_1 shown in figure 3.5. The stable and unstable states correspond to two different output voltages [SI87].

Figure 3.5 shows the circuit used in the construction of the one shot. The voltage V_1 at the inverting input of the 741 operational amplifier (op amp) can never be more positive than the diode turn-on voltage which is about 0.6 V. An op amp is a general purpose high-gain dc amplifier that has a differential input (two input leads) and a single-ended output (one output lead) [SI87]. R_1 and R_2 are chosen such that:

$$V_2 = \lambda V_{cc} = \left(\frac{R_1}{R_1 + R_2} \right) V_{cc} > 0.6V \qquad (3.4.1)$$

where: V_{cc} is the supply voltage (= 15 V)

This choice of V_2 makes the noninverting input more positive than the inverting input and the op amp output will be $+V_{cc}$. This is the stable state where $V_2 = V_c$

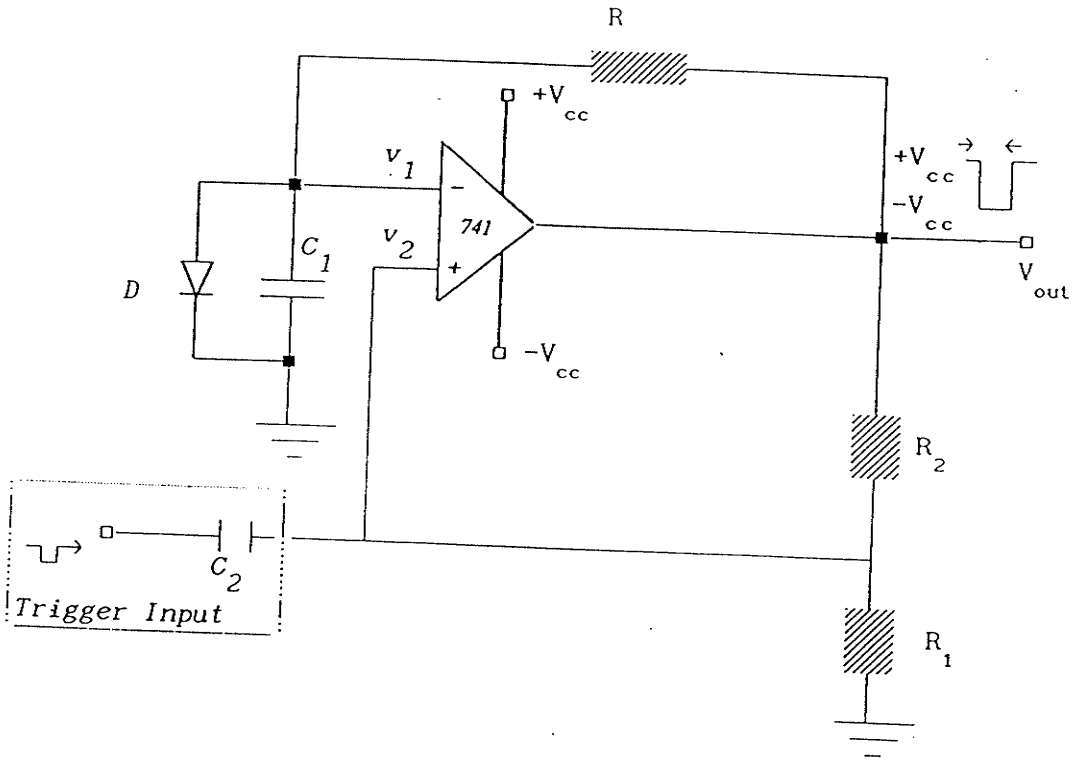

Figure 3.5 A circuit diagram for the one shot.

= 0.6 V and $V_{out} = +V_{cc}$.

If a negative trigger pulse is fed through the capacitor C_2 to the noninverting input then the op amp flips the output to the low state provided that V_2 is driven below V_1. The low state is then $V_{out} = -V_{cc}$. It can be shown that the time T over which the output remains low is given by [SI87]:

$$T = R\,C_1\,\ell n\left[\frac{1 + \frac{V_D}{V_{cc}}}{1 - \lambda}\right]$$

$$= R\,C_1\,\ell n\left[\frac{V_D - V_{cc}}{V_{cc}(1 - \lambda)}\right] \qquad (3.4.2)$$

where: V_D is the diode forward voltage.

An attenuator is used to reduce the output voltages obtained from the one shot. Unattenuated output from the one shot goes from +15 V to -15 V. The attenuator reduces the output voltage levels to ±2.0 V. This is done since V_{max} for both the triangular and ramp waves should not exceed 2.0 V.

(5) Megacom PC with GPIB interface board:

The GBIP (General-Purpose Interface Bus), or HPIB (Hewlett-Packard Interface Bus) as it is sometimes called, was developed by Hewlett-Packard to connect and control programmable instruments that they manufactured. GPIB quickly gained popularity in other applications because of its high data transfer rates. It was later accepted as an industry standard IEEE-488. The versatility of the system prompted

the name General Purpose Interface Bus. It is an asynchronous or handshaking bus intended mainly for interfacing instruments to one another and to a controller or a computer. The GPIB interface board connects three types of devices [NI84]:

(i) a " talker " instrument, such as an analog to digital converter (ADC) or counter that accepts input data, and presents a digital output to the bus.

(ii) a " listener " instrument, such as a pulse generator which accepts signals from the bus that control the output of the instrument.

(iii) a " talk/listen " instrument that can either talk or listen, such as a digital multimeter which accepts control signals from the bus and can output digital information to the bus. The role of the computer, or controller, is to manage the flow of information on the GPIB by sending commands to or receiving data from all devices.

These three types of devices are connected to the controller with 16 signal lines. The 16 lines are divided into three groups: 8 data lines, 3 handshake lines, and 5 interface management lines [NA84].

(6) Hewlett Packard 3457A Multimeter with a plug-in HP44491A Multiplexer card:

The Hewlett Packard 3457A multimeter is a versatile multimeter for both system GPIB and bench applications. It can make measurement of: DC voltage, AC voltage, AC+DC voltage, DC current, AC current, AC+DC current, 2- and 4-wire method resistances, frequency, and period. It also has reading and program storage and is

capable of making many repeated measurements quickly. In addition, the input of the HP 3457A can be expanded up to ten channels with optional plug-in multiplexer assemblies. The multimeter combines analog measuring capability with equally powerful measurement management. It has all the system features which make interfacing to a computer very easy. Features like formatting of ASCII, 16 bit binary, or 32 bit binary data and a buffer memory so that measurements may be taken with the HP 3457A while the contents of its memory is being transferred to the computer. In the experiment, the HP 3457A is used mainly for voltage measurements. Voltages are read across the 0.1 ohm resistor and from the secondary windings on the sample (see figure 3.2). These voltages are selected for the HP 3457A by a HP 44491 Armature Relay Multiplexer Card by using channels 0 and 1 on the multiplexer card [HE86].

3.5 Experimental Procedure

The experiments are performed without an electronic integrator which is frequently used in this type of magnetic measurement. The usage of the integrator would result in obtaining the usual hysteresis curves. Before the discovery of IC chips, integration was done using a ballistic galvanometer or fluxmeter which give an indication proportional to the integrated value of the volts/second induced in the sensing coil during a flux change. Present-day methods use electronic integrating circuits: e.g., the induced electromotive force (emf) can be used to generate a set of pulses whose frequency is proportional to that emf. The integral of emf over a

certain time is then simply the number of counted pulses in that time. Such a method can be made automatic, or the loop can be plotted step-by-step. However, in our experiment, the absence of the integrator produces curves of permeability versus magnetic excitation, **H**, and curves of unintegrated hysteresis loops. The integration of these curves is done later using appropriate computer programs.

When the waveform generator is externally triggered using the monostable multivibrator it generates a single ramp or a triangular wave depending on the output mode which is selected. A ramp wave was used for generating the unintegrated magnetization curves and a triangular wave was used for obtaining the unintegrated hysteresis loops. The monostable multivibrator also triggers the DVM so that it is ready to take data (see next section on data acquisition). The BOPS converts the voltage-control pulse to a current pulse which is fed to the primary windings on the torus sample. The output of the BOPS is measured as a voltage across the 0.1 Ohm resistor by channel 0 on the DVM.

If an alternating current is fed to the primary winding an alternating voltage is induced in the secondary windings. This induced voltage is then fed to channel 1 on the DVM which will read the voltage values from the secondary windings.

After the data taking is finished, the different measurements stored in the DVM's memory buffer are transferred to the PC via the GPIB interface card where the PC stores the data for further analysis. These voltage drops will be calibrated in terms of the appropriate units of **H** and μ.

3.6 Data Acquisition Algorithm

We describe here the algorithm used for linking the DVM and the GPIB interface card for reading and storing on the PC hard disk the measurements made by the DVM.

The program, DVM.BAS, is a composite of programs supplied by the GPIB manufacturer [NA84]. A copy of the program is found in Appendix A. The program is written in BASICA. There are two components to the DVM.BAS algorithm. DECL.BAS, which accounts for lines 1 to 99, and a user written code accounting for lines 110 to the end of the program. The DECL.BAS is a GPIB declaration file that contains codes that must be placed at the beginning of an application program to allow it to properly access the handler (i.e. the GPIB board). The DECL.BAS establishes a link between the BASIC program and the DVM. The user written code is specific to one's purposes. It contains the programming steps that must be used to program the DVM [NA84].

The DVM.BAS goes through a number of steps which may be summarized as follows [HE86]:

(1) resets the DVM and initializes the GPIB card. This takes approximately two seconds.

(2) selects the rear terminal which is the input source for making measurements. This step makes the connection to the plug-in multiplexer card where readings are taken on channels 0 and 1 on the multiplexer.

(3) sets the trigger event to hold (TRIG HOLD) to suspend any measurements. This is done to make sure that no measurements are taking place at that moment.

(4) sets scan advance (SADV) to auto which causes the event to advance to next channel in list.

(5) uses the autozero (AZERO) command with the control parameter OFF which makes one zero measurement and subtracts this from all subsequent measurements.

(6) the LOCK ON command is used to disable the DVM's keyboard (i.e. pressing keys has no affect). This causes the reading rate of the DVM to increase since it no longer scans the keyboard between measurements.

(7) memory format (MFORMAT) command clears the reading memory and designates the storage format for new readings. It is set at single-real (SREAL) which means 32 bits (4 bytes per reading).

(8) the number of power line cycles (NPLC) command designates the minimum integration time for the ADC converter. The integration time is the time, measured in power line cycles (PLCs), during which the DVM samples the input signal.

(9) the TIMER command defines the time interval for the TIMER sample event in the NRDGS (number of readings) command. The time interval is inserted between readings. The time interval selected is 30 msec to achieve high accuracy of readings and to increase reading rate. The number of readings per trigger is chosen to be 512 (i.e. 256 readings per channel).

(10) the trigger external (TRIG EXT) command allows the measurements to be made through an external input (i.e. through the monostable multivibrator).

(11) then the file DVM.DAT is opened for data to be sent to it.

(12) then a subroutine to split the one column sequential file DVM.DAT into a two column sequential files, one for each channel, for future analysis.

Chapter 4

Analysis and Discussion

4.1 Introduction and Review of Theory

As far as its magnetic properties are concerned, matter is equivalent to an assemblage of magnetic dipoles. In order to put this into quantitative terms, the magnetization **M** is defined as the magnetic dipole moment per unit volume. Then the dipole moment **dm** in a small volume $d\tau$ at **r** will be [WA86]

$$\mathbf{dm} = \mathbf{M}(\mathbf{r})\, d\tau \qquad (4.1.1)$$

Thus the total dipole moment of a volume V of material is

$$\mathbf{m}_{total} = \int_V \mathbf{M}(\mathbf{r})\, d\tau \qquad (4.1.2)$$

where: **M** will be in units of ampere/meter.

M can be regarded as a smoothly varying function of position provided that $d\tau$ is large enough to include enough material. It is found that as far as the effects outside the material are concerned, the material can be replaced by a distribution of volume and surface current densities which are related to the magnetization **M** by

$$\mathbf{J}_m = \nabla \times \mathbf{M} \qquad (4.1.3)$$

and

$$\mathbf{K}_m = \mathbf{M} \times \mathbf{n} \qquad (4.1.4)$$

where: $\mathbf{J}_m$ is the volume current density.

$\mathbf{K}_m$ is the surface current density.

n is the outward normal to the surface of the material.

The subscript m on $\mathbf{J}_m$ and $\mathbf{K}_m$ refers to the fact that they are usually called magnetization current densities. Sometimes they are called Amperian current densities [BO51].

From the integral form of Ampere's law we have

$$\oint_C \mathbf{B} \cdot d\mathbf{S} = \mu_o I_{enc} \qquad (4.1.5)$$

where the integral is taken about an arbitrary closed path C and I_{enc} is the total current passing through the area S enclosed by the curve C.

But since $$\left(dq/dt \right)_{\text{through S}} = I = \int_S \mathbf{J} \cdot da \qquad (4.1.6)$$

where: da is an element of area.

J is the total current density.

S is a surface bounded by the curve C.

Then substituting (4.1.6) in (4.1.5) and using Stokes' theorem, we have

$$\oint_C \mathbf{B} \cdot d\mathbf{S} = \mu_o \int_S \mathbf{J} \cdot da = \int_S (\nabla \times \mathbf{B}) \cdot da \qquad (4.1.7)$$

By equating the integrands, we have

$$\nabla \times \mathbf{B} = \mu_o \mathbf{J} \qquad (4.1.8)$$

This relation shows, in contrast to the electrostatic field, that the magnetic induction is not a conservative field since the curl of **B** is not always zero.

It is convenient to divide currents which arise from moving charges into two broad classes of magnetization currents and free currents. These two types are described by the respective densities $\mathbf{J}_m$ and $\mathbf{J}_f$. The magnetization currents are associated with constituents of matter and we do not have any real control over

them. On the other hand, $\mathbf{J}_f$ is a quantity upon which we can have some control, for example, varying the current which is applied to a certain circuit [WA86]. Therefore, the total current density can be written as

$$\mathbf{J}_{total} = \mathbf{J} = \mathbf{J}_f + \mathbf{J}_m \qquad (4.1.9)$$

Then equation (4.1.8) becomes

$$\nabla \times \mathbf{B} = \mu_o \mathbf{J} = \mu_o (\mathbf{J}_f + \mathbf{J}_m)$$

$$= \mu_o (\mathbf{J}_f + \nabla \times \mathbf{M}) \qquad (4.1.10)$$

where we have used $\mathbf{J}_m = \nabla \times \mathbf{M}$

$$\Rightarrow \quad \nabla \times \left(\mathbf{B}/\mu_o - \mathbf{M} \right) = \mathbf{J}_f \qquad (4.1.11)$$

From equation (4.1.11), the magnetic field $\mathbf{H}$ is defined as

$$\mathbf{H} = \mathbf{B}/\mu_o - \mathbf{M} \qquad (4.1.12)$$

thus equation (4.1.11) becomes

$$\nabla \times \mathbf{H} = \mathbf{J}_f \qquad (4.1.13)$$

The most important characteristic of $\mathbf{H}$ is that its curl depends only on the free current density. $\mathbf{H}$ has the dimensions of $\mathbf{M}$, namely ampere/meter. Equation (4.1.13) can be thought of as expressing Ampere's law of force between current elements plus the magnetic effect of matter [KR53]. The integral form of Ampere's law for $\mathbf{H}$ can be found by using Stokes' theorem and equation (4.1.6) to be

$$\oint \mathbf{H} \cdot d\mathbf{S} = \int_S \left(\nabla \times \mathbf{M} \right) \cdot da$$

$$\oint \mathbf{H} \cdot d\mathbf{S} = \int_S \mathbf{J}_f \cdot da = I_{f,enc} \qquad (4.1.14)$$

It is convenient to consider **M** to be a measurable function of **H**. That is, **M** = **M** (**H**). Generally speaking, the magnetization **M** is taken to be proportional to and parallel to the magnetic field **H** so that we can write

$$\mathbf{M} = \chi_m \mathbf{H} \qquad (4.1.15)$$

where the constant of proportionality χ_m is called the magnetic susceptibility and it is a constant characteristic of the material. χ_m is negative for diamagnetic substances and positive for the other materials [KR53].

Combining equations (4.1.12) and (4.1.15), we obtain

$$\begin{aligned} \mathbf{B} &= \mu_o (\mathbf{H} + \mathbf{M}) \\ &= \mu_o (\mathbf{H} + \chi_m \mathbf{H}) \\ &= \mu_o (1 + \chi_m) \mathbf{H} \\ &= \mu_o \kappa \mathbf{H} = \mu \mathbf{H} \qquad (4.1.16) \end{aligned}$$

where: $\kappa = 1 + \chi_m = \mu/\mu_o$ is called the relative permeability

and $\mu = \mu_o \kappa$ is called the normal permeability or simply the permeability.

One distinguishes between Dia-, Para-, Ferro-, Ferri-, and Antiferromagnetic materials by the value of κ where:

(i) $\kappa < 1$ for diamagnetic materials

(ii) $\kappa > 1$ for paramagnetic materials

(iii) $\kappa >> 1$ for ferromagnetic materials

(iv) $\kappa >> 1$ for ferrimagnetic materials

(v) $\kappa > 1$ for antiferromagnetic materials

In an antiferromagnetic material adjacent atoms have their dipoles oppositely

aligned. Antiferromagnetic materials thus have zero net magnetization per unit volume, and their relative permeabilities are slightly greater than unity. They are characterized by hysteresis and the Curie point. However, paramagnetic materials do not show hysteresis [BO51] even though they have relative permeability values close to the antiferromagnetic materials. The difference between ferromagnetic and ferrimagnetic materials is that in ferrimagnetic materials the dipoles, besides being of different strenghts, are oppositely aligned (see figure 2.1). However their relative permeability is sill much greater than unity.

The relation $\mathbf{B}=\mu\mathbf{H}$, or $\mathbf{H}=\mathbf{B}/\mu$, is an example of a constitutive equation and is not a fundamental equation of electromagnetism, in contrast to equation (4.1.12) which is. For ferromagnetic materials, such a relation is never more than a crude approximation which can be used over a limited range. Nevertheless, it has very important usefulness in practical applications even though it has no value in basic physical theory [JK53]. In ferromagnetism, permeability is not a quantity to be used in theoretical formulae but a quantity to be calculated by means of them.

4.2 Discussion

As eluded to previously in the experimental section, what one wants to do is to apply an external magnetic field **H**, produced by external free currents, and then measure **B** as a function of **H**. This has led to the choice of a ring sample in order to measure **B** and **H** conveniently and unambiguously. It can be assumed to a good approximation that **H** is confined to the interior of the sample and its magnitude can

be calculated from the free currents I_f in the N_1 turns of the magnetizing coil.

From the integral form of Ampere's law for **H** and for a ring sample of radius r, we have

$$\oint_C \mathbf{H} \cdot d\mathbf{S} = 2\pi r\, H_r(r) = I_{f,enc} = N_1\, I$$

$$\Rightarrow \qquad H_r(r) = N_1 I/2\pi r \qquad (4.2.1)$$

where: $d\mathbf{S} = r\, d\varphi\, \hat{\varphi}$ and $\hat{\varphi}$ is a unit vector as shown on figure 4.1.

$I_{f,enc}$ is the net free current passing through the surface S enclosed by the arbitrary path of integration C. See figure 4.1.

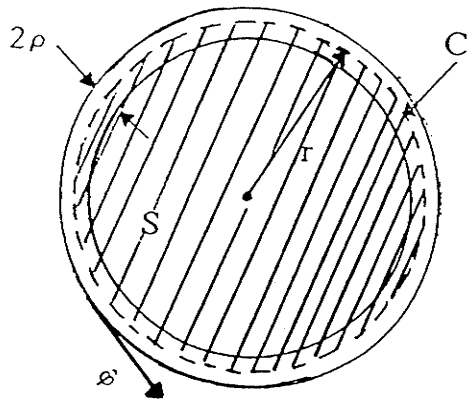

Figure 4.1 A ring sample showing the surface S enclosed by an arbitrary path of integration C.

In the case where $r >> \rho$, where ρ is the radius of the circular cross section of ring, $H_r(r)$ will be equal to

$$H = N_1 I/2\pi r = N_1 V_1/2\pi R_c r \qquad (4.2.2)$$

where: R_c is the resistance of the energizing coil at which the voltage drop V_1 is taken across.

The magnetizing field **H** inside the toroid has, on account of symmetry, the same

direction as the circles forming the ring and is approximately constant in magnitude. Then both **M** and **B** will also be approximately constant across the cross section of area $A = \pi\rho^2$, and the flux through A will be

$$\phi = A\,B \qquad (4.2.3)$$

where: B is the magnitude of **B**.

If the controllable external quantity I is changed by a small amount, ΔI in a time Δt, then the magnetic field will change by

$$\Delta H/\Delta t = N_1/2\pi r\ (\Delta I/\Delta t) \qquad (4.2.4)$$

and can be calculated from the known properties of the toroid.

Correspondingly, there will be changes in the induction, ΔB, and the flux, $\Delta\phi = A\,\Delta B$. The change in ΔB can be measured by finding the total charge ΔQ_c that passes through the sensing coil as a result of the induced current, $i_{c,ind}$, in the pickup coil.

Since R_c' is the resistance of the pickup coil circuit, then by using $I=\Delta Q/\Delta t$ and Faraday's law $\xi_{ind} = -\,d\phi/dt$, where ξ_{ind} is the induced emf, the magnitude of ΔQ_c can be found to be

$$\Delta Q_c = N_2 \int i_{c,ind}\, dt \qquad (4.2.5)$$

where: N_2 is the number of turns on the secondary windings.

$$\Rightarrow \qquad \Delta Q_c = N_2 \int |\xi_{ind}|\, dt \,/\, R_c'$$

$$= N_2/R_c' \int d\phi/dt \cdot dt$$

and therefore $$\Delta Q_c = N_2/R_c' \cdot \Delta\phi \qquad (4.2.6)$$

$$\Rightarrow \quad \Delta\phi = R_c'/N_2 \cdot \Delta Q_c \qquad (4.2.7)$$

and thus

$$\Delta B = R_c'/N_2 \cdot \Delta Q_c/A \qquad (4.2.8)$$

where we have used $\Delta\phi = A\ \Delta B$

Since $A = \pi \rho^2$ then equation (4.2.8) becomes

$$\Delta B = R_c'/N_2 \cdot \Delta Q_c/\pi \rho^2 \qquad (4.2.9)$$

Thus

$$\Delta B/\Delta t = R_c'/N_2 \,.\, I/\pi \rho^2$$

$$\Rightarrow \quad \Delta B/\Delta t = V_2/N_2 \pi \rho^2 \qquad (4.2.10)$$

where: V_2 is the induced voltage in the secondary windings, $V_2 = R_c' I$.

Therefore, from equations (4.2.4) & (4.2.10), we have

$$\mu = (\Delta B/\Delta t) / (\Delta H/\Delta t) = (V_2/N_2\pi\rho^2) / (N_1/2\pi r.\Delta I/\Delta t)$$

$$\Rightarrow \quad \mu = (2rV_2) / (N_1 N_2 \rho^2.\Delta I/\Delta t) \qquad (4.2.11)$$

$\Delta I/\Delta t$ will be different for both the unintegrated magnetization curves and the unintegrated hysteresis loops. Since a triangular pulse is used to generate the hysteresis loops then $\Delta I/\Delta t$ can be found using figure 4.2, where it is seen that

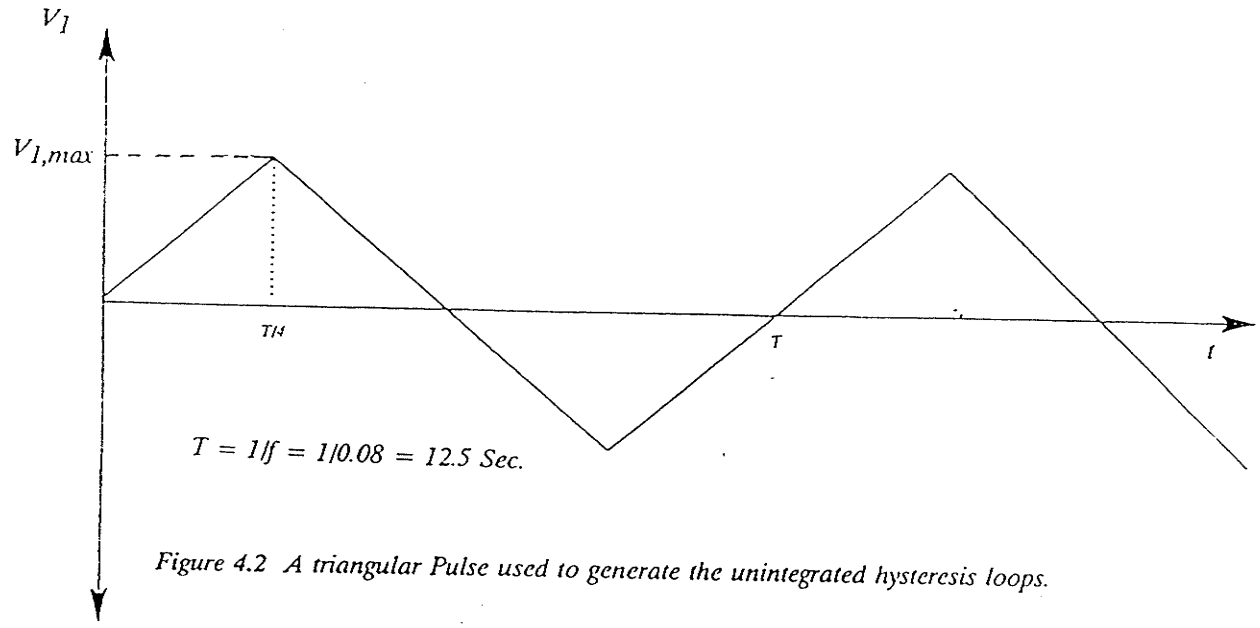

Figure 4.2 A triangular Pulse used to generate the unintegrated hysteresis loops.

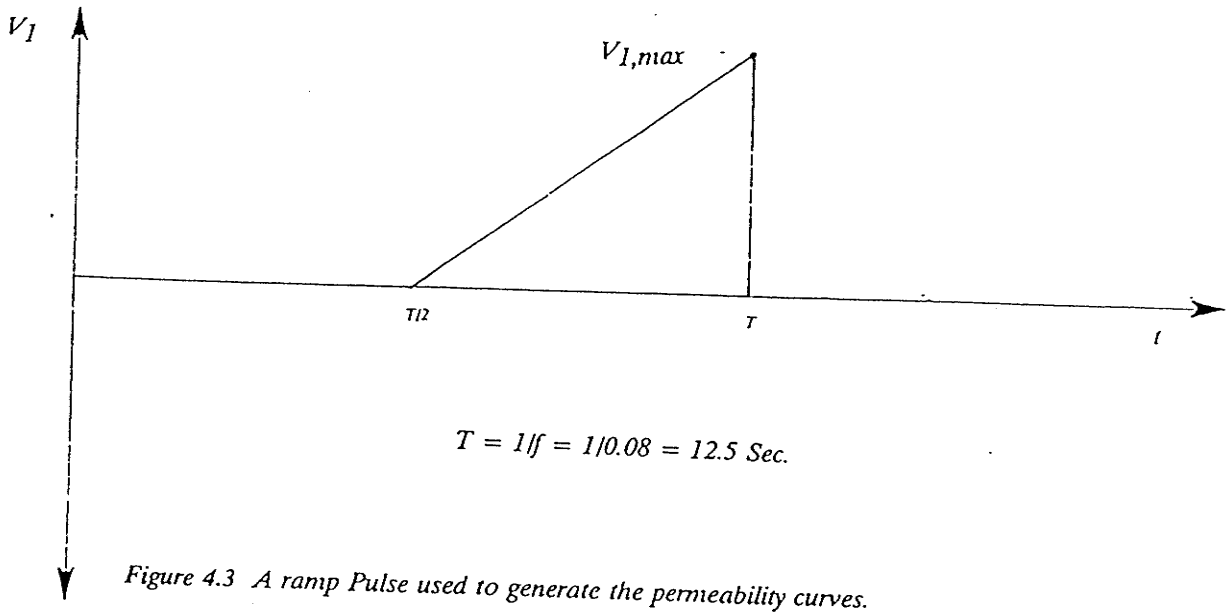

Figure 4.3 A ramp Pulse used to generate the permeability curves.

$$(\Delta V_1/\Delta t) = (V_{1,max})/(T/4) = 4V_{1,max}/T \qquad (4.2.12)$$

where: T is the period of the pulse, T=1/f=12.5 s.

Therefore, $$(\Delta I/\Delta t)_{triang.\ pulse} = 4V_{1,max}/R_cT \qquad (4.2.13)$$

On the other hand, a ramp pulse is used to generate the unintegrated magnetization curves and from figure 4.3, we have

$$(\Delta V_1/\Delta t) = (V_{1,max})/(T/2) = 2V_{1,max}/T \qquad (4.2.14)$$

and $$(\Delta I/\Delta t)_{ramp\ pulse} = 2V_{1,max}/R_cT \qquad (4.2.15)$$

4.3 Data Smoothing

Prior to data analysis, the raw data must be smoothed. It has been observed that there is a consistent fluctuation in the data. This fluctuation was particularly large for the one shot curves. The origin of this effect is not well understood. It is possible that the Barkhausen effect may play a role in this. See figure 2.5. The effect of the Barkhausen discontinuity has been the subject of investigation by Bozorth and Dillinger [BO30], by Preisach [PR29], and by Tebble et al [TE50]. Also it is possible that the 30 ms time interval between readings when the measurement is being taken by the DVM is the cause of the fluctuation. This time interval represents the sampling event for measurements (See section 3.6 on Data Acquisition). The fluctuations in the one shot case are larger than those in the hysteresis loop. This is probably caused by the higher resolution in the one shot data. The GPIB card is reading the same number of data points for both curves but using a smaller region

in the one shot case. The one shot data is only in the first quadrant, whereas for the hysteresis loop measurements are being made in all four quadrants. It is evident from the data that the largest fluctuations occur well beyond the place where d**B**/d**H** is maximum. The same conclusion has been reached by Bozorth [BORM51, p.528].

To do the fittings for the curves, use has been made of the OPDATA (OPerates on DATA) package on the VAX. We used the FIT command which allows the user to fit the data to any expression one specifies. Figures 4.4 and 4.5 show the unfitted and fitted data for both the one shot and hysteresis loop. For the one shot data, emphasis has been made on the middle range of the data where we tried to "fit" a curve to the data as best we can. Less emphasis has been given to the end points because the end points are often the least reliable because of experimental factors in the extremes of ranges [PA61].

The smoothing of data was done a portion of the data at a time to ensure that the function $y=f(x)$, which is being fitted, be a slowly varying function over each small portion of the curve being treated. A third-order power series was used to each portion of the curve to minimize the least square residual between the expression being fitted and the y-axis data. The fit accuracy was on the average about $\pm 0.3\%$ assuming the functional form used for the fit is appropriate.

4.4 Analysis

All of the calibrations are done through a computer program on the VAX. A copy of the program is found in appendix B. The integration is done by the program

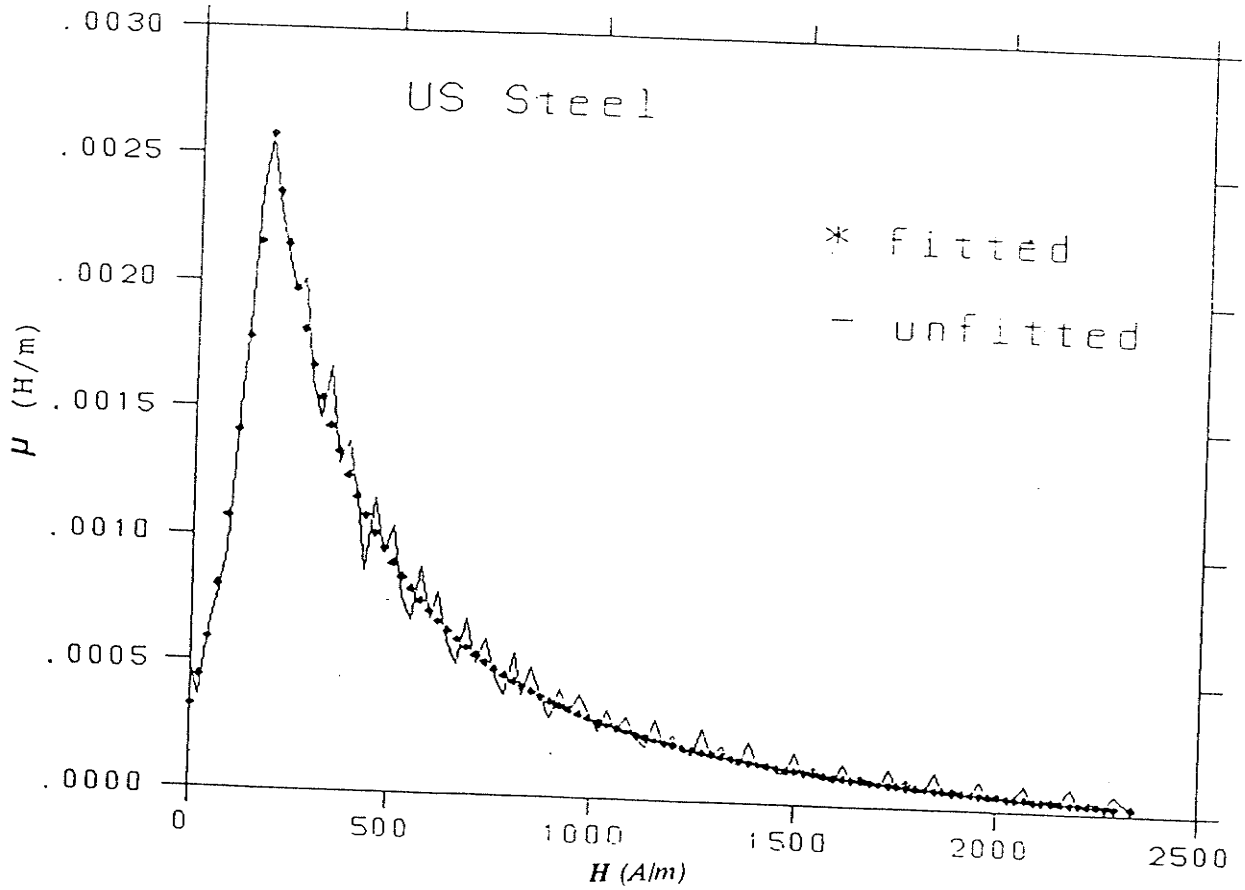

Figure 4.4 Unfitted and fitted data for the one shot curve for the US sample.

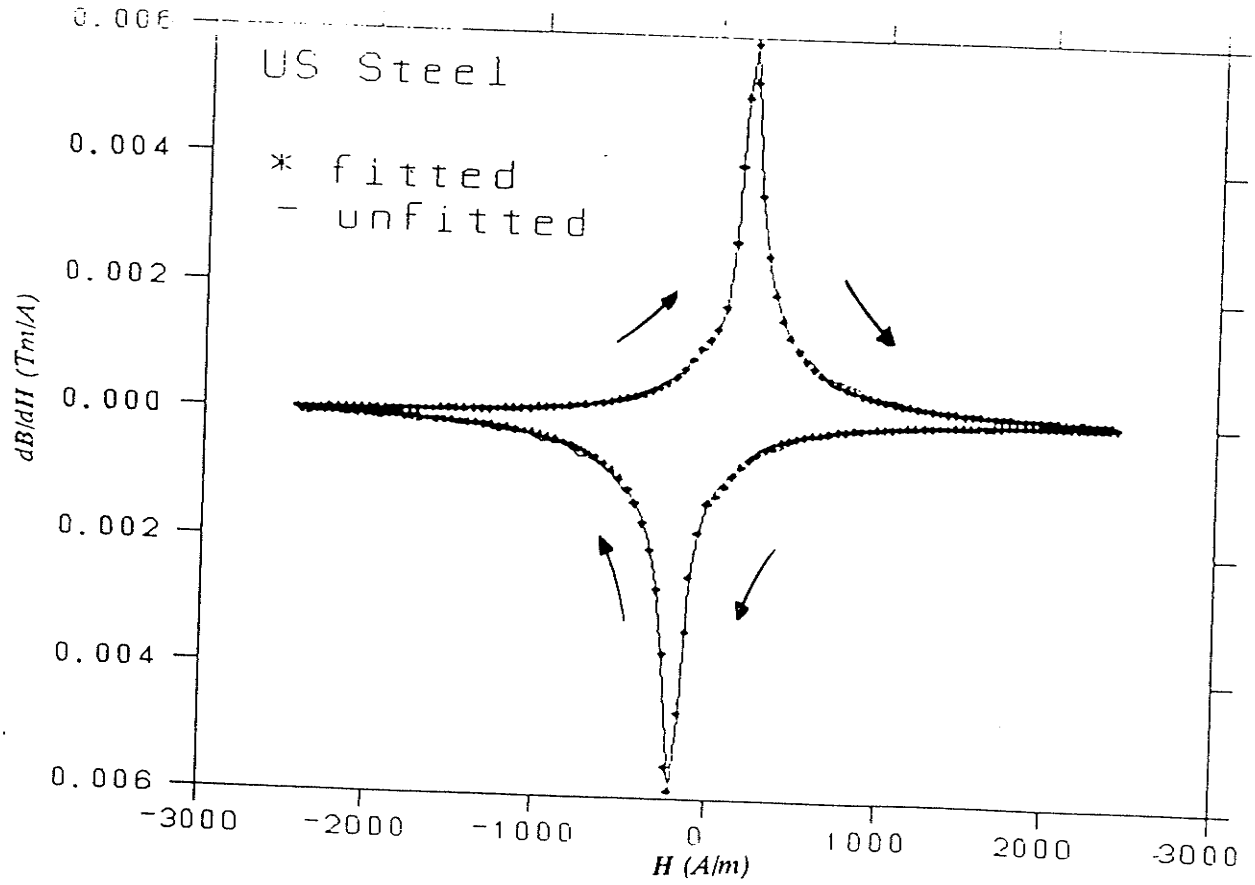

Figure 4.5 Unfitted and fitted data for the hysteresis loop for the US sample.

to produce the magnetization and hysteresis curves. However, we present here a sample calculation for purposes of illustration. To do a sample calculation of the results, we take the US sample as an example. We have from equation (4.2.2)

$$H = N_1 I/2\pi r = N_1 V_{1,i}/2\pi r R_c \qquad (4.4.1)$$

where: the $V_{1,i}$ are the different voltage drops across the resistor R_c read by the DVM via the multiplexer card on channel 0. See figure 3.2. The voltage drops comprise, in total, 256 points.

From table 2, we have:

$N_1 = 264 \pm 2$ turns

$N_2 = 513 \pm 2$ turns

$r = 23.59 \pm 0.01$ mm

$\rho = 1.43 \pm 0.01$ mm

$R_c = 0.112 \pm 0.001$ Ohm

The magnetizing current was set to alternate between +1.4 and -1.4 Amperes. The exact value of the current will be determined by V_{max} for the pulse which can be obtained from the DVM readings. The current was set at this value so that the field strength, **H**, would be sufficient to magnetize the sample to saturation. To make sure that saturation was reached many loops were measured for the same sample. It was found that one comes again and again to the same curve. This indicates that the magnetic field, **H**, was sufficient to drive the sample to saturation. Turning up the current on the BOPS more than this value may cause the samples to warm up and this introduces an additional unwanted new component into our experiment, namely

heat. However, data for the Dutch sample were obtained at a magnetizing current set to alternate between +1.8 and -1.8 Amperes since the material needed more current to be driven into saturation.

For purposes of illustration, we first take the unintegrated magnetization curve and do the calculation for the maximum voltage, i.e. $V_{1,max}$.

For the US sample, we have:

$$V_{1,max} = 0.149 \pm 0.001 \text{ V}$$

The $V_{1,i}$ voltages are read by the DVM and their accuracy will be determined mostly by the error in the resistor R_c since these points are read across the resistor.

Therefore,

$$H_{max} = (N_1 V_{1.max})/ (2\pi r R_c)$$
$$= \left((264)(0.149) / 2\pi(23.59\text{x}10^{-3})(0.112) \right) \text{ A/m}$$
$$= (2369.54) \text{ A/m}$$

and the error in H_{max} is given by

$$\Delta H_{max}/H_{max} = (\Delta N_1/N_1 + \Delta r/r + \Delta R_c/R_c + \Delta V_{1,max}/V_{1,max})$$

therefore,

$$\Delta H_{max} = (2/264 + 0.01/23.59 + 0.001/0.112 + 0.001/0.149) 2369.54 \text{ A/m}$$
$$= 56.02 \text{ A/m}$$

and thus $H_{max} = (23.7 \pm 0.6)\text{x}10^2$ A/m

To determine $\Delta I/\Delta t$ for the magnetization curve, we have

$$I_{max} = V_{1,max}/R_c = 0.149/0.112 = 1.330 \text{ A}$$

and we have

$$\Delta I_{max} = (\Delta V_{1,max}/V_{1,max} + \Delta R_c/R_c) I_{max}$$

$$= (0.001/0.149 + 0.001/0.112) 1.330 \text{ A}$$

$$= 0.021 \text{ A}$$

$$\Rightarrow \qquad I_{max} = (1.33 \pm 0.02) \text{ A}$$

and we have

$$(\Delta I/\Delta t)_{ramp\ pulse} = 1.33/6.250 = (21.0 \pm 0.3) \times 10^{-2} \text{ A/s}$$

where we have used $T/2 = (6.250 \pm 0.001)$ s for the ramp pulse. See figure 4.3.

The fractional errors are added linearly because the fractional errors (e.g. $\Delta N_1/N_1$) for all the quantities are much less than unity (i.e $<< 1$). And therefore we kept only magnitudes to first order. The errors are not correlated since these errors are random. However, for example, there is a correlation between the variations in the value of $V_{1,max}$ and the value of H_{max}.

Now to do the calculations for the hysteresis loop (i.e. unintegrated without the magnetization curve), we have to note that it has been observed that the maximum voltage obtained during the unintegrated magnetization curve run and that obtained during the unintegrated hysteresis loop run differ by about 1%. For example for the US sample it is found that:

$V_{1,max} = 0.149 \pm 0.001$ V for the unintegrated magnetization curve.

and $V_{1,max} = 0.151 \pm 0.001$ V for the unintegrated hysteresis loop.

This difference is probably due to the way these two curves were generated,

where a ramp pulse was used for the magnetization curve and a triangular pulse for the hysteresis loop. In the case of the ramp pulse the current goes gradually up and then drops suddenly to zero, whereas for the triangular pulse the current gradually drops to zero. See figures 4.2 and 4.3. This is, of course, due to the electronics used.

Therefore to determine $\Delta I/\Delta t$ for hysteresis loop we have:

$$I_{max} = V_{1,max}/R_c = 0.151/0.112 = 1.348 \text{ A}$$

$$\Rightarrow \qquad I_{max} = (1.35 \pm 0.02) \text{ A}$$

then we have

$$(\Delta I/\Delta t)_{\text{triangular pulse}} = 1.348/3.125 = 0.432 \text{ A/s}$$

$$\Rightarrow \qquad (\Delta I/\Delta t)_{\text{triangular pulse}} = (43.2 \pm 0.6)\text{x}10^{-2} \text{ A/s}$$

where we have used T/4 = (3.125 ± 0.001) s for the triangular pulse. See figure 4.2.

Therefore, the maximum permeability for both the magnetization curve and the hysteresis loop can now be calculated using the following equation:

$$\mu_{max} = \left(2r/N_1N_2\rho^2 (\Delta I/\Delta t) \right) V_{2,max} \qquad (4.3.2)$$

where: the $V_{2,max}$ is the maximum voltage drops read by the DVM across the sensing coils.

Therefore,

$$(\mu)_{\text{max,perm. curve}} = \left(2(23.59\text{x}10^{-3})(3.2\text{x}10^{-3})/(264)(513)(1.43\text{x}10^{-3})^2(0.21) \right) \text{H/m}$$

$$= (25.9 \pm 0.2)\text{x}10^{-4} \text{ H/m}$$

and $$(\mu)_{\text{max,hyst. loop}} = \left(2(23.59\text{x}10^{-3})(1.48\text{x}10^{-2})/(264)(513)(1.43\text{x}10^{-3})^2(0.43) \right) \text{H/m}$$

$$= (58.6 \pm 0.3)\text{x}10^{-4}\ \text{H/m}$$

where we have used for $(\mu)_{\text{max.hyst. loop}}$, $(\Delta I/\Delta t)_{\text{triang. pulse}}$ and $V_{2,\text{max; hyst.}}$ instead of that for the ramp pulse in equation (4.3.2).

When the calibration in terms of the appropriate units of **H** and μ is performed, we obtain figures 4.6 and 4.7. Figure 4.6 shows the μ-**H** curve and figure 4.7 shows **dB/dH** versus **H** curve. It is seen that for figure 4.6, as stated in chapter 2, the initial permeability is non-zero. Also for figure 4.7 many loops were measured for the same sample to insure that one obtains the same curve each time. This indicates that saturation was reached.

4.5 Description of the Integration Algorithm for the Curves

Prior to the description of the algorithm, the relation between the unintegrated and integrated hysteresis loops is illustrated in figures 4.8 and 4.9. In order to be able to do the integration the data for unintegrated hysteresis loop has to be sorted in the manner shown in figure 4.8.

The algorithm is used to do the calibration in terms of the appropriate units of **H** and μ, to sort the data in the correct order and to perform the integration for the curves. The algorithm is shown in appendix B. For each sample two data sets, the one shot and the hysteresis loop, are normalized, combined and integrated. The algorithm proceeds as follows:

(1) the appropriate physical constants for the normalization (i.e. calibration) of the raw data of the one shot and hysteresis loop are read. These constants are

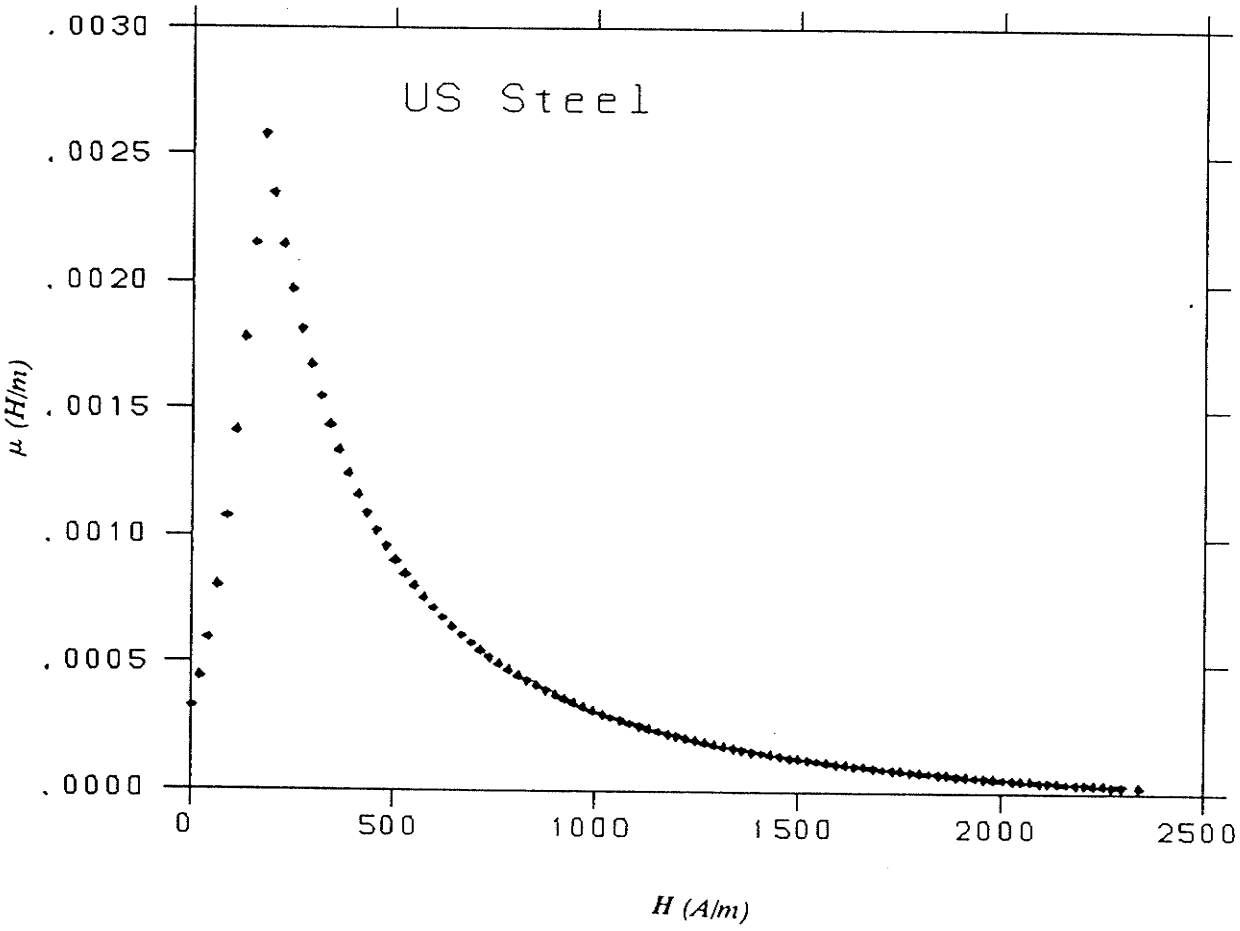

Figure 4.6 *μ-$\dot{H}$ curve for the US sample.*

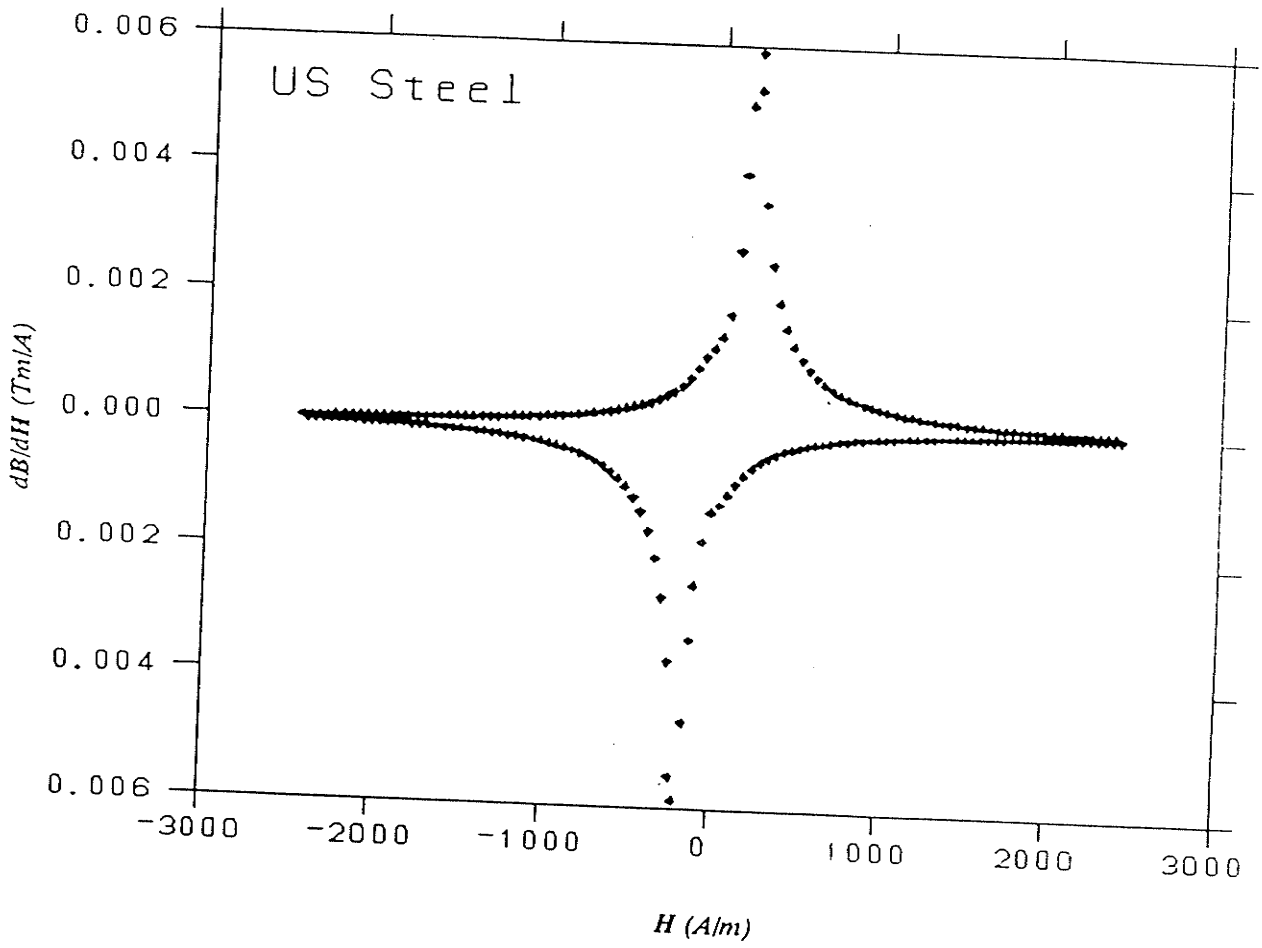

Figure 4.7 dB/dH versus H for the US sample.

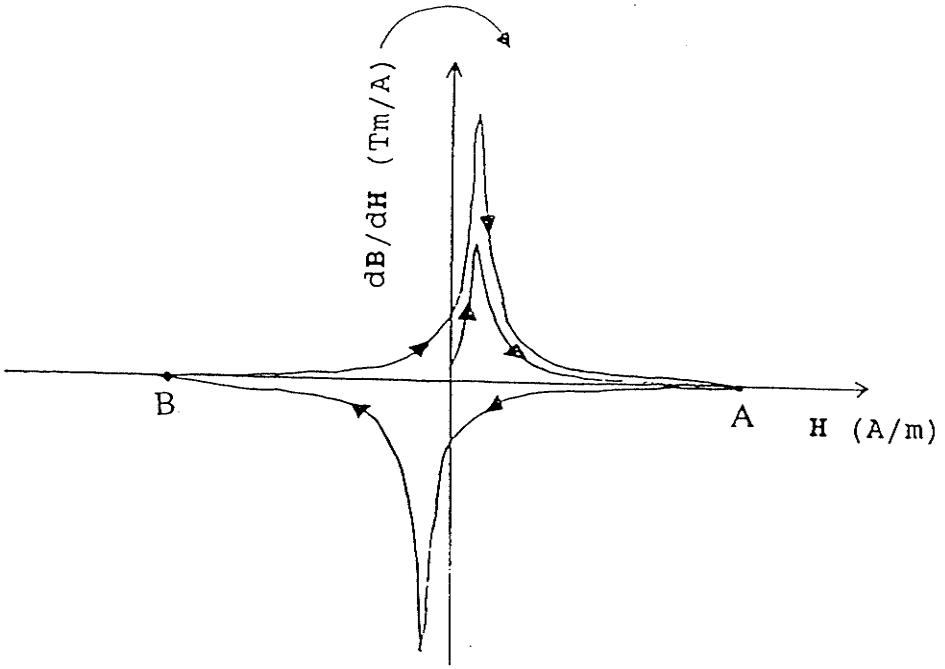

Figure 4.8 Relation between the unintegrated magnetization curve and hysteresis loop, obtained without the aid of an integrator.

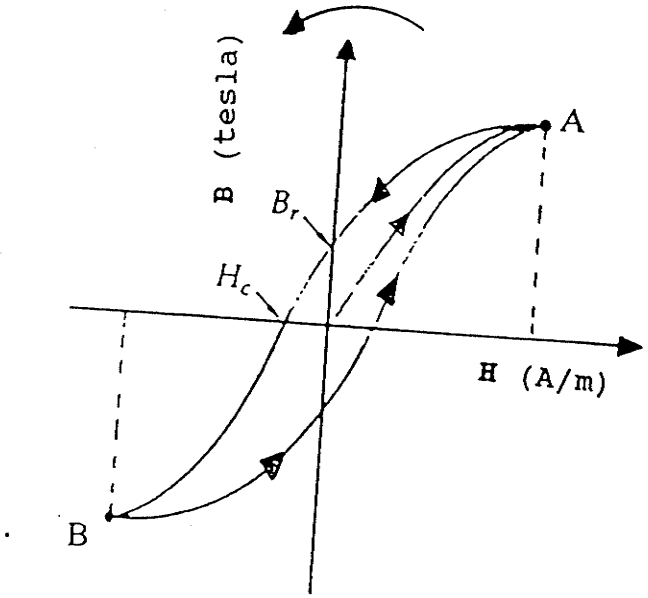

Figure 4.9 Relation between the magnetization curve and the hysteresis loop.

a) the value of the resistor R_c.

b) the value of π.

c) the radius of the steel ring, r.

d) the radius of the circular cross section, ρ.

e) the maximum voltage during the hysteresis loop run, $V_{1,max,\ hyst}$.

f) the maximum voltage during the one shot run, $V_{1,max,\ perm}$.

g) the time constant for the hysteresis run.

h) the time constant for the one shot run.

i) the number of turns of the excitation coil, N_1.

j) the number of turns of the sensing coil, N_2.

(2) All of the one shot data is read and normalized then the end point (i.e. H_{max}) of the one shot is determined.

(3) the hysteresis loop data is read and the end point is determined. This point is called HEND. Then the first point where both the x and y axes are positive is found, this point is called HPOS.

(4) the point at which the y axis goes from positive to negative is determined. Note this point also corresponds to the maximum value in x (i.e **H**) axis. This point is called HMAX.

(5) the raw data for the hysteresis loop is corrected by multiplication by the appropriate constants to get the proper units of **H** and μ as given by the formulae.

(6) the data for the hysteresis loop is sorted because it is multi-valued over the

range of **H**. The sorting is done according to the relation between the unintegrated and integrated hysteresis loops as shown in figures 4.8 and 4.9.

(7) the data for both the one shot and hysteresis loop are combined into one file and the total number of points used is determined.

(8) once the data is sorted and written in the proper order the integration is performed using the trapezoidal rule. The trapezoidal rule is chosen because it achieves an accurate answer when a large number of evaluations is used [MA87]. This is the case since more than 300 points (when the unintegrated magnetization and hysteresis curves are combined) are utilized in the integration.

Note that this algorithm will combine the data such that if there is an overlap in the raw data of the hysteresis loop, this overlap will *not* be used in the integration.

When the integration is performed we obtain the figure 4.10 for the **B-H** curve. Appendix D lists the **B-H** data for the US sample. The μ-**H** curves, d**B**/d**H**-**H** loops and **B-H** curves for the rest of the samples are shown in figures 4.11-4.25.

To determine the accuracy for the integration algorithm, it is necessary to examine the second derivative of the function y=f(x) which is being integrated. This is done because the error term for the trapezoidal rule is given by [MA87]

$$E(f,h) = -(b-a)h^2/12 \bullet f^2(c)$$

where: [a,b] is the interval over which the integration is carried out.

h is the step size.

c is some value in [a,b] such that the error term has the above value.

$f^2(c)$ is the second derivative of f(x) at c.

The investigation of the error term revealed an average accuracy of the integration algorithm to be $\pm 0.1\%$.

Table 3 contains the experimental values for B_{sat}, H_{sat}, B_r, and H_c for all the samples. Table 4 lists the different experimental values of the maximum relative permeability, κ_{max}, and the maximum permeability, μ_{max}, for the samples; where $\kappa_{max} = \mu_{max} / \mu_o$.

4.6 Heat Treatment

The main purposes of heat treatment are to relieve the internal strains introduced during fabrication and to purify the steels from their carbon content [YE24]. However, the steels used in this study were *not* heat treated. The reason is that the steels that actually go into the construction of the ZEUS detector are worked steels, not treated ones. In order to investigate the real properties of the steels, they should be tested as they are without any annealing because some properties of the magnetic materials are structure-sensitive (μ is among them) and can be affected by heat treatment. However, some properties, such as saturation magnetization, are not affected by fabrication or heat treatment [BO51]. Heat treatments may also affect crystal orientation and/or atomic ordering [FO29].

4.7 Discussion of Results

We may summarize all of the concepts discussed in previous sections. We began

from a stage where the sample was demagnetized (i.e. **H**=0 and **B**=0). Then we measured the permeability as a function of the excitation field, **H**. d**B**/d**H** as a function of the excitation field was also calculated for the sample. From these two measurements we were able to obtain the hysteresis loop. From the magnetization curves and the hysteresis loops, we were able to draw some information about the magnetic properties of the sample.

It is evident from the experimental values in table 3 that the steels have different magnetic properties, which indicate that the magnetic properties of the substances are sensitive functions of the structure and constitution of the materials.

From table 3, we see that the saturation magnetic fields, H_{sat}, are comparable in values for all the steels except for the case of the Dutch steel where it is seen that the value of H_{sat} is larger. This indicates that the Dutch steel requires a larger external magnetic field to reach its saturation value.

On the other hand, the values of the saturation magnetic flux, B_{sat}, are larger for both the German and US steels. And the value of the remanent field, B_r, for the German steel is larger than those of the other samples indicating that this steel retains higher residual flux density.

For the coercive force, H_c, we see again that the values of this force are different indicating that different magnetic field strengths are required to get rid of the residual flux density. It is desirable to have a large coercive force, H_c, and a large remanent field, B_r, in a permanent magnet. The large value of H_c is important so that the magnetization will not be effected by small stray fields [TI82].

From the values of table 4, we see that the values of relative permeabilities fall close to the representative values given by Skitek [SK68] and Kraus [KR53] for relative permeabilities of mild steel and iron. Skitek gives a representative value of 2,000 for mild steel and 5,000 for iron.

4.8 Conclusion

In conclusion, this study was initiated in order to understand the changes in the solenoidal magnetic field due to the presence of the different types of construction steel. Because of a lack of knowledge about the exact composition of the different steels, it was very difficult to make reasonable comparison with previous results. However, the results show that each steel used in the construction of the ZEUS detector exhibits a unique magnetic behaviour. Since the forces on the solenoid and calorimeters in the detector are very dependent on the magnetization curves, these differences in the magnetic properties of the steels should be considered in future analysis. Also for proper operation of the PMT's these different characteristics of the steels have to be well understood for effective analysis of the data obtained via the PMT's.

Possible directions for improvements would be a detailed study of the various steels at different temperatures, not only room temperature. This would give an indication of the magnetic properties of the steels at different conditions which can be compared to the properties at room temperature.

The PMT's performed perfectly in the cosmic ray tests of september 1991 [ZE91].

Table 2: *the different dimensions of the samples and the number of turns for the primary and the secondary windings.*

Material	*Primary windings* N_1 (±2)	*Secondary windings* N_2 (±2)	*Outer diameter (mm) (±0.01)*	*Inner diameter (mm) (±0.01)*	*Thickness of ring (mm) (±0.01)*
Dutch	*137*	*246*	*27.36*	*21.10*	*3.12*
US	*264*	*513*	*49.98*	*44.32*	*2.86*
German	*268*	*498*	*50.23*	*44.34*	*2.92*
C-Arm	*272*	*499*	*50.28*	*44.27*	*2.95*
Can.St I	*213*	*382*	*41.28*	*34.86*	*3.21*
Can.StII	*219*	*385*	*41.19*	*34.80*	*3.21*

Table 3: *The experimental values of B_{sat} , H_{sat} , B_r and H_c for all of the samples. Errors shown are the statistical errors (as estimated in section 4.4) plus the systematic errors (i.e ± 0.1% integration accuracy as estimated in section 4.5).*

Material	B_{sat} *(tesla)*	H_{sat} *(A/m)*	B_r *(tesla)*	H_c *(A/m)*
Dutch	*0.812 ±0.001±0.001*	*2987 ±89±3*	*0.378 ±0.001±0.001*	*351 ±11±1*
US	*1.208 ±0.002±0.001*	*2410 ±60±2*	*0.639 ±0.001±0.001*	*211 ±9±1*
German	*1.643 ±0.002±0.002*	*2441 ±57±2*	*0.888 ±0.001±0.001*	*180 ±5±1*
C-Arm	*0.811 ±0.001±0.001*	*2490 ±63±3*	*0.414 ±0.001±0.001*	*203 ±5±1*
Can.St.I	*0.725 ±0.001±0.001*	*2411 ±61±2*	*0.511 ±0.001±0.001*	*261 ±7±1*
Can.St.II	*0.708 ±0.001±0.001*	*2406 ±60±2*	*0.497 ±0.001±0.001*	*265 ±7±1*

Table 4: *The experimental values for the maximum permeability and the maximum relative permeability for all of the samples.*

Material	μ_{max} *(H/m)*	κ_{max}
Dutch	$(14.2 \pm 0.8)10^{-4}$	$(1.1 \pm 0.1)10^{3}$
US	$(25.9 \pm 1.0)10^{-4}$	$(2.1 \pm 0.1)10^{3}$
German	$(43.9 \pm 2.0)10^{-4}$	$(3.5 \pm 0.2)10^{3}$
C-Arm	$(16.1 \pm 0.6)10^{-4}$	$(1.3 \pm 0.1)10^{3}$
Can. Steel I	$(15.0 \pm 0.7)10^{-4}$	$(1.2 \pm 0.1)10^{3}$
Can. Steel II	$(15.1 \pm 0.7)10^{-4}$	$(1.2 \pm 0.1)10^{3}$

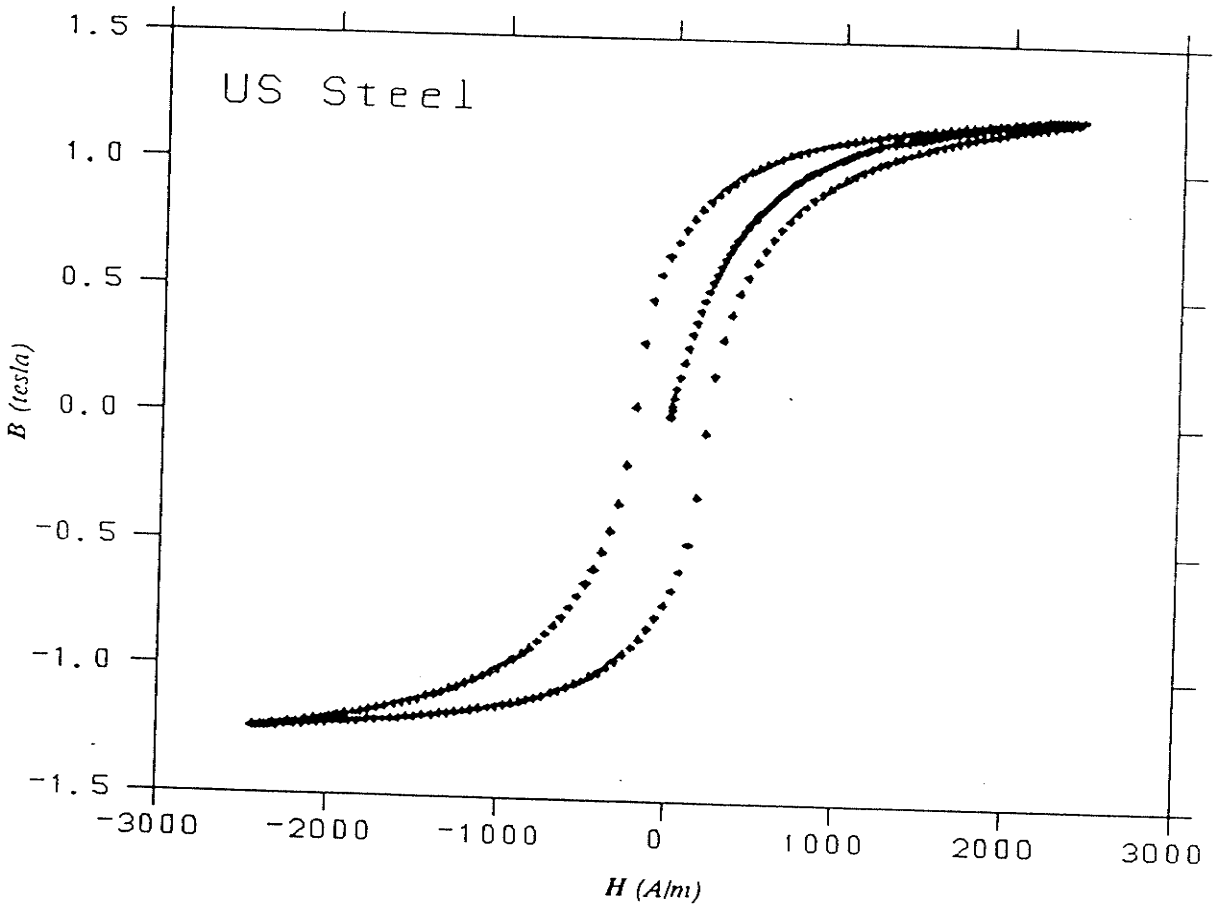

Figure 4.10 B-H curve for the US sample.

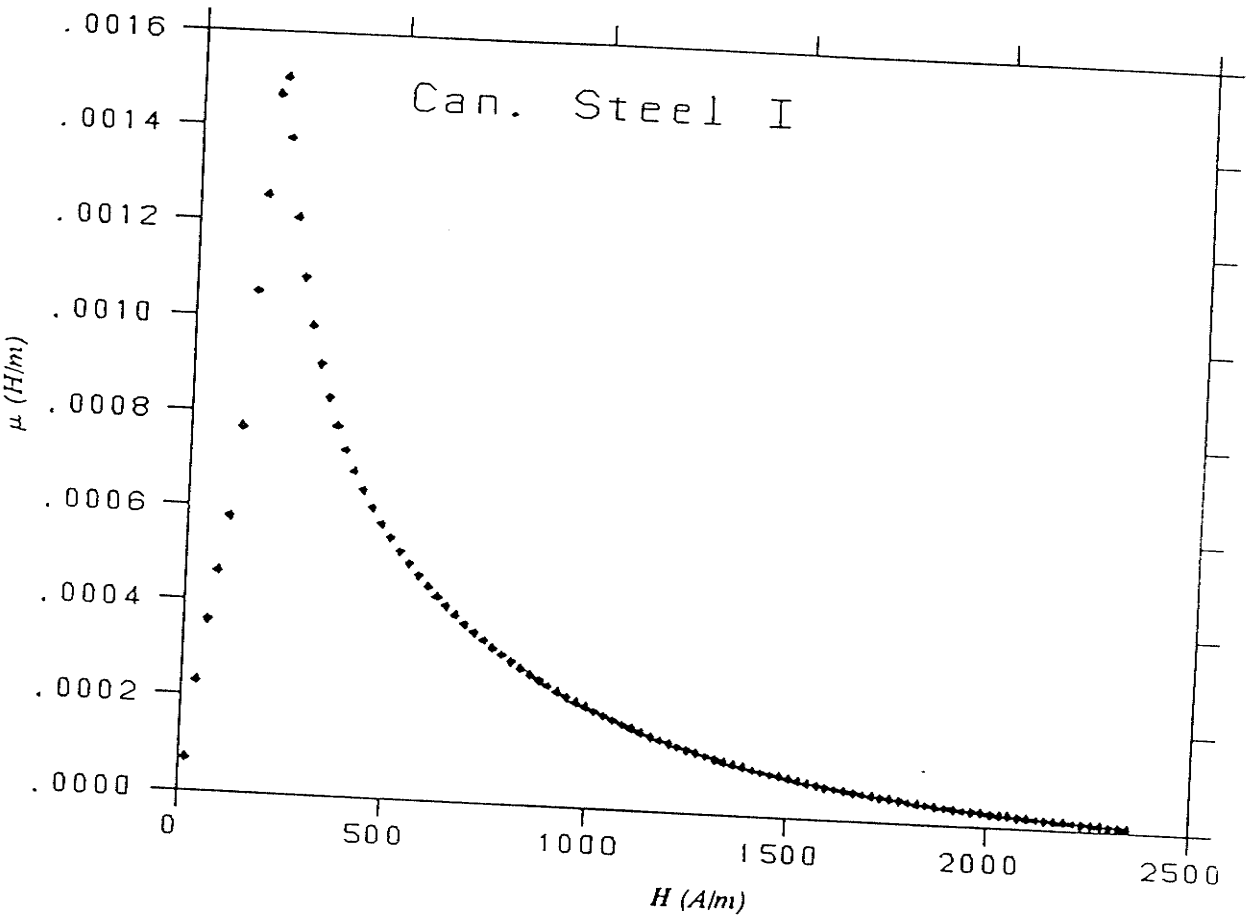

Figure 4.11 μ-H curve for the Canadian St. I sample.

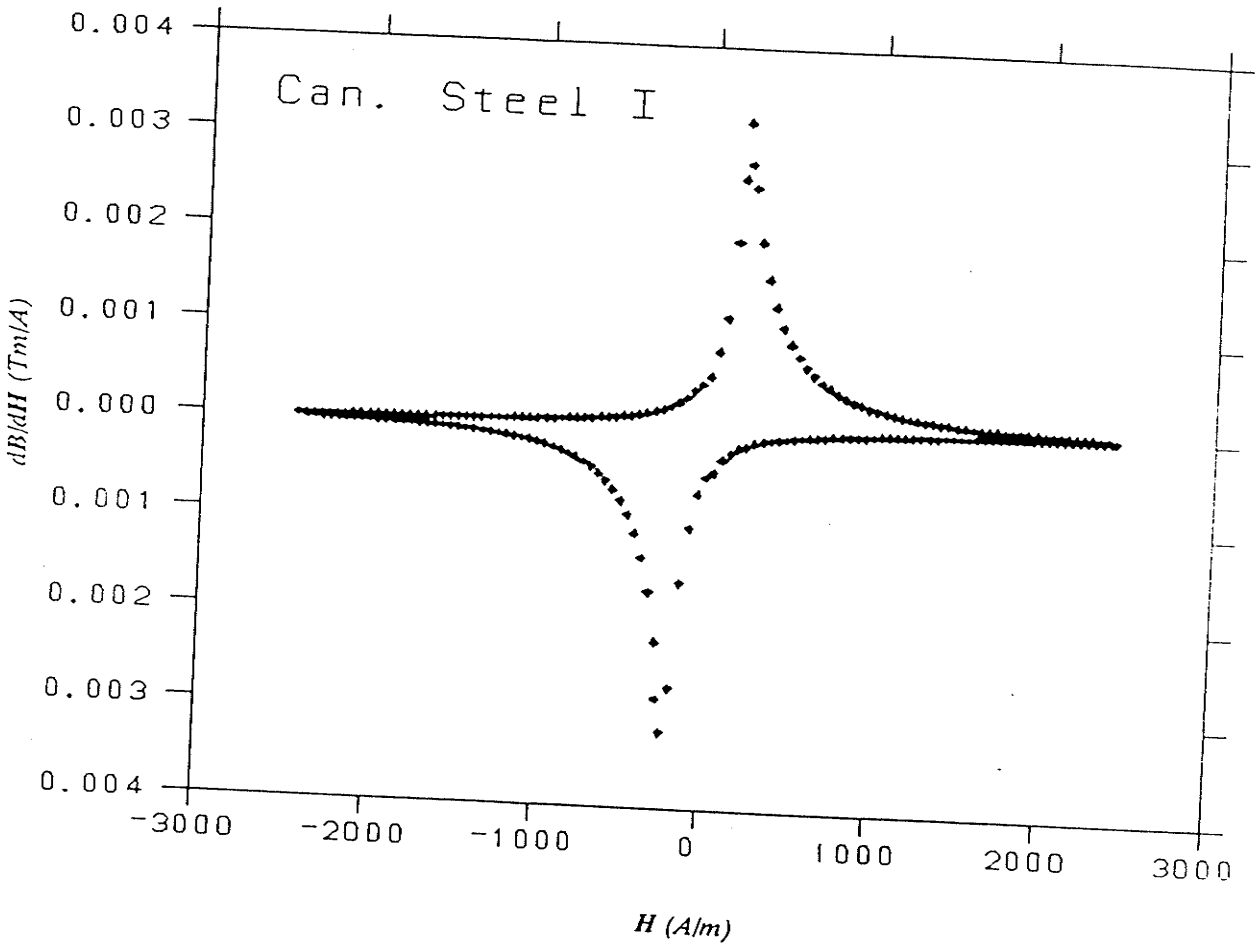

Figure 4.12 dB/dH versus H for the Canadian St. I sample.

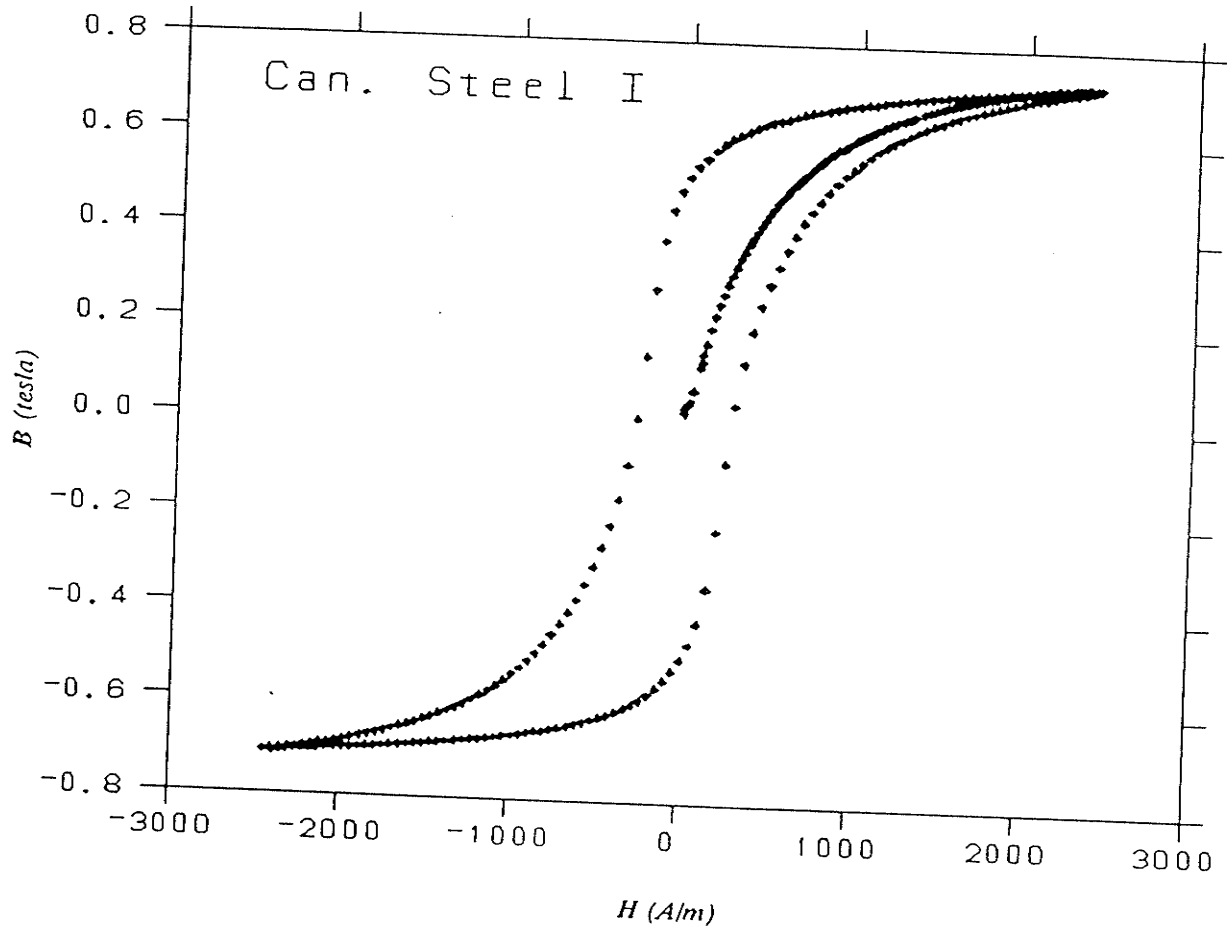

Figure 4.13 ***B-H*** *curve for the Canadian St. I sample.*

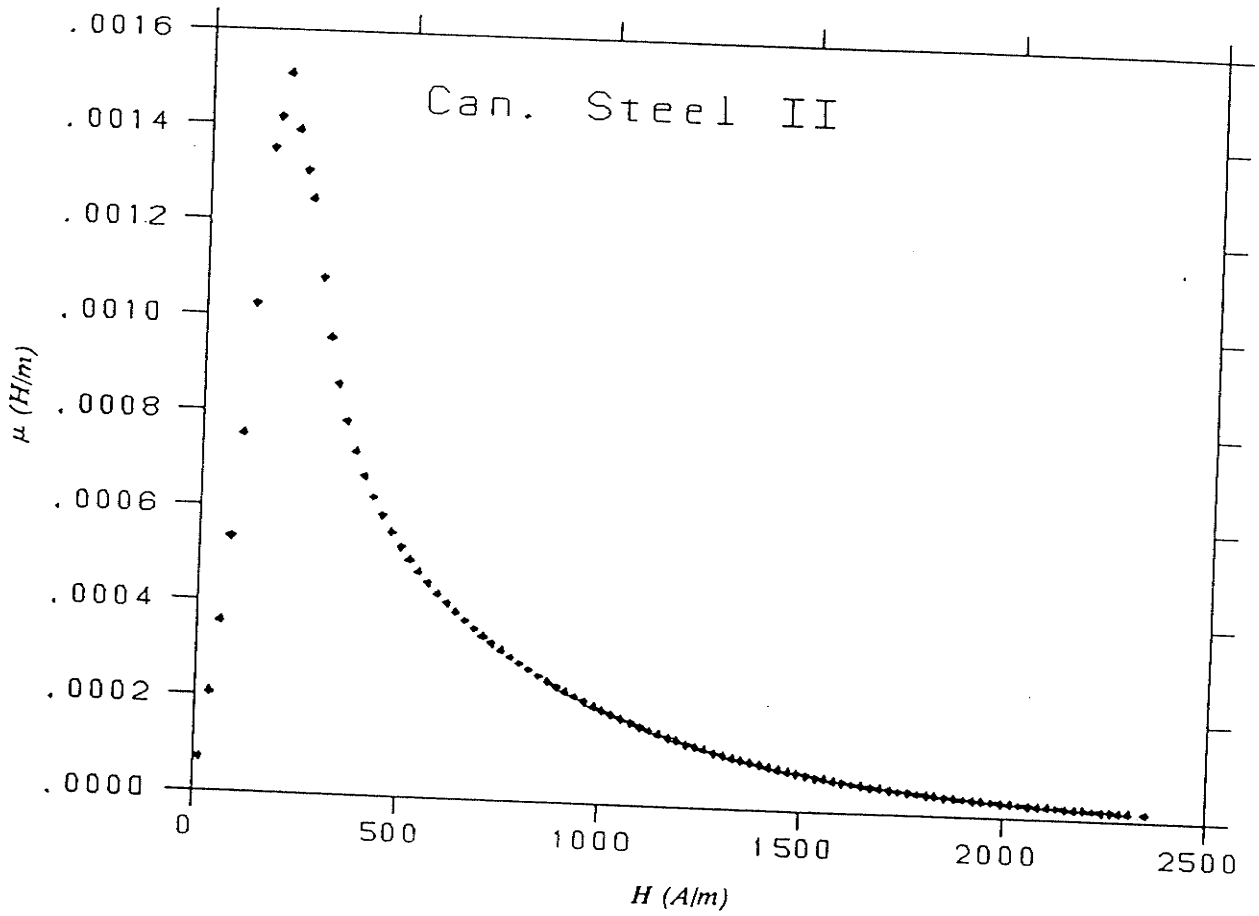

Figure 4.14 μ-H *curve for the Canadian St. II sample.*

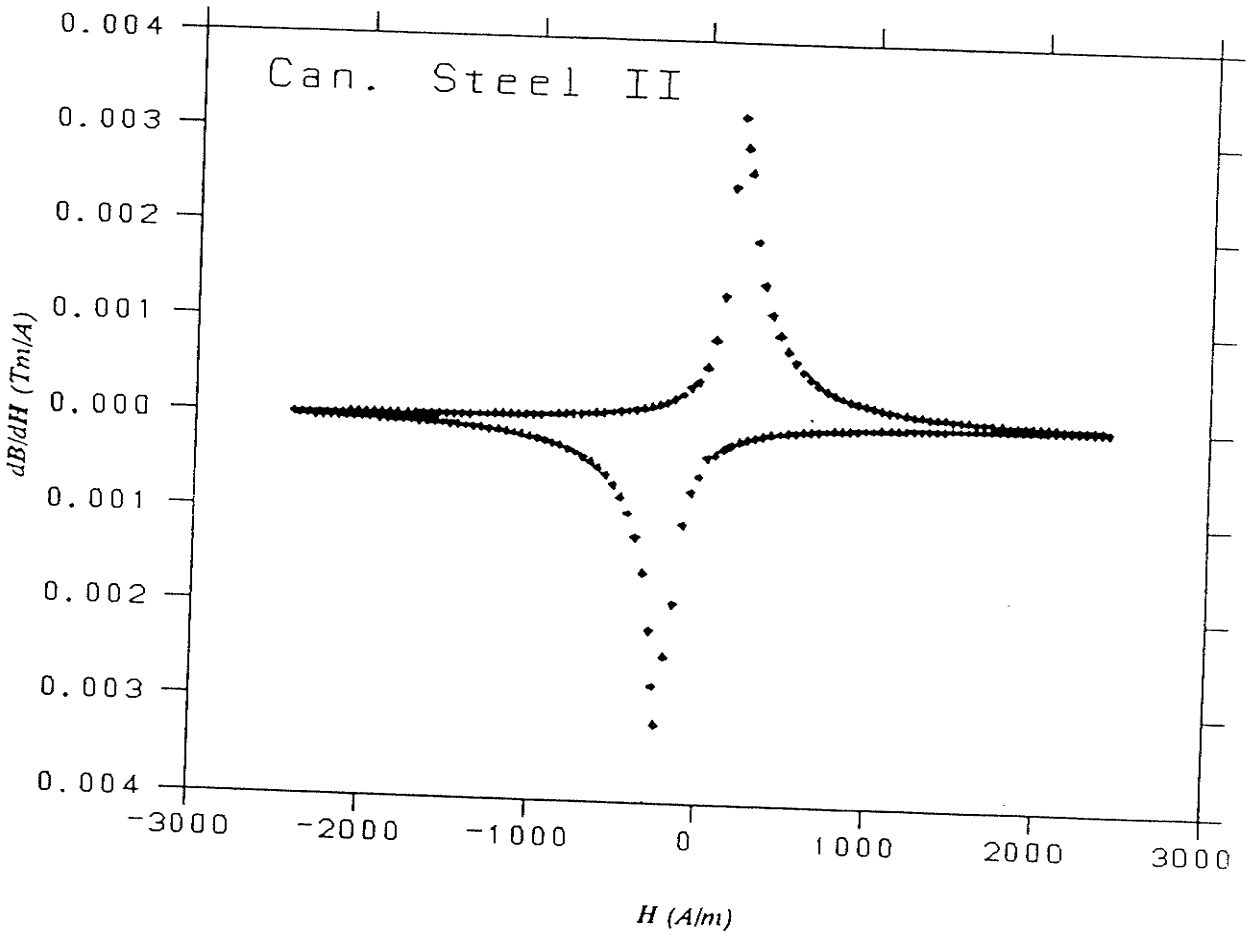

Figure 4.15 dB/dH versus H for the Canadian St. II sample.

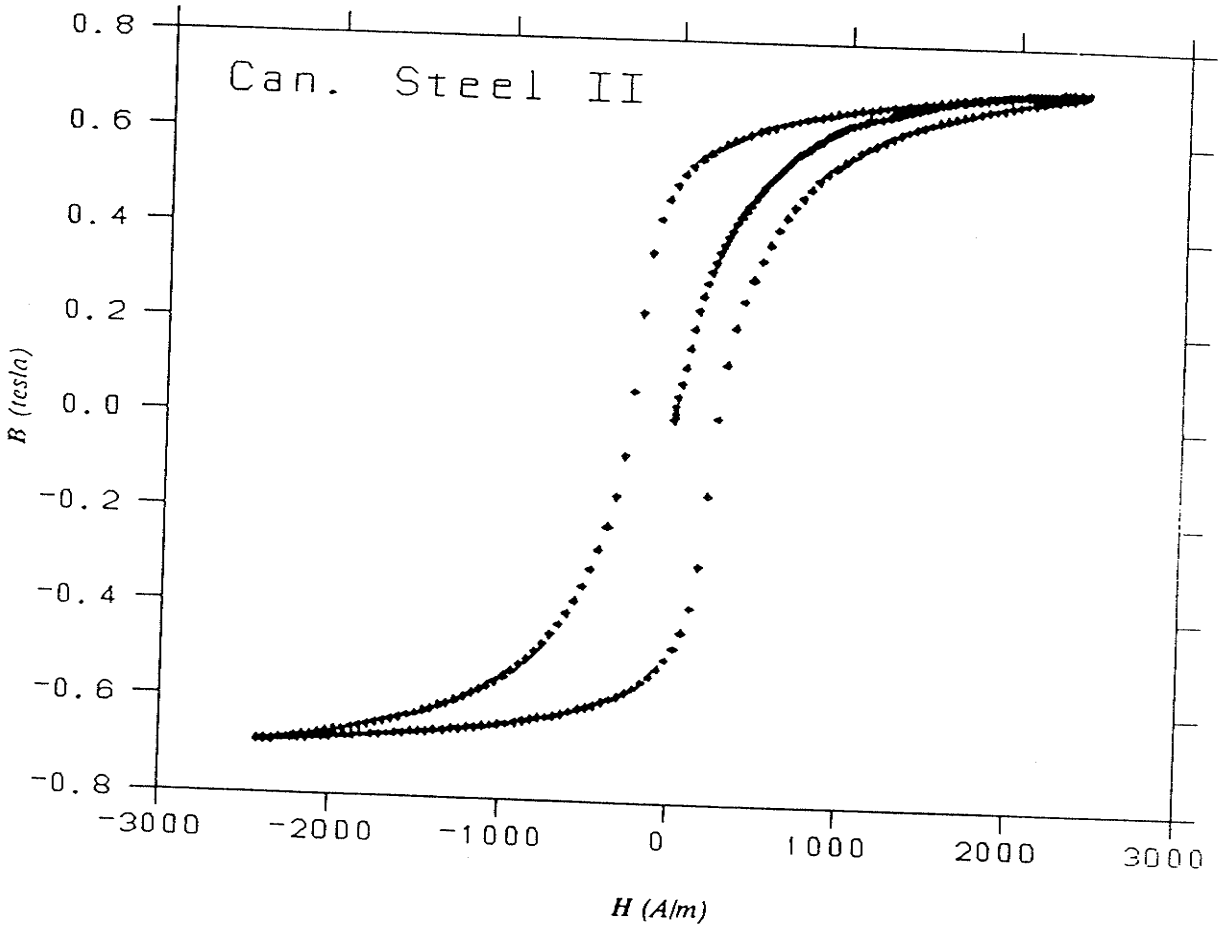

Figure 4.16 B-H curve for the Canadian St. II sample.

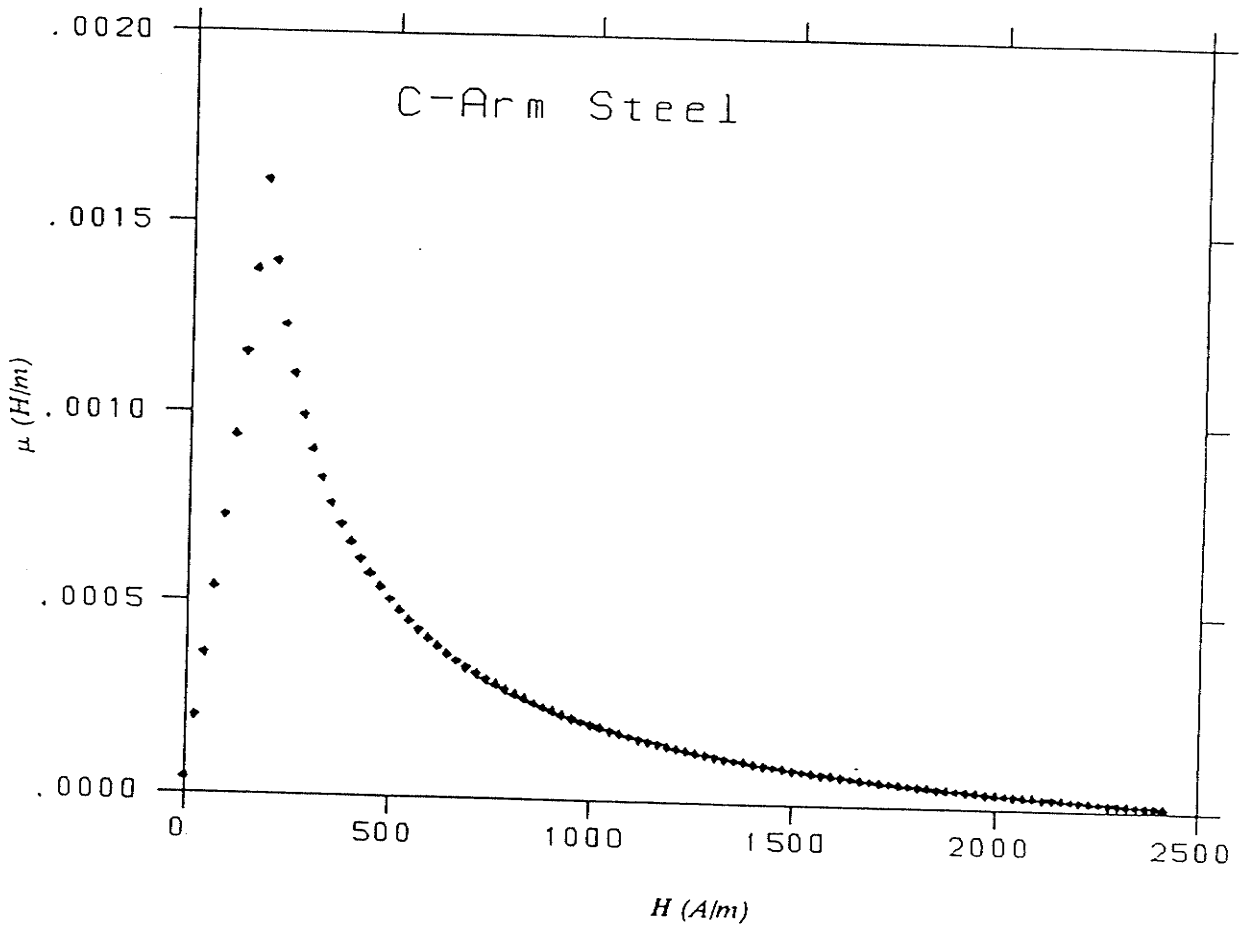

Figure 4.17 μ-H curve for the C-Arm sample.

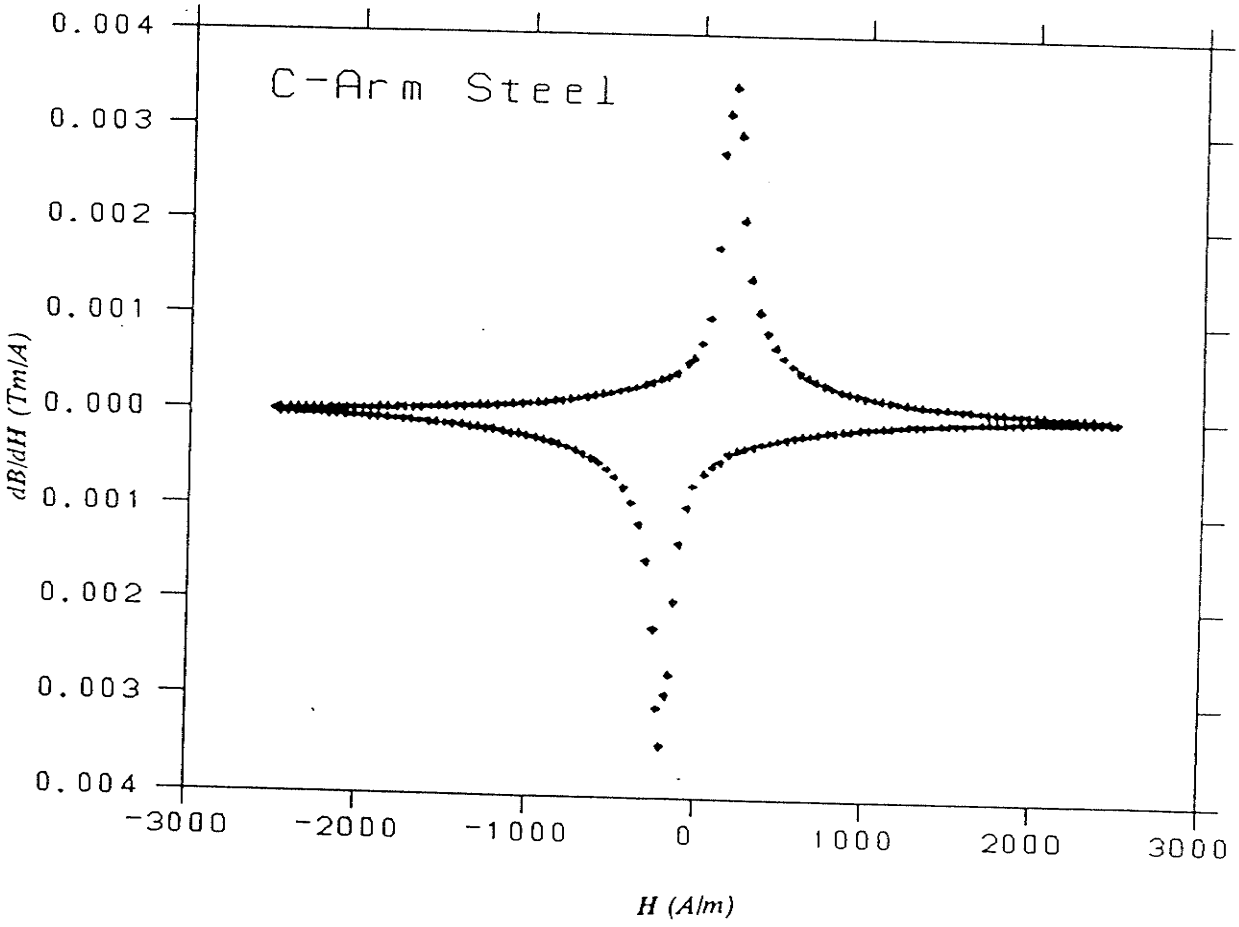

Figure 4.18 dB/dH versus H for the C-Arm sample.

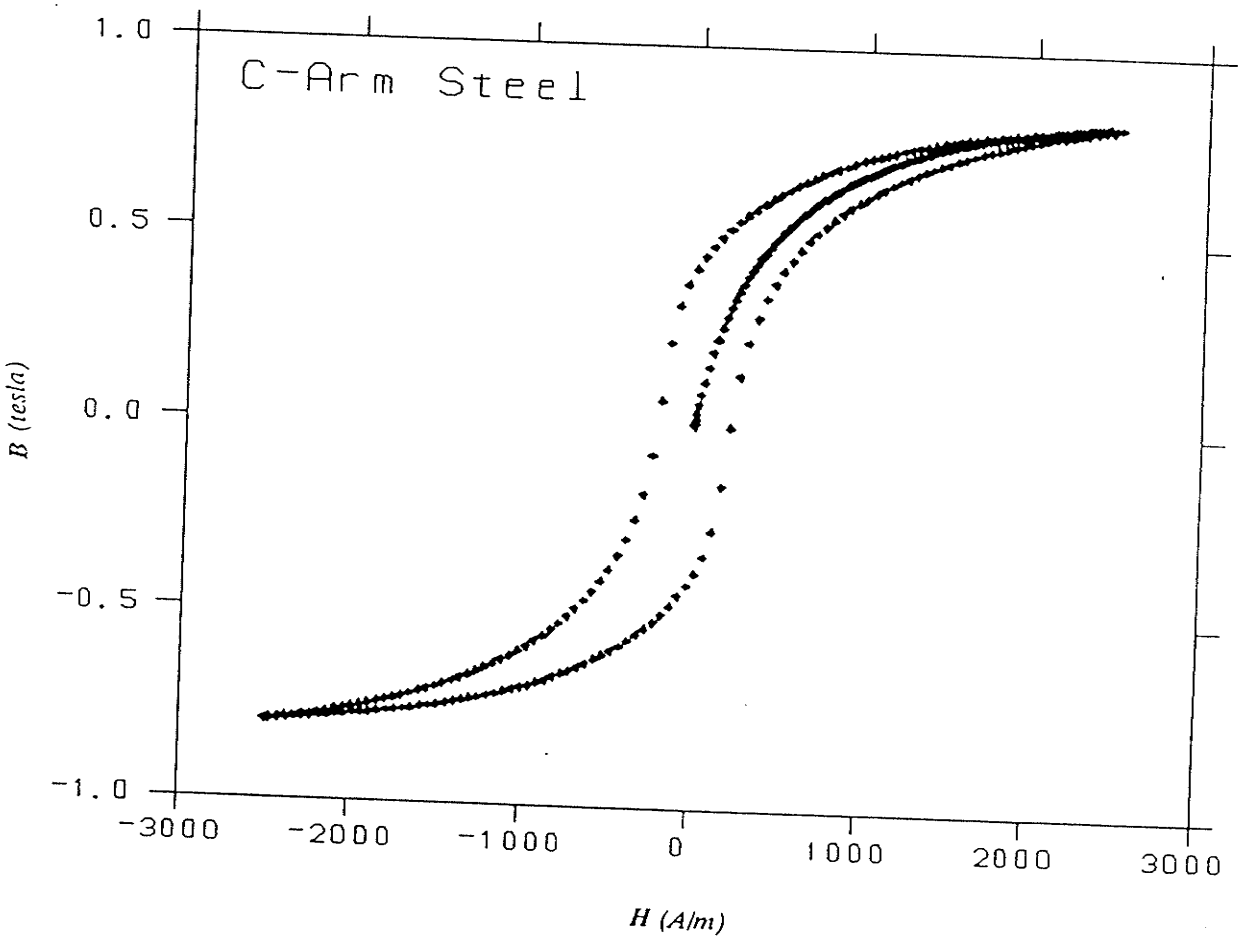

Figure 4.19 B-H curve for the C-Arm sample.

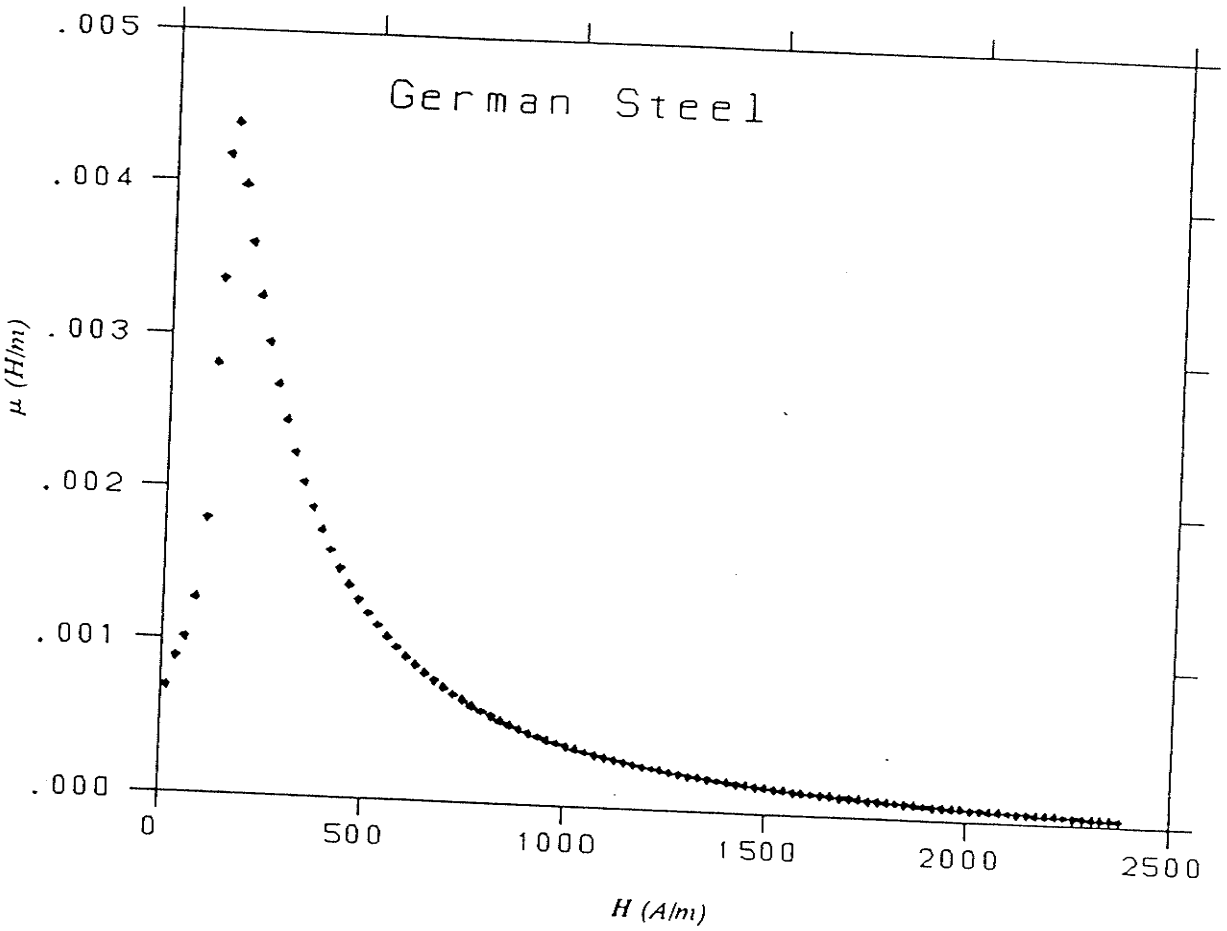

Figure 4.20 μ-H curve for the German sample.

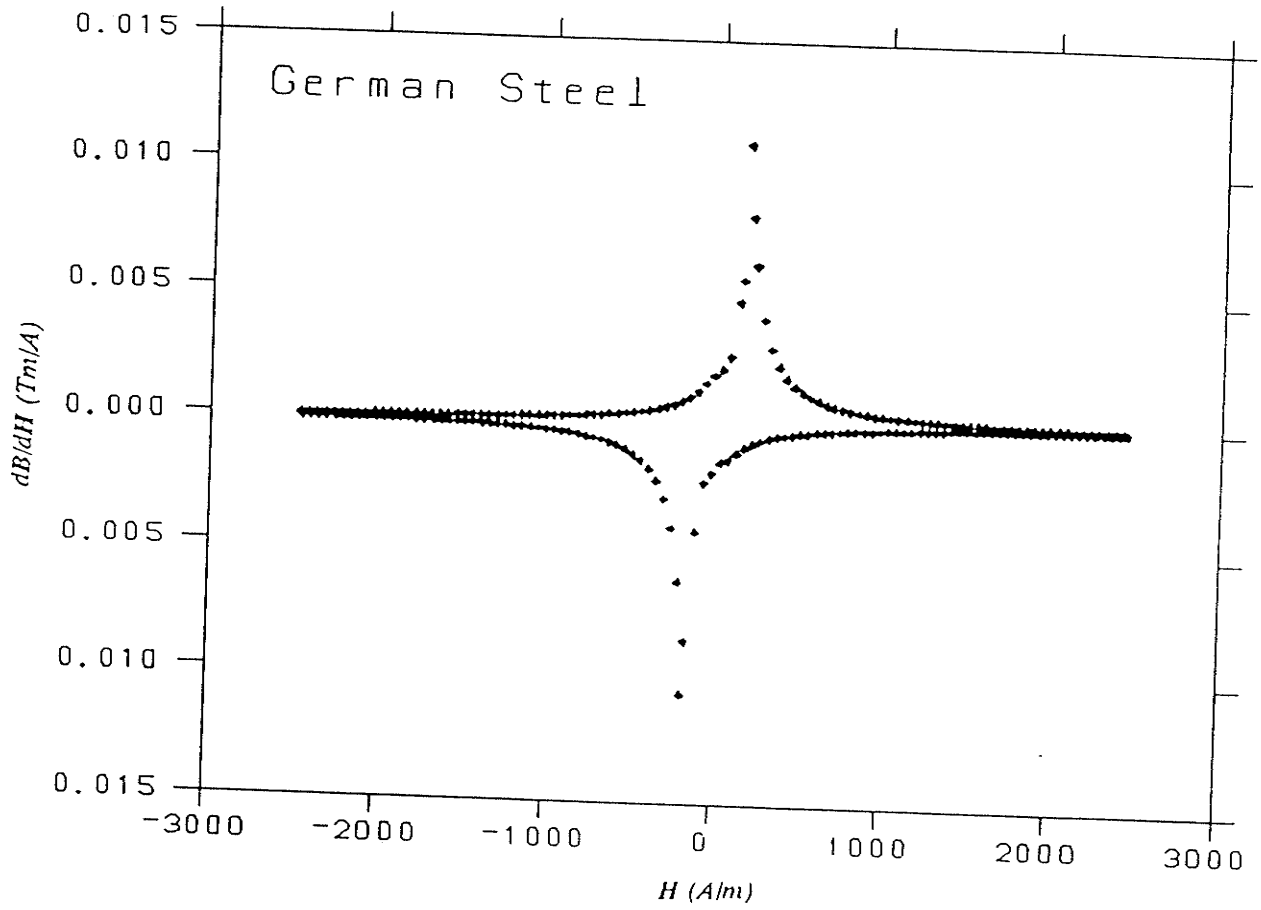

Figure 4.21 *dB/dH versus H for the German sample.*

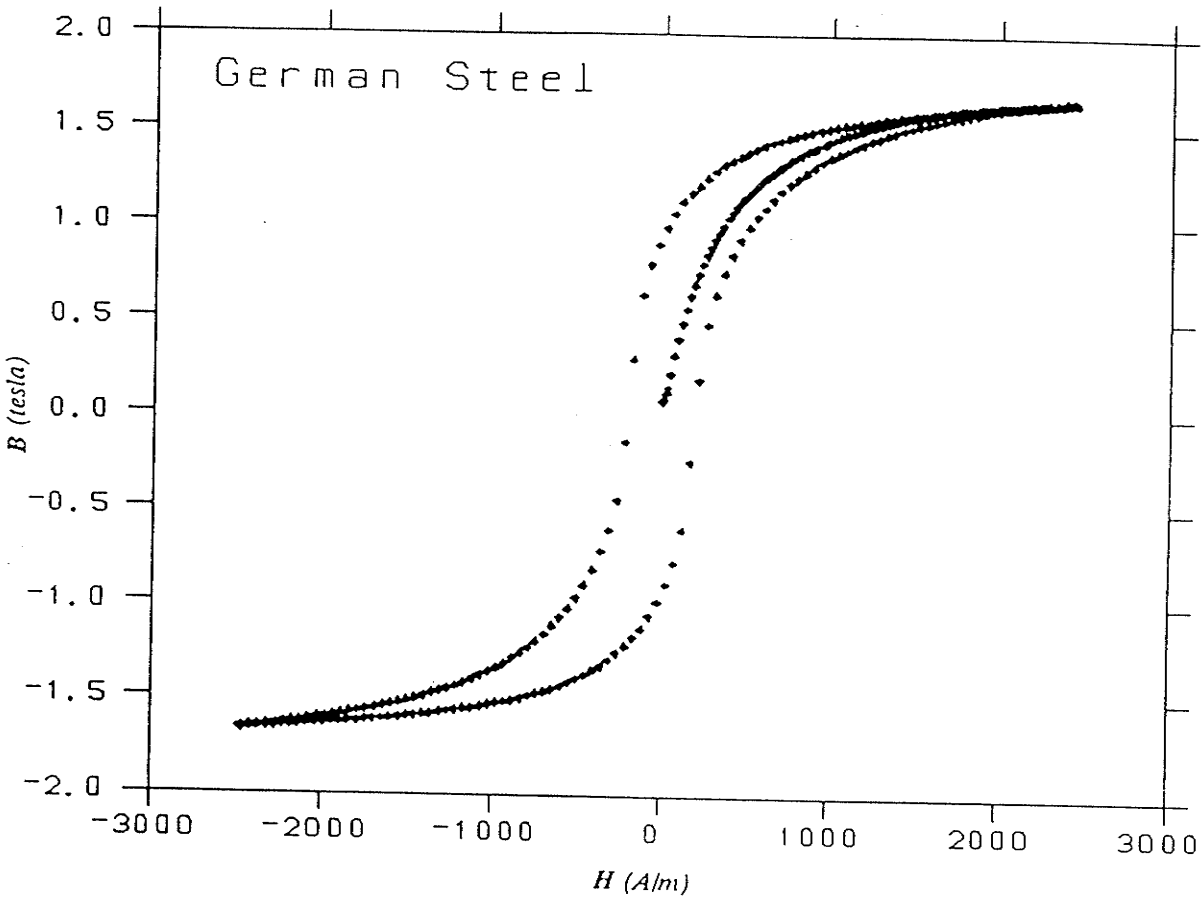

Figure 4.22 B-H curve for the German sample.

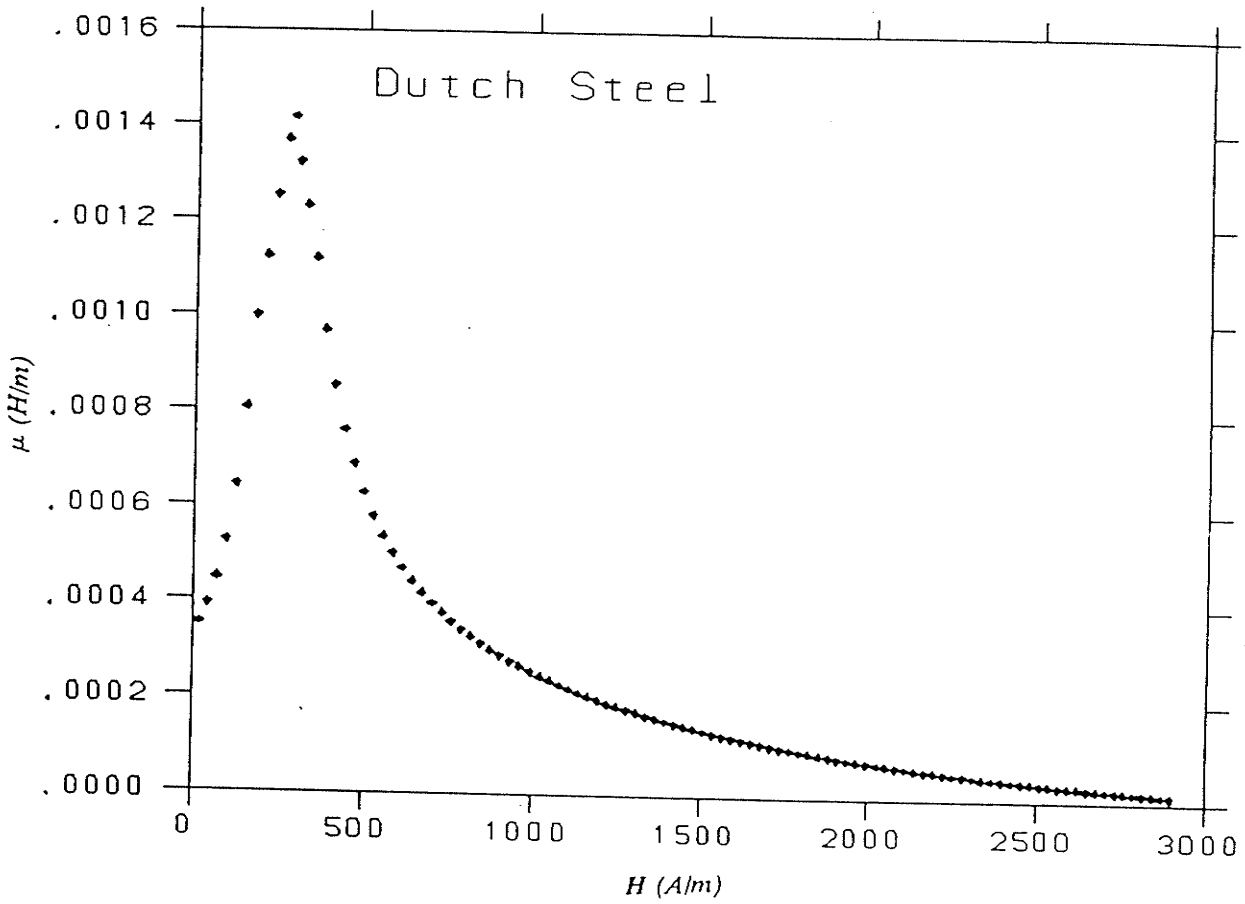

Figure 4.23 *μ-H curve for the Dutch sample.*

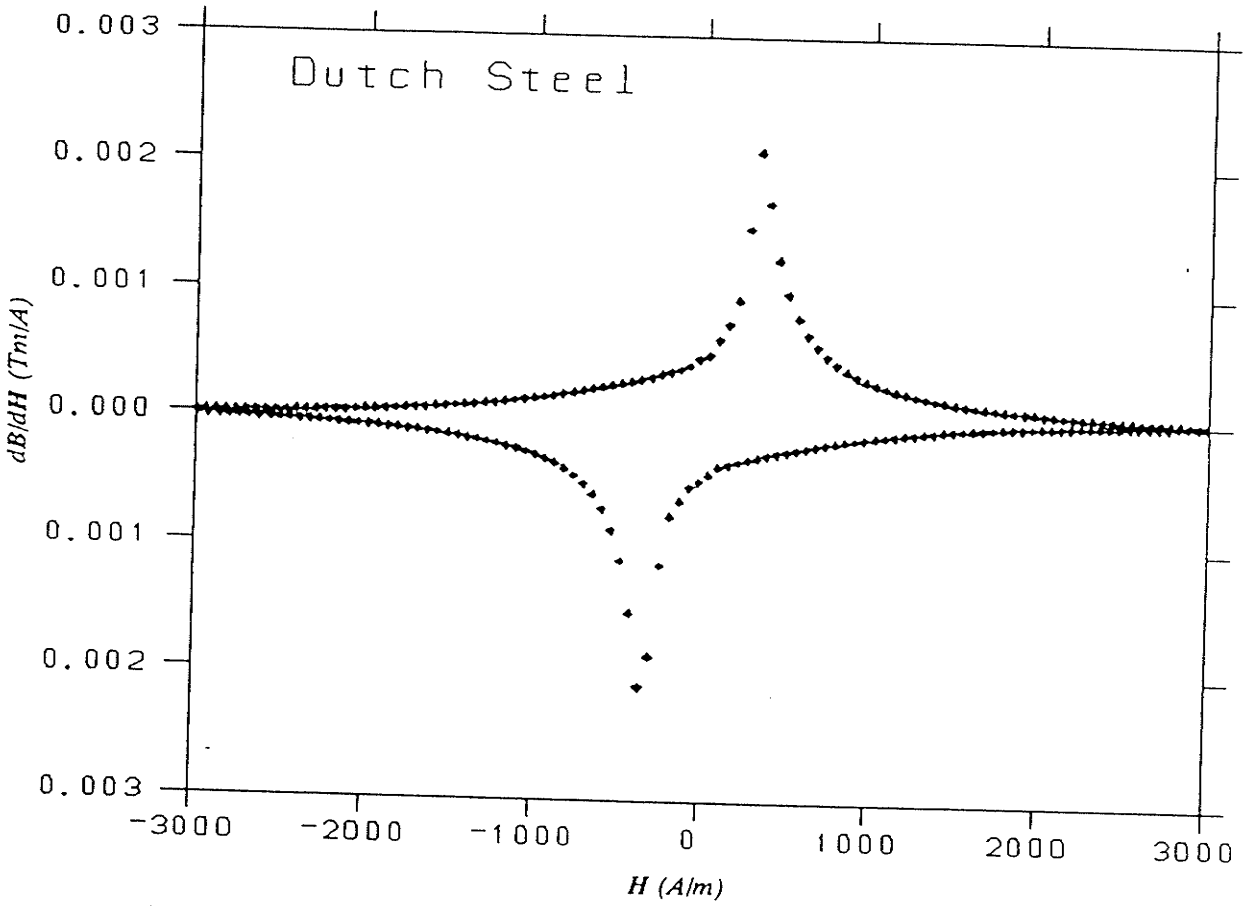

Figure 4.24 dB/dH versus H for the Dutch sample.

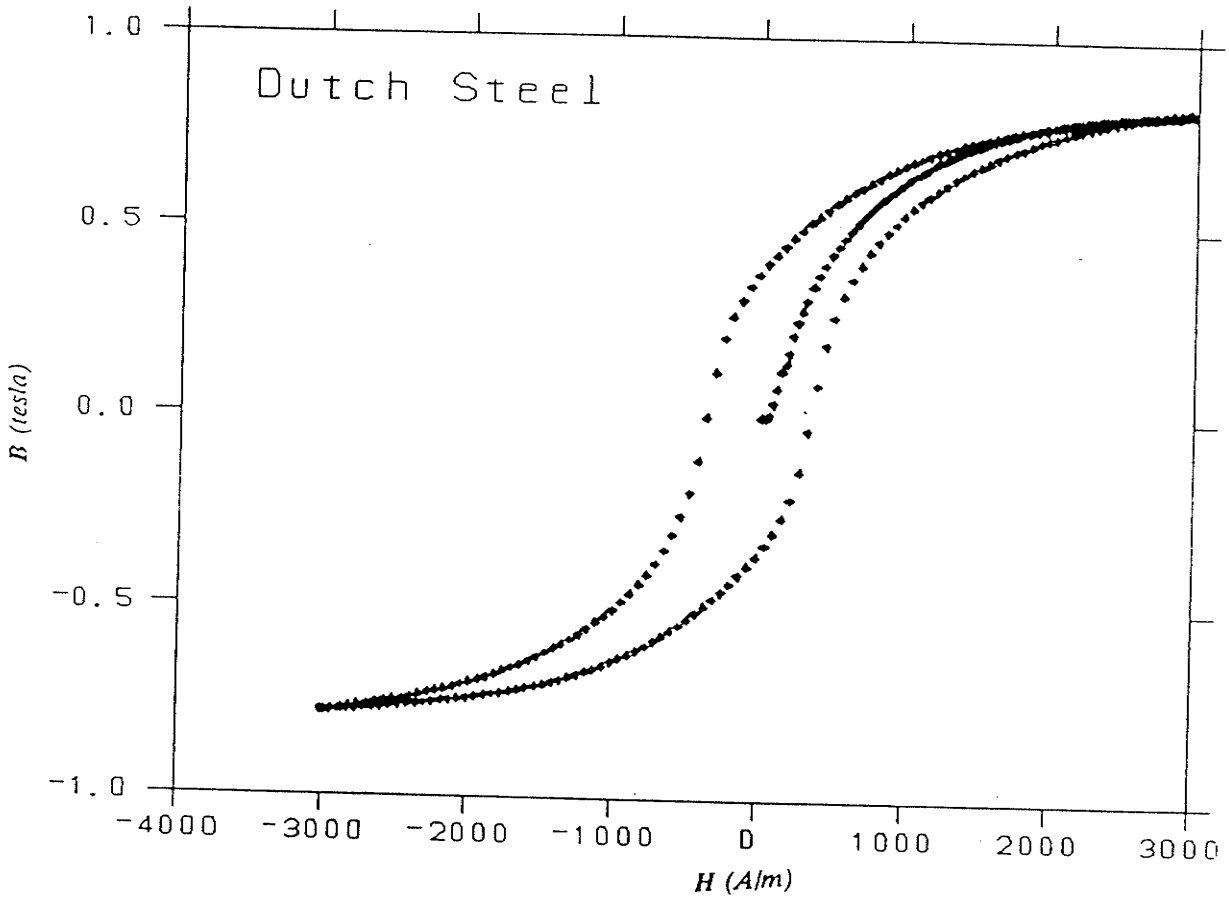

Figure 4.25 B-H curve for the Dutch sample.

```
1       CLEAR   ,59982          ' BASIC Declarations
2       IBINIT1 = 59982
3       IBINIT2 = IBINIT1 + 3 ' Lines 1 to 6 MUST be included in your program.
4       BLOAD "bib.m",IBINIT1
5       CALL IBINIT1(IBFIND,IBTRG,IBCLR,IBPCT,IBSIC,IBLOC,IBPPC,IBBNA,IBONL_
        ,IBRSC,IBSRE,IBRSV,IBPAD,IBSAD,IBIST,IBDMA,IBEOS,IBTMO,IBRDF,IBWRTF)
6       CALL IBINIT2(IBGTS,IBCAC,IBWAIT,IBPOKE,IBWRT,IBWRTA,IBCMD,IBCMDA,IBRDA_
        ,IBSTOP,IBRPP,IBRSP,IBDIAG,IBXTRC,IBRDI,IBWRTI,IBRDIA,IBWRTIA,IBSTA%,_
        IBERR%,IBCNT%)
10      REM Optionally include the following declarations in your program.
11      REM They provide appropriate mnemonics by which
12      REM to reference commonly used values.  Some mnemonics (GET%, ERR%,
13      REM END%, ATN%) are preceded by "B" in order to distinguish them
14      REM from BASIC keywords.
15      REM GPIB Commands
16      UNL% = &H3F      ' GPIB unlisten command
17      UNT% = &H5F      ' GPIB untalk command
18      GTL% = &H1       ' GPIB go to local
19      SDC% = &H4       ' GPIB selected device clear
20      PPC% = &H5       ' GPIB parallel poll configure
21      BGET% = &H8      ' GPIB group execute trigger
22      TCT% = &H9       ' GPIB take control
23      LLO% = &H11      ' GPIB local lock out
24      DCL% = &H14      ' GPIB device clear
25      PPU% = &H15      ' GPIB ppoll unconfigure
26      SPE% = &H18      ' GPIB serial poll enable
27      SPD% = &H19      ' GPIB serial poll disable
28      PPE% = &H60      ' GPIB parallel poll enable
29      PPD% = &H70      ' GPIB parallel poll disable
30      REM
31      REM GPIB status bit vector
32      REM global variable IBSTA% and wait mask
33      BERR% = &H8000   ' Error detected
34      TIMO% = &H4000   ' Timeout
35      BEND% = &H2000   ' EOI or EOS detected
36      SRQI% = &H1000   ' SRQ detected by CIC
37      RQS% = &H800     ' Device needs service
38      CMPL% = &H100    ' I/O completed
39      LOK% = &H80      ' Local lockout state
40      REM% = &H40      ' Remote state
41      CIC% = &H20      ' Controller-In-Charge
42      BATN% = &H10     ' Attention asserted
43      TACS% = &H8      ' Talker active
44      LACS% = &H4      ' Listener active
45      DTAS% = &H2      ' Device trigger state
46      DCAS% = &H1      ' Device clear state
47      REM Error messages returned in global variable IBERR%
48      EDVR% =  0       ' DOS error
49      ECIC% =  1       ' Function requires board to be CIC
50      ENOL% =  2       ' Write function detected no Listeners
51      EADR% =  3       ' Interface board not addressed correctly
52      EARG% =  4       ' Invalid argument to function call
53      ESAC% =  5       ' Function requires board to be SAC
54      EABO% =  6       ' I/O operation aborted
55      ENEB% =  7       ' Non-existent interface board
56      EOIP% = 10       ' I/O operatation started before previous operatation completed
57      ECAP% = 11       ' No capability for operation
58      EFSO% = 12       ' File system operation error
59      EBUS% = 14       ' Command error during device call
60      ESTB% = 15       ' Serial poll status byte lost
61      ESRQ% = 16       ' SRQ remains asserted
62      REM EOS mode bits
63      BIN% = &H1000    ' Eight bit compare
64      XEOS% = &H800    ' Send EOI with EOS byte
65      REOS% = &H400    ' Terminate read on EOS
```

```
67      REM Timeout values and meanings
68      TNONE% =   0    ' Infinite timeout  (disabled)
69      T10us% =   1    ' Timeout of 10 us  (ideal)
70      T30us% =   2    ' Timeout of 30 us  (ideal)
71      T100us% =  3    ' Timeout of 100 us (ideal)
72      T300us% =  4    ' Timeout of 300 us (ideal)
73      T1Ms% =    5    ' Timeout of 1 ms   (ideal)
74      T3Ms% =    6    ' Timeout of 3 ms   (ideal)
75      T10ms% =   7    ' Timeout of 10 ms  (ideal)
76      T30ms% =   8    ' Timeout of 30 ms  (ideal)
77      T100ms% =  9    ' Timeout of 100 ms (ideal)
78      T300ms% = 10    ' Timeout of 300 ms (ideal)
79      T1s% =     11   ' Timeout of 1 s    (ideal)
80      T3s% =     12   ' Timeout of 3 s    (ideal)
81      T10s% =    13   ' Timeout of 10 s   (ideal)
82      T30s% =    14   ' Timeout of 30 s   (ideal)
83      T100s% =   15   ' Timeout of 100 s  (ideal)
84      T300s% =   16   ' Timeout of 300 s  (ideal)
85      T1000s% =  17   ' Timeout of 1000 s (maximum)
86      REM
87      REM Miscellaneous
88      S% = &H8        ' Parallel Poll sense bit
89      LF% = &HA       ' Line feed character
90      REM
91      REM Application program variables passed to
92      REM GPIB functions
93      REM
94      CMD$ = SPACE$(10)       ' command buffer
95      RD$ = SPACE$(255)       ' read data buffer
96      WRT$ = SPACE$(255)      ' write data buffer
97      BNAME$ = SPACE$(7)      ' board name buffer
98      BDNAME$ = SPACE$(7)     ' board or device name buffer
99      FLNAME$ = SPACE$(50)    ' file name buffer
110     BDNAME$="HPDVM"         ' name of device as per GPIB.COM file
120     CALL IBFIND(BDNAME$,HPDVM%)
130     CALL IBRSP(HPDVM%,SPR%):IF SPR%=0 THEN PRINT "DVM is not responding."
140     :N%=4:GOTO 220
150     REM clear the dvm . attempt 3 times then quit
160     N%=1
170     CALL IBCLR(HPDVM%)
180     WRT$="RESET"     'remote reset the device (approx 2 sec.)
190     CALL IBWRT(HPDVM%,WRT$)
200     CALL IBRSP(HPDVM%,SPR%):IF SPR%=0 GOTO 190 'loop until the DVM responds
210     CALL IBRSP(HPDVM%,SPR%):IF SPR%<>16 AND N%<4 THEN N%=N%+1:GOTO 160
220     IF N%>3 THEN PRINT "Could not clear the DVM. Device Status: "SPR%
230     IF N%>3 THEN INPUT "Press RETURN to exit. ",X$:GOTO 740
240     WRT$="TERM REAR"                'select rear terminals
241     CALL IBWRT(HPDVM%,WRT$)
242     CALL IBRSP(HPDVM%,SPR%):IF SPR%=0 GOTO 241
243     WRT$="TRIG HOLD"        'suspends trigerring
244     CALL IBWRT(HPDVM%,WRT$)
245     CALL IBRSP(HPDVM%,SPR%):IF SPR%=0 GOTO 244
250     WRT$="SADV AUTO;SLIST 0,1"      'sets scan advance to auto
260     CALL IBWRT(HPDVM%,WRT$)
261     CALL IBRSP(HPDVM%,SPR%):IF SPR%=0 GOTO 261
270     WRT$="SLIST 0,1"        'sets up scan list
280     CALL IBWRT(HPDVM%,WRT$)
282     CALL IBRSP(HPDVM%,SPR%):IF SPR%=0 GOTO 282
290     WRT$="AZERO OFF"        'disables autozero
300     CALL IBWRT(HPDVM%,WRT$)
310     WRT$="LOCK ON"          'disable the dvm keyboard
320     CALL IBWRT(HPDVM%,WRT$)
330     WRT$="DISP MSG,ZEUS_RULES"
340     CALL IBWRT(HPDVM%,WRT$)
341     CALL IBRSP(HPDVM%,SPR%):IF SPR%=0 GOTO 341
390     WRT$="TARM AUTO"        ' trigger armed
400     CALL IBWRT(HPDVM%,WRT$)
401     CALL IBRSP(HPDVM%,SPR%):IF SPR%=0 GOTO 401
410     WRT$="MFORMAT SREAL"    '4 byte real no. w/ autoranging
420     CALL IBWRT(HPDVM%,WRT$)
421     CALL IBRSP(HPDVM%,SPR%):IF SPR%=0 GOTO 421
430     WRT$="MSIZE 2048"       'reading memory size = 512  bytes
440     CALL IBWRT(HPDVM%,WRT$)
441     CALL IBRSP(HPDVM%,SPR%):IF SPR%=0 GOTO 441
450     WRT$="MEM FIFO"         'reading buffer first in first out
460     CALL IBWRT(HPDVM%,WRT$)
461     CALL IBRSP(HPDVM%,SPR%):IF SPR%=0 GOTO 461
470     WRT$="F12"              'select dc 300mV range
480     CALL IBWRT(HPDVM%,WRT$)
```

```
481     CALL IBRSP(HPDVM%,SPR%):IF SPR%=0 GOTO 481
490     WRT$="NPLC .1"          'no. of power cycles for sample time
500     CALL IBWRT(HPDVM%,WRT$)
501     CALL IBRSP(HPDVM%,SPR%):IF SPR%=0 GOTO 501
502     REM number of measurements is 512, according to the time
503     REM interval in the TIMER.
510     WRT$="TIMER .03;NRDGS 512,TIMER"   '512 measurements
520     CALL IBWRT(HPDVM%,WRT$)
521     CALL IBRSP(HPDVM%,SPR%):IF SPR%=0 GOTO 521
530     WRT$="TRIG EXT"             'external trigger
540     CALL IBWRT(HPDVM%,WRT$)
541     CALL IBRSP(HPDVM%,SPR%):IF SPR%=0 GOTO 541
550     WRT$="DISP OFF;TONE 500"    'display off while taking data
560     CALL IBWRT(HPDVM%,WRT$)
570     INPUT "Press return after externally triggering the DVM.",X$
575     PRINT " "
580     CALL IBRSP(HPDVM%,SPR%):PRINT"Status register bit:",SPR%:GOSUB 1000
590     WRT$="DISP MSG,SENDING_DATA"
600     CALL IBWRT(HPDVM%,WRT$)
610     FLNAME$="DVM.DAT"       'name of file to be opened for data input
620     PRINT " ":PRINT "File "FLNAME$" is being opened for data input."
621     REM the DVM data is read into the DVM.DAT
622     REM and I/O errors is checked.
630     CALL IBRDF(HPDVM%,FLNAME$):GOSUB 2000 'read dvm data into flname$
640     WRT$="TONE 1400;TONE 1620;TONE 1280"
650     CALL IBWRT(HPDVM%,WRT$)
655     CALL IBRSP(HPDVM%,SPR%):IF SPR%=0 GOTO 655
660     WRT$="DISP ON"      'turn the dvm display back on
670     CALL IBWRT(HPDVM%,WRT$)
680     WRT$="LOCK OFF"     'enable the dvm keyboard
690     CALL IBWRT(HPDVM%,WRT$)
700     CLOSE               'close all open dos files
710     PRINT FLNAME$ " closed."
711     REM proceed to split the channels in DVM.DAT
720     IF SPR%=16 AND IBCNT%>0 THEN GOSUB 3000   'split channels in dvm.dat
730     INPUT "Reset the DVM? (n)  ",X$
740     IF X$ = "Y" OR X$="y" THEN WRT$="RESET":CALL IBWRT(HPDVM%,WRT$)
750     SYSTEM
760     END

1000    REM Subroutine to evaluate the serial response bit.
1001    REM DVM isn't ready when this occurs.
1010    IF SPR%=0 THEN PRINT "Measurement failed.Exit program.":GOTO 720
1011    REM when measurement completed then DVM is ready.
1020    IF SPR%=16 THEN PRINT "Measurment cycles completed.":RETURN
1030    IF SPR%=1 THEN RETURN   'program memory execution completed
1050    IF SPR%=32 OR SPR%=34 OR SPR%=35 OR SPR%=48 THEN PRINT _
      "An error has occured. Data will not be transfered."_
      :INPUT "Try again? ",X$:IF X$="Y"OR X$="y" GOTO 110 ELSE GOTO 730
1060    IF SPR%=64 OR SPR%=80 THEN PRINT "SRQ line is set true._
      (Check data to be sent.)":RETURN
1070    PRINT "An unusual condition (error?) on the DVM has occurred._
      Check data sent."
1080    RETURN

2000    REM  Subroutine to evaluate the data transfer
2001    REM  and the GPIB Status Word.
2010    PRINT "Number of bytes read: "IBCNT%
2020    IF IBSTA%=-32512 THEN PRINT "I/O completed.":RETURN
2030    PRINT "Unusual GPIB state. Device status: "IBSTA% :RETURN
2040    RETURN

3000    REM Subroutine to split the one column sequential file dvm.dat
3001    REM into a two column sequential file channels.dat.
3010    PRINT " "       'print a blank line
3011    TRUE%=1
3012    WHILE TRUE%
3013    PRINT " "
3014      INPUT "Name of output file? (8 characters or less) ",OUTNAME$
3015    REM set the expressionn false(0) or true(1)
3016      IF OUTNAME$="" THEN TRUE%=1 ELSE TRUE%=0
3017    WEND
3018    PRINT " "
3020    PRINT "Splitting the one column sequential file DVM.DAT into a "
3030    PRINT "two column sequential file "OUTNAME$".DAT for "
3031    PRINT " graphing purposes. Please wait."
3032    INFILE$="DVM.DAT"
3033    OUTFILE$=OUTNAME$+".DAT"
3040    OPEN INFILE$ FOR INPUT AS #1
3050    OPEN OUTFILE$ FOR OUTPUT AS #2
```

```
3060    WHILE NOT EOF(1)
3070      INPUT#1,CHAN0#
3080      INPUT#1,CHAN1#
3090      PRINT#2,CHAN0#,CHAN1#
3100    WEND
3110    CLOSE#1,#2
3120    PRINT "Done.":PRINT " ":RETURN
3130    RETURN
```

```
C*********************************************
C                                             *
C                                             *
C Algorithm used for normalizing, sorting and *
C integrating data files from studies of magnet*
C properties of some of the steels used in ZEUS*
C detector.                                   *
C                                             *
C INPUT:  data files transfered to VAX from PC*
C         normalization data                  *
C OUTPUT: data file containing normalized and *
C         sorted data for one-shot and hysteresis*
C         curves                              *
C         integrated data for the hysteresis  *
C         loops.                              *
C*********************************************
C
      IMPLICIT NONE
*
      REAL*8 XOS(200),YOS(200)
      REAL*8 XH(300),YH(300)
      REAL*8 XNEW(500),YNEW(500)
      REAL*8 R,RAD,RHO,PI,VMAXH,VMAXOS,TH,TOS
      INTEGER N1,N2
      INTEGER OSEND,HEND,HPOS,HMAX,DATAEND
      REAL*8 CONSTH,CONSTMU
      REAL*8 LASTH
      INTEGER IOS,JOS,IH,JH,JHH,KH,LH,MH,MHH,NH,I,J
      INTEGER MAXH,HLP
      REAL*8 SUM, YNORM, XDIFF
*
* OPEN THE VARIOUS FILES FOR READING AND WRITING
*
*
* define values of the constants used ni the normalization
*       the value of the resistor
        R=0.112
*       the value of pi
        PI=3.1415926
* open file to read the normalization constants
        OPEN (UNIT=11,STATUS='OLD',
     +  FILE='CONSTANTS')
*       radius of the ring
        READ (11,*) RAD
*       radius of the circular cross section in the ring
        READ (11,*) RHO
*       maximum voltage for H during the hysteresis run
        READ (11,*) VMAXH
*       maximum voltage for H during the one-shot run
        READ (11,*) VMAXOS
*       time constant for the hysteresis run
        READ (11,*) TH
*       time constant for the ono shot run
        READ (11,*) TOS
*       number of turns of the primary coil
        READ (11,*) N1
*       number of turns of the sensing coil
        READ (11,*) N2
*
*       group constants for calculations
        CONSTH=N1/(2.0*PI*RAD*R)
        CONSTMU=(2*RAD*R)/(RHO*RHO*N1*N2)
*
* open file to read the one shot data
        OPEN (UNIT=7,STATUS='OLD',
     +  FILE='ONE SHOT DATA')
* read in the one shot data
        DO IOS=1,200
                READ (7,*,END=101) XOS(IOS),YOS(IOS)
```

```
                OSEND=IOS
        ENDDO
*
* write check
101     write (6,*) 'end of one-shot is ',ios
* normalize the one shot dat  & write data to a new file
        OPEN(UNIT=3,STATUS='NEW',FILE='NORMALIZED ONE SHOT')
        DO JOS=1,OSEND
                XNEW(JOS)=CONSTH*XOS(JOS)
                YNEW(JOS)=CONSTMU*TOS*YOS(JOS)/VMAXOS
                write (3,*) xnew(jos), ynew(jos)
        ENDDO
        close (unit=3)
*
* open file to read the hysteresis data
        OPEN (UNIT=8,STATUS='OLD',
     +  FILE='HYSTERESIS DATA')
* read in hysteresis data
        DO IH=1,300
                READ (8,*,END=102) XH(IH),YH(IH)
                HEND=IH
        ENDDO
*
* write check
102     write (6,*) 'end of hysteresis is ', hend
*
* find the max H value point
*       if the data starts out in a negative quad,
*       find the 1st +ve,+ve value
        DO JH=1,HEND
                HPOS=JH
                IF ((XH(JH).GT.0.0).AND.(YH(JH).GT.0.0)) GOTO 103
        ENDDO
* write check
103     write (6,*) 'H goes +ve at ', hpos
*       now find where the data goes -ve, ie max H value
        DO JHH=HPOS,HEND
                HMAX=JHH
                IF (YH(JHH).LE.0.0) GOTO 1030
        ENDDO
*
* write check
1030    write (6,*) 'hmax is ', hmax
* normalize the hysteresis data
        DO KH=1,HEND
                XH(KH)=CONSTH*XH(KH)
                YH(KH)=CONSTMU*TH*YH(KH)/VMAXH
        ENDDO
* write first part of hysteresis data out to the sorted (new) file
        DO LH=1,(HEND-HMAX)
                XNEW(OSEND+LH)=XH(HMAX+LH-1)
                YNEW(OSEND+LH)=YH(HMAX+LH-1)
                        LASTH=XNEW(OSEND+LH)
        ENDDO
*
*write check
        write(6,*) 'h value for last hyst point is ', lasth
*
* write out the last part of the hysteresis loop using data
* from the beginning of the original file
*
* find point where loop ends and fill in
*       check starting quadrant
        IF (YH(1).LT.0.0) GOTO 1044
*
        DO MH=1,HEND
                HLP=MH
                IF (XH(MH).GT.LASTH) GOTO 104
        ENDDO
                GOTO 104
*
1044    DO MHH=1,HEND
                HLP=MHH
                IF (XH(MHH).LT.LASTH) GOTO 104
        ENDDO
*write check
104     write (6,*) 'restart of loop is at ',hlp
* determine where to start writing to sorted arrays
        MAXH = OSEND + (HEND-HMAX)
* write out the last bit of the loop
```

```
        DO NH=1,(HMAX-HLP)
                XNEW(MAXH+NH)=XH(HLP+NH-1)
                YNEW(MAXH+NH)=YH(HLP+NH-1)
        ENDDO
*
* determine th number of points to write out
        DATAEND=OSEND+HEND-HLP
*write check
        write (6,*) 'total number of data points uses is ', dataend
* write out sorted data to new file
        DO I= 1,DATAEND
        WRITE (9,*) XNEW(I),YNEW(I)
        ENDDO
        CLOSE (UNIT=9)
*
*
* integrate the  data for one-shot plus hysteresis data
* and write out result to a new file
* open file to write file combining integrated one-shot and hysterisis data
        OPEN (UNIT=10,STATUS='NEW',
     +  FILE='INTEGRATED HYSTERESIS')
*
        SUM=0.0
        DO J=2,DATAEND
                        IF (YNEW(J).EQ.0.0) GOTO 105
                YNORM=YNEW(J)/ABS(YNEW(J))
                XDIFF=XNEW(J)-XNEW(J-1)
                        IF (XDIFF.EQ.0.0) GOTO 105
                SUM=SUM+((YNEW(J)+YNEW(J-1))/2.0*XDIFF)*YNORM
105             WRITE (10,*) XNEW(J), SUM
        ENDDO
        CLOSE (UNIT=10)
*
*
        STOP
        END
```

Appendix C: List of Abbreviations of Technical Terms

ADC	Analog to Digital Converter
BAC	Backing Calorimeter
BCAL	Barrel Calorimeter
BOPS	Bipolar Operational Power Supply
CC	Charged Current
CTD	Central Track Detector
DESY	Deutsches Elektronen-Synchrotron Laboratory
DVM	Digital Voltimeter
FCAL	Forward Calorimeter
FTD	Forward Tracking Detector
GPIB	General-Purpose Interface Bus
HAC	Hadron Calorimeter
HERA	Hadron Electron Ring Accelerator
HP	Hewlett-Packard
HPIB	Hewlett-Packard Interface Bus
MOV	Monostable Multivibrator
MUD	Muon Detector
NC	Neutral Current
PMT	Photomultiplier Tube
QCD	Quantum Chromodynamics
RCAL	Rear Calorimeter

RTD	Rear Tracking Detector
TRD	Transition Radiation Detector
VXD	Vertex Detector
ZEUS	Search to Elucidate Underlying Symmetry

Appendix D: List of B-H data for the US sample

H (A/m)	*B (tesla)*
0.20055747409866	8.3406964580788427E-03
3.09707074126601	1.9781401792334411E-02
5.29762821536467	3.5916576703608146E-02
8.41867079879678	5.7303539144466186E-02
19.9054818792950	8.5916240092304497E-02
32.1855542440602	0.1221147061446850
55.0063278653579	0.1676125962500993
78.4314146557213	0.2236032813254200
101.3158001895522	0.2806768063342275
124.5341482641826	0.3335299928230740
147.1958921041472	0.3808419957645237
170.3665312443777	0.4253686706697781
193.7598120784745	0.4668256009374529
217.0576750437714	0.5050085989249191
240.3396350309350	0.5404005968053422
263.1604086522327	0.5726846894663107
286.3151448143299	0.6032516291665664
309.9946792548262	0.6324490500892301
333.3084451982565	0.6593483103779919
356.6699200760867	0.6846333211324015
379.3634698723179	0.7077345203669910
402.7408477282814	0.7301548673170003
426.4044791906444	0.7515443231617952
449.5910213090082	0.7713308982060322
472.9843021431050	0.7902099684409244
495.9482025676025	0.8077642679849126
519.1665506422328	0.8246009402476004
542.8142791264626	0.8408733872174686
566.2552688949593	0.8561937803076979
589.4895199477230	0.8706384719747933
612.4852263284871	0.8842573196593361
635.7353803593841	0.8973866628632648
659.4308177780137	0.9101478330606312
682.7922926558439	0.9221549912759251
706.1378645555408	0.9331969577419150
728.9586381768385	0.9443414697853411
752.2405981640021	0.9548147544249985
775.9042296263652	0.9650057112719221
799.1543865726622	0.9745977608517711
822.4840525788257	0.9838273937031200
845.4479530033232	0.9925466386156375
868.5072712966205	1.000956345407190
892.2345146715168	1.009267156179201
915.6277955056614	1.017138567006509
938.8461435802244	1.024650870124166
961.6351112452275	1.031747668734792
984.710332516706	1.038667791353308
1008.501187804135	1.045536009169949
1031.687729922499	1.051961902178756
1055.128719690996	1.058261591422909
1077.869978421627	1.064136603729496
1100.945199693057	1.069889206239952
1124.465704352221	1.075546029433979
1147.699955404984	1.080938112814110
1170.870594545215	1.086129637267745
1193.707271144646	1.091072740008372
1216.798395394210	1.095903213147614
1250.318900053373	1.100656975725184
1293.425927281070	1.105170389222451
1336.676081311967	1.109561480999220
1379.321922173799	1.113699052416323
1412.333531532696	1.117768010565636
1455.869939169993	1.121794198565230
1478.913354485157	1.125608232463804
1502.020381712854	1.129310642757435
1524.713931509085	1.132832158616007
1547.598317042916	1.136272650486633
1570.991597877013	1.139678992014039
1594.114528082843	1.142939700929372
1617.014816594808	1.146086644827397
1639.756075325439	1.149080732046223
1662.497334056070	1.152001346329045
1685.874711912033	1.154911147687134
1708.775000423998	1.157673829578085
1731.675288935962	1.160352854123041
1754.257517885260	1.162915509686036
1776.998776615891	1.165419359047691
1800.217124690521	1.167898481606765
1823.117413202486	1.170269834128940
1846.017701714450	1.172570261933286
1868.440900882415	1.174755849472367
1891.023129831713	1.176892294952254
1914.082448125010	1.179009170371597
1936.982736636974	1.181048579298550
1959.564965586272	1.183000121209585
1981.829134972904	1.184867987814105
2004.252334140869	1.186694456798144
2027.470682215500	1.188529517819353
2050.211940946131	1.190273233009787
2072.635140114096	1.191942106707127
2094.740279719395	1.193539490621000
2117.004449106027	1.195101655333789
2140.063767399324	1.196671733037878
2162.645996348622	1.198163419282719
2184.910165735254	1.199590672847465
2207.015305340553	1.200966347248406
2229.120444945851	1.202301885410108
2252.020733457816	1.203644182944997
2274.125873063114	1.204901080963307
2296.390042449746	1.206129691160254

H (A/m)	*B (tesla)*
2340.123232316345	1.208437790870438
2410.462104599968	1.207776377349650
2364.025408450707	1.205928028653269
2317.700192178161	1.203713527217470
2271.072501261519	1.201384490590936
2225.287668185943	1.199142221136869
2178.660136299082	1.197249885277302
2131.921442595070	1.195261843530752
2085.500649423942	1.192870682111964
2038.920826471482	1.190225905571620
1992.865801797420	1.187548093860950
1946.269916837045	1.185229737524131
1899.451549212585	1.182726746511806
1853.014853063324	1.179827375698556
1806.212388416997	1.176786452669769
1760.141460764803	1.173811038540223
1713.498184929590	1.171144492274633
1666.616205392597	1.168188987213298
1619.972611497822	1.164804341487248
1573.249709451096	1.161230721892023
1527.083475250948	1.157600594056730
1480.328767247955	1.154343832244327
1433.399031067628	1.150754392950365
1386.723822052323	1.146592461752072
1339.905422621907	1.142134577357394
1293.707318853580	1.137627586777304
1246.857145272853	1.133532326227298
1199.832023029682	1.128953829619748
1153.188556358732	1.123702623438634
1106.211127146982	1.118056343452063
1059.949395563144	1.112252371548357
1013.067447832107	1.106690747153712
966.0264226108025	1.100559544489533
919.2557003088297	1.093477996035469
872.3419307185478	1.085532655883268
825.9211693533766	1.077154538593595
778.8801441320719	1.068994898967344
731.7914576853017	1.060018470309439
685.0843791018184	1.049656660226035
638.0592568586471	1.037572731395912
591.5908024620541	1.024571041190592
544.5497931437275	1.011629434947898
497.3815440973564	0.9971618935962451
450.5949983321410	0.9803192680856825
403.5062800794145	0.9603910317398455
357.0377620709090	0.9386308514319859
309.9649626992940	0.9157518975528118
262.7331017403896	0.8902981844830895
215.9147341159294	0.8614589806987115
168.8737407005810	0.8271591460425980
122.2780004573068	0.7886563672464159
75.17337445555362	0.7459005018938150
27.84611312112536	0.6965247181568784
-18.98815589117034	0.6392196555985185
-66.06096798516785	0.5656965372852072
-112.6885030526240	0.4656301806418875
-159.8090431645952	0.2974542307054339
-207.1044683270984	4.8508186367954099E-02
-253.9864478640918	-0.1794636860339463
-301.0751820197964	-0.3319804334284751
-347.7027298096350	-0.4389702268661202
-394.8709470500499	-0.5222505696172085
-442.2459189091759	-0.5914666895965799
-489.1914785527463	-0.6497872660210633
-536.2166485048520	-0.7018665730640044
-582.9077604982895	-0.7475905352491544
-630.0600747605710	-0.7868108251867117
-677.4191277385856	-0.8222943446430007
-724.2852202004239	-0.8542811593215869
-771.4852911060397	-0.8847461172587051
-818.0173574151660	-0.9118836710538986
-865.1220104519820	-0.9348148721659020
-912.4811111389309	-0.9560772813577632
-959.3472036007692	-0.9761124742003645
-1006.404099994251	-0.9956324360246946
-1052.967988162622	-1.013294357198367
-1099.961336255483	-1.028276739827221
-1147.352115674873	-1.042599862741350
-1194.138740954980	-1.056101372990364
-1241.211476714682	-1.069538493967107
-1287.775476203900	-1.082039966274636
-1334.721131265339	-1.092564621276640
-1382.000589837796	-1.102841237290140
-1428.723587302391	-1.112705177009582
-1475.844095608406	-1.122653037258414
-1522.296678832822	-1.132079215624736
-1569.226255983369	-1.139899039032548
-1616.394600447608	-1.147372109819440
-1663.165100107887	-1.154754771552258
-1710.142815573243	-1.162408460212555
-1756.547546736456	-1.169887308636497
-1803.381976368831	-1.176210899565561
-1850.454632613643	-1.182245194123603
-1897.113970456770	-1.188099049221120
-1944.091526892345	-1.194203647312942
-1990.400999216539	-1.200384072667183
-2037.044275051751	-1.205635257363663
-2084.069222362163	-1.210525697765494
-2130.712816256938	-1.215285469730499
-2132.812168400316	-1.215520589756835

H (A/m)	*B (tesla)*
-2179.582668060595	-1.220521453299191
-2226.098879100523	-1.224578466682246
-2273.346468104801	-1.229012666026333
-2319.481166699310	-1.233684500777139
-2365.901959870438	-1.238765718995855
-2412.545394735432	-1.243279750936731
-2435.668324941262	-1.242882725908053
-2389.613141237419	-1.240950715672628
-2341.999624706294	-1.239157716804777
-2294.608908898816	-1.237530301530675
-2247.647255441374	-1.235505287208695
-2200.335895494782	-1.233132870270287
-2153.835587432988	-1.230991655089012
-2106.094847076796	-1.228914415955648
-2058.847258072517	-1.226840196927749
-2011.917728630905	-1.224413673521967
-1964.590465706179	-1.221855773471996
-1917.851453942604	-1.219502937460272
-1870.174166469164	-1.217009842658540
-1822.926577464886	-1.214400935966817
-1775.901471124693	-1.211510703532814
-1728.431240426548	-1.208537540038604
-1681.676484714621	-1.205718659394447
-1633.935585328648	-1.202737858337223
-1586.608322403922	-1.199570494693434
-1539.599134944840	-1.195993322916159
-1492.160567076159	-1.192318685174504
-1445.246765679921	-1.188931844295181
-1397.331092564262	-1.185257645935707
-1350.115023262644	-1.181185676186286
-1303.090075952232	-1.176708124932468
-1255.635525590527	-1.172208186549186
-1208.562694412956	-1.167918953586572
-1160.742502778010	-1.163113759118936
-1113.478899474751	-1.157700518070827
-1066.405988782289	-1.151794776073479
-1018.951438420584	-1.145868931166979
-971.8945202710127	-1.140130466200444
-923.8835623634913	-1.133423192790847
-876.5881053950318	-1.125745421237331
-829.4834205225595	-1.117372539963903
-781.9971755551348	-1.108844448238569
-734.8448135839188	-1.100218687900458
-686.9291404682603	-1.090084257984256
-639.6496023809123	-1.078479226569654
-592.5131592908078	-1.065640123586366
-544.9791735533269	-1.051598330818215
-497.7950533347787	-1.037153540714873
-449.8793325101858	-1.020998271932931
-402.5679884665712	-1.002222030111736
-355.4156423983334	-0.980509634025314 2
-307.8498348016077	-0.956008213619982 2
-260.7770195270145	-0.929960544965110 3
-212.8295404550894	-0.900182589603019 0
-165.5500023677414	-0.866373018633223 7
-118.4453795465838	-0.827137254120365 6
-70.97498981865799	-0.781770884072930 3
-23.77495230929620	-0.731431902711693 6
24.14072239666010	-0.670372897783662 5
71.30895872064872	-0.595117775874501
118.4453811368817	-0.488018002880408 1
165.9634797992074	-0.301947636639313 7
213.0521980519339	-4.889856076076566 6E-02
260.8883562769258	0.174220903531259 0
308.0407023451636	0.316059888256106 5
355.0498739012673	0.416972789929909 7
402.5202795321713	0.499351028611578 6
449.4181620472980	0.565033442960913 2
497.2225302190015	0.621883869749205 2
544.3430226220383	0.671338141213783 1
591.3522100811200	0.715603349815964 0
638.6954077899357	0.756247937158185 5
685.6409833364842	0.790487356997305 1
733.4453515081877	0.821314371311976 4
780.4863290205579	0.849583959643883 0
827.5114194577730	0.875825427952658 2
874.8545853606324	0.900101315546476 5
921.7843056379820	0.920804683045121 5
969.3819509969306	0.939805992995351 3
1016.454702659611	0.957872174538267 0
1063.368567667762	0.974998628352648 0
1110.616236186931	0.991122251213532 3
1157.402893272993	1.005043695818007
1205.000522728964	1.017896972545614
1251.930099879510	1.030231050453579
1298.732644040728	1.042285180151428
1345.853152346743	1.053584552084198
1392.655632896048	1.063227842041708
1440.157749065349	1.072366497852410
1486.944379573 68	1.081531835938137
1533.587809210449	1.090578089589136
1580.740187084643	1.099005448732923
1627.463232258173	1.106289455793100
1674.806239131251	1.113383754730672
1721.672474719892	1.120644362923363
1768.220332686305	1.127610427516005
1815.181827113965	1.134106944463288
1861.777553044559	1.139852811930739
1909.200233838084	1.145423066498114
1955.795959768678	1.151241666646984

H (A/m)	*B (tesla)*
2002.248399866291	1.157024246803057
2049.082829498666	1.162342642719097
2095.662652451127	1.166986845355196
2142.894497507053	1.171502527956303
2189.394964598628	1.176383788832553
2235.656568958641	1.181294133959330
2282.347871787816	1.185758137172881
2328.641441133877	1.189714418824980
2375.873286189804	1.193631082453171

BIBLIOGRAPHY

[BL32] F.Bloch, Z. Physik, 74, 295 (1932).

[BO30] R.M.Bozorth, J.F.Dillinger, *Barkhausen effect II. Determination of the average size of the discontinuities in magnetization*, Phys. Rev., 35, 733-52 (1930).

[BO51] R.M.Bozorth, *Ferromagnetism*, Princeton, D.Van Nostrand, 1951.

[CO91] F.Corriveau and J.Mayer, *Analysis results from the ZEUS field and force monitoring,* ZEUS Notes, 1991.

[EW89] J.A.Ewing, *Time lag in the magnetization of iron*, Proc. Roy. Soc. (London), 46, 269-86 (1889).

[FE66] R.Feynman, R.Leighton and M.Sands, *The Feynman lectures on physics volume II*, London, Addison-Wesley Publishing Company, Inc., 1966.

[FO29] D.D.Foster, *Magnetic properties of iron crystals*, Phys. Rev., 33, 1071 (1929).

[HA79] G.C.Hadjipanayis, Ph.D. thesis, University of Manitoba, 1979.

[HE86] Hewlett-Packard, HP 3457A Multimeter Operating Manual, (1986).

[HO52] K.Hoselitz, *Ferromagnetic properties of metals and alloys*, New York, Oxford University Press, 1952.

[KE79] KEPCO Instruction Manual, (1979).

[KR53] J.Kraus, *Electromagnetics*, New York, McGraw-Hill Book Company, Inc., 1953.

[MA87] J.H.Mathews, *Numerical methods*, New Jersey, Prentice-Hall, Inc., 1987.

[MA91] J.Mayer and F.Corriveau, *Force and field monitoring during the ZEUS solenoid mapping*, ZEUS Notes, 1991.

[MI70] MICRODOT Inc., Instruction Manual, (1970).

[MO65] A.H.Morrish, *The physical principles of magnetism*, New York, John Wiley & Sons, Inc., 1965.

[NA84] National Instruments, IEEE-488 Instrumentation Interface Manual, (1984).

[PA61] L.G.Parratt, *Probability and experimental errors in science*, New York, Dover Publications, Inc., 1961.

[PA69] D.Paris and F.Hurd, *Basic electromagnetic theory*, New York, McGraw-Hill Book Co., 1969.

[PR29] F.Preisach, *Investigations of the Barkhausen effect*, Ann. Physik [5], 3, 737-99 (1929).

[RE66] R.Resnick and D.Halliday, *Physics II*, New York, John Wiley & Sons, Inc., 1966.

[SA86] See for example, D.H.Saxon, Proc. Roy Soc. Lond., A404, 233 (1986).

[SI87] R.E.Simpson, *Introductory electronics for scientists and engineers*, Boston, Allyn & Bacon, Inc., 1987.

[SK68] G.Skitek and S.Marshall, *Electromagnetic concepts and applications*, New Jersey, Prentic-Hall, Inc., 1968.

[ST34] E.C.Stoner, *Magnetism and matter*, New York, 1934.

[ST48] E.C.Stoner, *Ferromagnetism*, Rep. Progr. Phys., 11, 43 (1948).

[ST50] E.C.Stoner, *Ferromagnetism-Magnetization curves*, Rep. Progr. Phys., 13, 83 (1950).

[TE50] R.S.Tebble, I.C.Skidmore, W.D.Corner, *Barkhausen effect*, Proc. Phys. Soc. (London), A63, 739-61 (1950).

[TI82] P.Tipler, *Physics volume II*, New York, Worth Publishers, Inc., 1982.

[WA86] R.K.Wangsness, *Electromagnetic fields*, New York, John Wiley & Sons, 1986.

[WE07] P.Weiss, J. Phys., 6, 661 (1907).

[YE24] T.D.Yensen, *Magnetic properties of ternary Fe-Si-C alloys*, Trans. Am. Inst. Elect. Engrs., 43, 145-75 (1924).

[ZD86] The ZEUS Detector Technical Proposal, March 1986.

[ZE86] The ZEUS Detector Status Report, March 1986.

[ZE89] The ZEUS Detector Status Report, March 1989.

[ZE91] ZEUS Meeting, september 23-27, 1991, DESY, Germany.